

*Disorder and entropy rate in
discrete time quantum walks*

by

Bálint Kollár

A dissertation submitted in partial fulfillment of
the requirements for the degree of

**Doctor of Philosophy
(Physics)**

At the

Doctoral School of Physics
Institute of Physics
Faculty of Sciences
University of Pécs

Quantum optics and quantum informatics program

Supervisor:

Tamás Kiss, PhD

Senior research fellow

MTA Wigner RCP SZFKI



Pécs, Hungary

2014

Contents

| | |
|--|-----------|
| Introduction | 1 |
| Part I | 5 |
| 1. Definitions of quantum walks | 7 |
| 1.1. Discrete time quantum walks | 7 |
| 1.1.1. Basic properties, the one-dimensional Hadamard walk | 10 |
| 1.1.2. Two-dimensional quantum walks | 13 |
| 1.1.3. Quantum search | 15 |
| 1.2. Continuous time quantum walks | 18 |
| 1.3. Scattering quantum walks | 20 |
| 1.4. Szegedy's quantum walk | 22 |
| 1.5. Optical realizations | 24 |
| 2. Entropy rates of stochastic processes | 29 |
| 2.1. Definition of the entropy rate | 29 |
| 2.2. Examples | 31 |
| 3. Asymptotics of random unitary operations | 33 |
| 3.1. Random unitary evolution of quantum Markov chains | 33 |
| 3.2. Properties and asymptotics of RUO maps | 34 |
| 3.3. Example | 36 |
| 4. Walks on percolation graphs | 41 |
| 4.1. Definition and some properties of percolation graphs | 41 |
| 4.2. Overview of quantum walks on percolation graphs | 42 |
| *** | |
| Part II | 49 |
| 5. Asymptotics of quantum walks on percolation graphs | 51 |
| 5.1. Definitions | 51 |
| 5.2. Formal solution and a polynomial construction | 53 |
| 5.3. General method | 55 |
| 5.4. Shift conditions on regular lattices | 57 |
| 5.5. Conclusions | 59 |
| 6. Determining asymptotics through pure states | 61 |
| 6.1. Pure state ansatz | 61 |
| 6.2. Percolation quantum walks | 63 |
| 6.3. Conclusions | 64 |
| 7. One-dimensional quantum walks on percolation graphs — complete analysis | 67 |
| 7.1. Explicit solutions | 67 |
| 7.2. Edge states | 73 |
| 7.3. Conclusions | 74 |

| | |
|---|-----|
| 8. Two-dimensional quantum walks on percolation graphs | 77 |
| 8.1. Description and asymptotics | 77 |
| 8.2. The two-dimensional Hadamard walk: breaking the directional symmetry | 79 |
| 8.3. The Grover-walk: preserving trapping on percolation lattice | 83 |
| 8.4. Conclusions | 85 |
| 9. Entropy rate of quantum walks | 87 |
| 9.1. Periodically measured walks in a black box | 87 |
| 9.2. Entropy rate of some classical random walks | 88 |
| 9.3. Discrete time quantum walks as stochastic processes | 90 |
| 9.4. Solution — employing the quantum Markov property | 91 |
| 9.5. Calculating the entropy rate of one-dimensional QWs | 95 |
| 9.6. Upper bound for the entropy rate | 100 |
| 9.7. Analysis of independent systems — the “most quantum” case | 103 |
| 9.8. The quantum entropy rate of periodically measured QWs | 105 |
| 9.9. Conclusions | 106 |
| Summary | 109 |
| List of new scientific results | 119 |
| Összefoglalás | 121 |
| Új tudományos eredmények | 131 |
| List of publications | I |
| Acknowledgement | III |
| Appendix | V |
| A. Entropy rate of one-dimensional Hadamard walk for waiting time $w = 2$ | V |
| B. Approximating entropy rates of one-dimensional QWs | VII |
| Bibliography | XI |

Introduction

Walks are elementary processes that consist of a sequence of atomic steps. If the sequence of steps is random, we call the process *random walk* [1–7]. In general, random walks follow the Liouville equation, thus can be fully described and understood in terms of classical mechanics. Random walks are basic mathematical tools, used to model a rich variety of physical systems. The path of a single dye molecule in water (diffusion) [8–12], the fluctuation of stocks [13–15] and temperature [16], the spreading of diseases [17–19], mass transport [20], steady states in nonequilibrium [21, 22], Ising spin chains [23, 24], evolutionary games [25], and surfing on the internet [26, 27] are amongst the typical examples of such systems. In computational sciences it was also found beneficial to employ random walks, *e.g.* as an approach to describe probabilistic Turing machines. Throughout this thesis we will use the term *classical walk* as a synonym for random walks.

However, there are countless walk-like phenomena in nature, which do not fit in the framework of classical mechanics, *e.g.* the propagation of a single excitation in a crystal, the efficient energy transport during photosynthesis [28] in plants or the spreading of quantum information on quantum networks. Such phenomena called for the extension of walks to the quantum domain. We call these extensions *quantum walks* [29–38]. Similarly to classical walks, quantum walks can model physical systems of many kind. In fact, most quantum processes can be viewed as generalized quantum walks. Here, we have to note that classical walks can be generalized to quantum walks in several ways. Naturally, these definitions are all competing and complementing each other, however, most of them share a common point: They satisfy the Schrödinger (von Neumann) equation or a Master equation.

By design, quantum walks are perfect candidates for modeling quantum transport [39–44], *i.e.* the propagation of a single excitation on a graph structure. In quantum information theory [45, 46], quantum walks are widely used to construct quantum algorithms, for example, to perform search on an unstructured database [47–53]. Quantum walks are also universal primitives of quantum computation [54–56]: On a quantum computer, the computation process is described by unitary (reversible) transitions between elements of the state space. One can consider these elements as vertices of a graph, and the unitary computation process as a quantum walk on this very graph.

Since their introduction, quantum walks gained considerable attention. Up to date, several aspects of quantum walks were studied, all aimed to shed some light on the quantum features of this simple model. The straightforward construction of quantum walks makes them suitable tools for studying some properties of solid states materials. In particular, using quantum walk based models in the novel research field of topological insulators [57–61] is rather prosperous. The spreading nature of quantum walks also makes them suitable for generating entanglement [62–66]. The von Neumann entropy, that is used

to quantify the entanglement also allows for studying the thermodynamical aspects of quantum walks [67, 68]. Similarly to transport [39–43], perfect state transfer [69] can be understood in terms of quantum walks. Decoherence in quantum walks can also lead to interesting behaviors, for a review see [70]. Several other quantum phenomena are studied in terms of quantum walks, *e.g.* aperiodic behavior in chains [71], effects of non-local initial conditions [72], movement in electric field [73], movement including jumps [74], self-avoidance [75], and the effect of more internal states [76–79], localization in regular lattices [80, 81] and symmetries [82]. Quantum walks can exhibit a self similar spectral structure [83] commonly known as Hofstadter’s butterfly [84]. The Google PageRank algorithm have also been generalized to the quantum domain using a quantum walk based definition [85]. The two-particle extension of quantum walks [86, 87] and its algorithmic uses [88, 89] are particularly interesting. Introducing even more particles can lead to many-particle interference [90] and universal quantum computation [56], once again.

The universality and other promising aspects of quantum walks have caught the attention of experimentalists. To implement quantum walks, several experimental schemes were proposed based on various physical systems: cavity quantum electrodynamics [91, 92], Bose-Einstein condensate [93], linear optics [94–96], optical angular momentum of light [97], parametric down-conversion in nonlinear crystals [98], neutral trapped atoms [99, 100] and Rydberg atoms [101] in optical lattices, ion traps [102], optical cavity [103], superconducting qubits [104], semiconductor quantum rings [105, 106], array of quantum dots [107], and artificial graphene [108]. For a review on realization schemes, see [109].

In the recent years the number of actual realizations have grown significantly. Quantum walks have been successfully demonstrated in optical lattices using single neutral atoms [110, 111] and trapped ions [112, 113]. These experiments all share a similar approach: the internal state of the atom is rotated by an electromagnetic field, then the atom is coherently displaced in the lattice corresponding to its internal state. The repetition of this process realizes a discrete time quantum walk. A nuclear magnetic resonance based experiment (realizing a quantum information processor consisting of three qubits) is reported in [114]. Another promising realization family is the photonic quantum walk: These experiments are quite diverse considering the media where the photons propagate. In integrated waveguide arrays [115–118] photons scatter between parallel waveguides of close proximity; their final position density is given by a continuous time quantum walk. These arrangements are very well suited to study multi-photon (*i.e.* multi-particle) walks and decoherence, as well. Experiments are also performed with linear optics efficiently mimicking the optical Galton board [119, 120], using linear interferometer network [121], and by the time bin encoding of the position of the walker [122–125]. This latter approach is also suitable for studying higher dimensional walks, multi-particle walks with interaction, and decoherence.

Errors in the underlying graph or lattice are a special source of noise in walks. For example, hot water (liquid) passing through ground coffee (porous or granular material) or the robustness of computer networks [126, 127] under attacks or power outage can be modeled with graphs, where connections are

broken with some probability. This concept is called *percolation* [128–130]. Percolation is extensively studied in relation to classical walks. On the other hand, the question of the effect of percolation on quantum walk models is rather new and there exist only a few studies on this topic [131–137]. Most quantum walks are defined via a unitary time evolution, having a closed system dynamics. The effect of percolation can make the time evolution open, and in some cases the system can be described in terms of random unitary operations [138–140] (*RUO* maps). The first part of this very thesis aims to explore the properties of quantum walks on percolation graphs using the analytical tools available for RUO maps.

In physics, the *entropy* is the most well known measure of the information content (or disorder) [45, 46, 141–144]. However, the definition of the entropy is very special, since it is the average asymptotic information content *per symbol* for an independent and identically distributed (*i.i.d.*) sequence of random variables (thus, for a stochastic process). Even for simple stochastic processes, *e.g. Markov chains* (which, in fact, can be interpreted as classical walks on weighted, directed graphs), the entropy is not a suitable measure for the asymptotic per symbol information content. In information theory, however, there exists a generalization, which is a suitable measure for general stochastic processes: the *entropy rate*. As classical walks are the textbook examples of Markov chains, for which the entropy rate is a meaningful definition. It is a rather interesting question whether for quantum walks (which are quantum Markov chains) the concept of entropy rate is applicable. In this thesis, we address this question in detail.

This thesis is organized as follows. In Part I. we overview the literature, give the basic definitions, and establish the context of the thesis. In Chapter 1 we review the most influential definitions of quantum walks and some experimental schemes. Chapter 2 is devoted to define the entropy rate of stochastic processes and also to give its most important properties on which we later rely. The next chapter outlines the asymptotic theory of random unitary operations (RUO maps). Finally, in Chapter 4, we review some interesting aspects of walks on percolation graphs and also give a brief review of the literature.

Part II. is devoted to our own results. In Chapter 5 we adapt the asymptotic theory of RUO maps reviewed in Chapter 3 to the problem of quantum walks on dynamical percolation lattices. We introduce a pure state ansatz approach in Chapter 6, which gives a direct physical meaning for the asymptotics of RUO maps, considerably simplifying their asymptotic analysis. We also show that percolation quantum walks benefit from the ansatz. In Chapter 7 we elaborate on the complete problem of percolation walks on one-dimensional graphs using the newly given methods. After acquiring the complete solution for the one-dimensional system, we study some notable cases of the two-dimensional problem in Chapter 8: The Hadamard and Grover walks. Chapter 9 is devoted to study another disturbed quantum walk based system, the periodically measured discrete time quantum walk in terms of the entropy rate. We develop methods to perform the analysis and also compare different definitions of the entropy rate. Finally, we summarize the new scientific results of the thesis.

Part I

Chapter 1

Definitions of quantum walks

Quantum walks are always non-trivial generalizations of classical walks. The non-triviality is ensured by the no-go lemma of Meyer [30]:

Lemma: "In one dimension there exists no nontrivial, homogeneous, local, scalar quantum cellular automaton".

Consequently all non-trivial (useful) quantum walk definitions have to violate some of the conditions in the above lemma. In this chapter we review the major types of quantum walks and their most important properties. In Section 1.1 we review the discrete time quantum walk, that we will use later as the basis of our own research. In Section 1.2 we give the definition of continuous time quantum walks, which is particularly popular among those, who study quantum transport. In the next section another discrete time model, the scattering quantum walk, is presented which is a straightforward model of computation in quantum networks. In Section 1.4 we give Szegedy's quantum walk which is based on the quantization of classical Markov chains, and is widely used as a tool for the theoretical studies in quantum information theory. Finally, in Section 1.5 we briefly sketch some basic experimental arrangements realizing quantum walks.

1.1. Discrete time quantum walks

A discrete time random (classical) walk on a graph can be described by the following protocol: At the beginning, the walker (particle) resides in a single (initial) vertex. Next, some random (stochastic) process picks one from the immediate neighboring vertices. Following that, the walker is shifted to the just picked new vertex. The repeated application of this algorithm is a discrete time random walk. The most basic example is the unbiased walk of a particle on a one-dimensional integer lattice. Initially the walker resides at the origin, labeled by 0. Next, a random process chooses from the nearest neighbors: in this case the nearest neighbors are the sites ± 1 . The choice can be based on a fair coin toss. Following the coin toss, we place the particle to its new position depending on the state of the coin: either to the site labeled by +1, or to the site labeled by -1. Then, the protocol is repeated again and again: following every coin toss, we move the particle. The properties of this textbook example is well known, *e.g.* if one asks for the probability distribution of the position of the particle, the answer is a binomial distribution, and asymptotically it is the Gaussian distribution.

The discrete time quantum walk (QW) extends the previous classical model using the mathematical apparatus of quantum mechanics. Similarly to the classical walk, a single iteration step of the QW is split into two operations: the coin toss and the displacement. To define this system we give its Hilbert space first. Given a d -regular graph (or lattice) $G(V, E)$ we define a position Hilbert space spanned by state vectors corresponding to the vertices of the graph:

$$\mathcal{H}_P = \text{Span} \{ |v\rangle_P \mid v \in V \} . \quad (1:1)$$

Next, we use the fact that $G(V, E)$ is a d -regular graph, *i.e.* that every vertex of G has d nearest neighbors: We define an additional coin (or spin) Hilbert space using the d directions pointing to nearest neighbors

$$\mathcal{H}_C = \text{Span} \{ |c\rangle \mid c \in [1..d] \} . \quad (1:2)$$

Thus, the total Hilbert space of the system is a composite one:

$$\mathcal{H} = \mathcal{H}_P \otimes \mathcal{H}_C . \quad (1:3)$$

We denote the Hilbert vectors of the position space by $|v\rangle_P$, the coin space by $|c\rangle$ and the a vector on the total Hilbert space by $|v, c\rangle \equiv |v\rangle_P \otimes |c\rangle$. Throughout this thesis all matrixes are represented in this natural basis, unless noted otherwise. Note that this construction breaks the *scalarity* in Meyer's no-go lemma by introducing the coin space.

Let us now move on to constructing the discrete time evolution on this Hilbert space. Mimicking the classical discrete time walk, we should define a coin tossing operation first. As in the classical case, the coin toss should not affect the position state (distribution) of the walker and also should be local. Furthermore, quantum mechanics requires unitarity. Thus, a general coin toss operator has the following form:

$$\Gamma = \sum_{v \in V} |v\rangle_P \langle v|_P \otimes C_v \quad \text{where} \quad C_v \in U(d) . \quad (1:4)$$

In most cases the coin is assumed to be independent from the position:

$$\Gamma = I_P \otimes C \quad \text{where} \quad C \in SU(d) , \quad (1:5)$$

where I_P is the identity operator in the position space¹. In this way, the homogeneity property of Meyer's lemma is kept. Throughout this thesis, we will always assume that the coin is position independent, unless

¹ As the coin become homogeneous, the global phase of the coin will be neglected in the dynamics: $SU(d)$ coins can be used without losing generality.

it is noted otherwise.

We now continue with the definition of the displacement operator, that is:

$$S = \sum_{v \in V} \sum_{c \in [1..d]} |v \oplus c, c\rangle \langle v, c|. \quad (1:6)$$

Here, the abstract sum $v \oplus c$ denotes the nearest neighbor of vertex v in direction c . As in the classical case, the outcome of the coin toss determines the direction of the displacement. We note here that the time required for the displacement is negligible for both the classical and quantum discrete time models, thus the transition is considered to be instantaneous. Finally, a single time evolution step is defined as

$$U = S\Gamma = S(I_P \otimes C). \quad (1:7)$$

The actual discrete time quantum walk procedure is given by the repeated application of the single time evolution step U

$$|\psi(t)\rangle = U|\psi(t-1)\rangle = U^t|\psi(0)\rangle. \quad (1:8)$$

We note that measurement is not included in the definition of the system, so the whole process is unitary, and thus deterministic. We also note that this unitary time evolution definition is rather general, in some cases even stricter (less general) definitions can cover all possible dynamics [145]. In case of discrete time quantum walks, measurement usually means a position von Neumann measurement, *i.e.* the measurement of the observable

$$P = \sum_{v \in V} \sum_{c \in [1..d]} v|v, c\rangle \langle v, c|. \quad (1:9)$$

The first discrete time quantum analogue of the classical walk using an additional coin (spin) degree of freedom was proposed by Aharonov *et al* [29]. However, that very protocol included a von Neumann measurement, thus it is not a purely unitary process. Later, Meyer [30] have given a full unitary definition, which we summarized above. Since the combination of the coin space and the coin operator is the key driving mechanism of the discrete time quantum walk, we also refer to this model as the *coined quantum walk*. We note that recently an analogous model, called the "coinless quantum walk" has also been introduced [146]. This model can be understood as a coined quantum walk where the tensor product form of the Hilbert space is not enforced and is actually hidden: unitary rotations simply act on position states instead, breaking the homogeneity in Meyer's no-go lemma.

In this thesis we focus on discrete time quantum walks. Some of their most important properties are reviewed in the following.

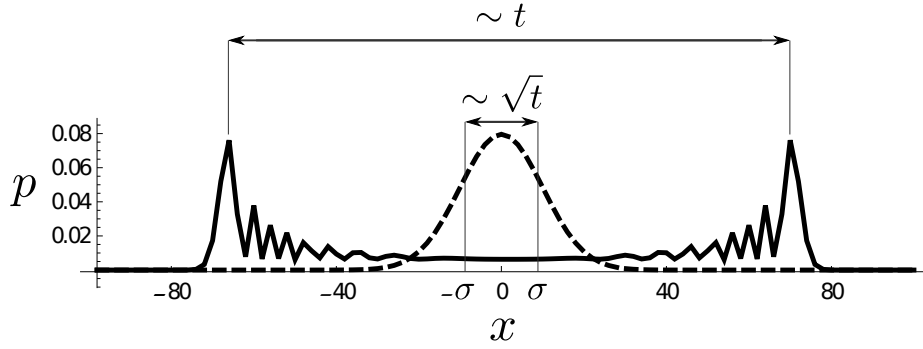


Figure 1:1. Comparison of the classical walk (dashed line) and the discrete time quantum walk (continuous line) on a one-dimensional integer lattice after 100 time steps. Probabilities at the odd sites of the lattice are not plotted, since for even number of steps the probabilities at all odd labeled sites are zeros. The data points are connected to guide the eye, and to emphasize the interference fringes.

1.1.1. Basic properties, the one-dimensional Hadamard walk

Let us employ the definition given above to describe the motion of a quantum particle on a one-dimensional integer lattice. The Hilbert space (*cf.* Eqs. (1:1)-(1:3)) is a composite:

$$\mathcal{H} = \mathcal{H}_P \otimes \mathcal{H}_C, \quad (1:10)$$

where

$$\mathcal{H}_P = \text{Span} \{ |v\rangle_P \mid v \in \mathbb{Z} \}, \quad (1:11)$$

and

$$\mathcal{H}_C = \text{Span} \{ |L\rangle, |R\rangle \}. \quad (1:12)$$

Here, $|L\rangle$ and $|R\rangle$ represent the directions left (decreasing the position state index) and right (increasing the position state index), respectively. According to Eq. (1:6), the displacement operator is given as

$$S = \sum_{v \in \mathbb{Z}} \left(|v-1, L\rangle \langle v, L| + |v+1, R\rangle \langle v, R| \right). \quad (1:13)$$

We represent the coin operator using the usual $SU(2)$ parametrisation

$$C(\mathbf{n}) = \exp(-i(\mathbf{n} \cdot \boldsymbol{\sigma}) \pi/2), \quad (1:14)$$

where $\boldsymbol{\sigma}$ denotes the vector of the Pauli matrices. The typical textbook example of the one-dimensional quantum walk is the one driven by the Hadamard coin:

$$C_H = \frac{1}{\sqrt{2}} \begin{pmatrix} 1 & -1 \\ 1 & 1 \end{pmatrix}, \quad (1:15)$$

which we can obtain from Eq. (1:14) by choosing $\mathbf{n} = (0, 1/2, 0)$. This coin has an interesting property: the magnitude of each of its elements is equal, consequently it shows a well defined classical correspondence: Should one measure the position of the walker after each single timestep, the walk reverts to the classical one-dimensional discrete time walk. Such coins are called *balanced* or *unbiased*. If one measures a biased discrete time quantum walk after each step one will not obtain a classical walk².

Since the definition of the system is homogeneous in space, *i.e.* translation-invariant, the quasi-momentum of the particle is a good quantum number. Consequently, the time evolution simplifies considerably in the momentum picture:

$$\tilde{U}(k) = \tilde{D}(k) \cdot C = \begin{pmatrix} e^{-i \cdot k} & 0 \\ 0 & e^{i \cdot k} \end{pmatrix} \cdot C. \quad (1:16)$$

The position and momentum pictures are connected through the Fourier and inverse Fourier transformations:

$$\tilde{\psi}(k, t) \equiv \sum_{v \in \mathbb{Z}} \psi(v, t) e^{i(vk)} \quad (1:17)$$

and

$$\psi(v, t) = \frac{1}{2\pi} \int_0^{2\pi} \tilde{\psi}(k, t) e^{-i(vk)} dk. \quad (1:18)$$

Here, $\psi(v, t)$ denotes the two-component (coin) spinor of probability amplitudes:

$$\psi(v, t) = \begin{pmatrix} \langle v, L | \psi(t) \rangle \\ \langle v, R | \psi(t) \rangle \end{pmatrix}. \quad (1:19)$$

The unitary (undisturbed) evolution of quantum walks exhibits interesting properties. The spreading (average mean distance from the expected value) of the system is ballistic, thus, linear in time. On the other hand, classical walks show diffusive spreading, *i.e.* a square-root dependence with respect to time (number of steps). Thus, the quantum walk spreads quadratically faster. This is quite an usual but

² The obtained classical process is not a walk in the sense that it is not a classical Markov chain, however it is still a classical stochastic process (See Chapter 2). A similar quantum system is discussed in Chapter 9.

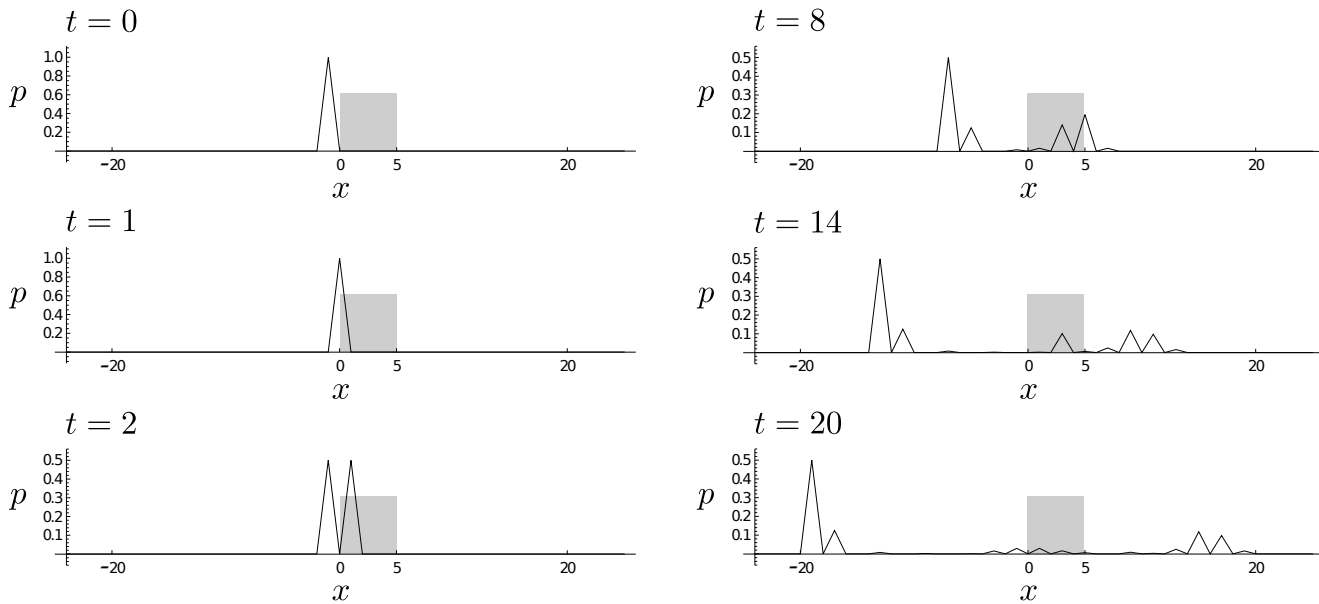


Figure 1:2. Modeling scattering through a potential barrier (gray area) using a discrete time quantum walk. Between positions 0 and 5 the Hadamard coin (1:15) is used. At the other positions the particle can fly without scattering, thus the coin operator is the identity. The strength (height) of the potential barrier can be tuned with the parameters of the coin.

expected property of quantum walks on regular lattices. We show the typical two-peaked quantum walk distribution in FIG. 1:1. Naturally, the spreading also affects the so-called *hitting time*, which is the expectation of the time it takes for the particle to reach a given vertex. On regular lattices the hitting times are usually quadratically lower, *i.e.* quantum walks hit quadratically faster. On some special graphs the hitting time of a quantum walk can even be exponentially larger or smaller compared to the classical hitting times [35, 147, 148].

The ballistic spreading also affects the return probability — the so-called *Pólya-number* — of the walk [149]. While in the classical case the Pólya number is determined by the dimension of the underlying graph, in quantum walks the graph, the coin and also the initial state affect the Pólya number [150–155]. We have to note here that in the definition of all these probabilities — hitting times and Pólya numbers — the measurement and the preparation process must be taken into account.

One can also observe quantum interference effects in quantum walks. The interference fringes between the peaks of a typical two-peaked distribution is one such place, and it is arising from the interference between the left and the right propagating parts of the wave function. Also, one might employ quantum walks to model scattering through potential barriers, or even single- and double-slit experiments [156]. This scattering behavior is illustrated in FIG. 1:2.

1.1.2. Two-dimensional quantum walks

This section is devoted to the description of the two-dimensional quantum walk model [80]. We will focus on the two-dimensional Cartesian lattice (square lattice), however, there are several other two-dimensional graph structures of interest in the research of quantum walks, e. g. the triangular, the honeycomb and the Kagome lattices [V] [50, 157, 158].

The position space is spanned by state vectors with two integer indices, corresponding to the coordinate labels of the square lattice:

$$\mathcal{H}_P = \text{Span} \{ |x, y\rangle_P \mid (x, y) \in \mathbb{Z}^2 \} . \quad (1:20)$$

The coin space is four-dimensional because a single lattice point has 4 immediate neighbors. However, the definition of the coin basis states and the corresponding unit shifts are ambiguous in the literature. It is possible to define the shifts to represent hopping in the diagonal direction, *e.g.* $|x, y\rangle \rightarrow |x+1, y+1\rangle$. The advantage of this approach is that the corresponding step operator has the form of $S \otimes S$, *i.e.* the tensor product of steps of one-dimensional quantum walks. Thus, such definition might allow us to see the single two-dimensional particle as two non-interacting one-dimensional particles, as long as the coin also has a tensor product structure. On the other hand, shifts can represent displacement to the actual nearest neighbor, *e.g.* $|x, y\rangle \rightarrow |x+1, y\rangle$. In this thesis, we will follow this latter approach. Thus, the coin space is defined as:

$$\mathcal{H}_C = \text{Span} \{ |L\rangle, |D\rangle, |U\rangle, |R\rangle \} . \quad (1:21)$$

A single step of the time evolution is given by

$$U = S(I_P \otimes C) , \quad (1:22)$$

where

$$S = \sum_{(x,y) \in \mathbb{Z}^2} \left(|x-1, y, L\rangle \langle x, y, L| + |x, y-1, D\rangle \langle x, y, D| \right. \\ \left. + |x, y+1, U\rangle \langle x, y, U| + |x+1, y, R\rangle \langle x, y, R| \right) , \quad (1:23)$$

and $C \in SU(4)$. We note that 4×4 matrices acting on the coin space will be represented in the $|L\rangle, |D\rangle, |U\rangle, |R\rangle$ basis. The boundary conditions (topology) of the underlying graph are reflected in the displacement operation S , *e.g.* periodic boundary conditions (tori) are considered by taking modulo addition and subtraction operations in Eq. (1:23).

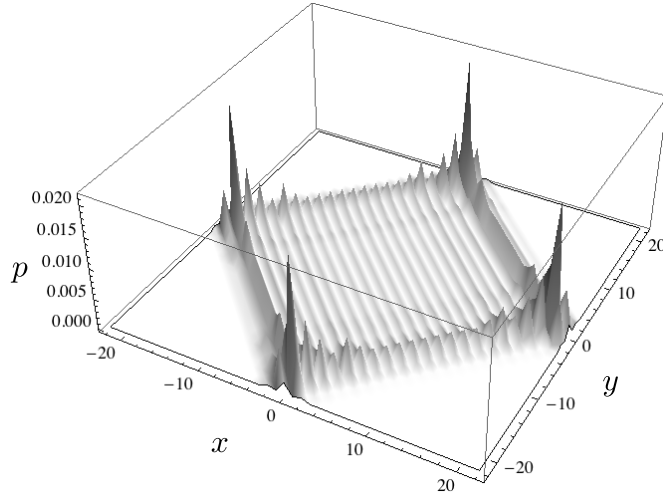


Figure 1:3. Position distribution of the Hadamard walk driven by the coin (1:24) on the Cartesian square lattice after 30 steps. The initial state of the system was $|\psi\rangle = |0,0\rangle_P \otimes (|L\rangle - i|D\rangle - i|U\rangle - |R\rangle)/2$.

Let us show the three most prominent examples of the two-dimensional quantum walks. The first is the walk driven by the 4×4 Hadamard coin, *i.e.*:

$$C_H^{2D} = C_H \otimes C_H = \frac{1}{2} \begin{pmatrix} 1 & -1 & -1 & 1 \\ 1 & 1 & -1 & -1 \\ 1 & -1 & 1 & -1 \\ 1 & 1 & 1 & 1 \end{pmatrix}. \quad (1:24)$$

The key feature of the Hadamard walk is that it is similar to a two-particle one-dimensional quantum walk, its distribution is dominated by four, ballistically moving peaks. We illustrate this walk on FIG. 1:3.

The next is the Fourier walk, driven by a discrete Fourier transform matrix:

$$C_F = \frac{1}{2} \begin{pmatrix} 1 & 1 & 1 & 1 \\ 1 & i & -1 & -i \\ 1 & -1 & 1 & -1 \\ 1 & -i & -1 & i \end{pmatrix}. \quad (1:25)$$

This walk exhibits a slowly propagating central peak. Also, for a family of initial states $|\psi^{\text{Ring}}\rangle = |x_0, y_0\rangle_P \otimes (a|L\rangle + b|D\rangle + a|U\rangle - b|R\rangle)$, (with $|a|^2 + |b|^2 = 1/2$) the central peak vanishes, and a ring like distribution emerges. This walk is illustrated in FIG. 1:4.

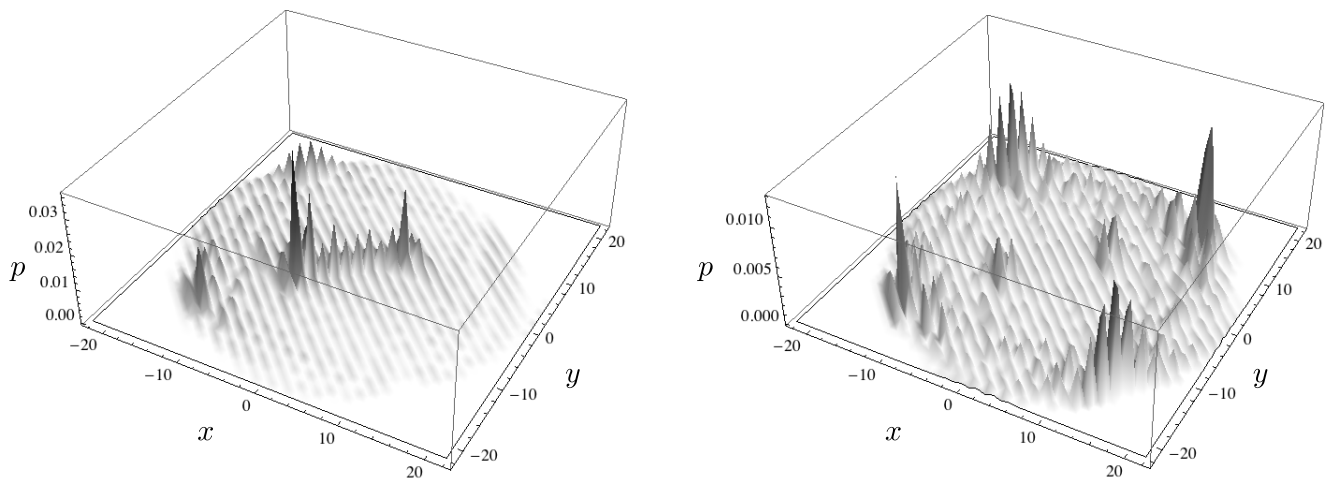


Figure 1:4. Two possible position distributions of the Fourier walk driven by the coin (1:25) on the Cartesian square lattice after 30 steps. The plot on the left shows a typical distribution, which is dominated by a slowly propagating central peak. The initial state of the system was $|\psi\rangle = |0, 0\rangle_P \otimes (|L\rangle + |D\rangle + |U\rangle + |R\rangle) / 2$. The plot on the right shows the ring like distribution we get by using $|\psi\rangle = |0, 0\rangle_P \otimes (|L\rangle + |D\rangle + |U\rangle - |R\rangle) / 2$ as the initial state.

Finally, we show the Grover walk, which is driven by the Grover diffusion operator:

$$C_G = \frac{1}{2} \begin{pmatrix} -1 & 1 & 1 & 1 \\ 1 & -1 & 1 & 1 \\ 1 & 1 & -1 & 1 \\ 1 & 1 & 1 & -1 \end{pmatrix}. \quad (1:26)$$

The Grover walk exhibits some rather interesting behavior. Almost all spatially local initial states remain spatially local (trapped) during the whole time evolution, *i.e.* the probability of finding the particle at the origin never decays to zero. This characteristic phenomenon is called *trapping* or *localization* [80, 81]. However, for a well defined initial state $|\psi^{\text{NT}}\rangle = |x_0, y_0\rangle_P \otimes (|L\rangle - |D\rangle - |U\rangle + |R\rangle) / 2$ this localization type of behavior is avoided; the walk exhibits a ring like distribution. We illustrate this behavior in FIG. 1:5. Furthermore, the Grover walk serves as the basis for several quantum walk based search algorithms [47–53]. We overview one such search algorithm in the next section.

1.1.3. Quantum search

Quantum walks — similarly to classical walks — are suitable for performing and modeling searches on graphs. It is well known in the field of quantum information that the Grover algorithm [159] provides quadratic speedup in terms of oracle queries over any classical algorithms. That corresponds to $O(\sqrt{N})$ expected queries in the quantum case, in contrast to the expected number of $O(N)$ queries for classical algorithms (Turing machines). It is shown in the literature of quantum walks that this quadratic speedup

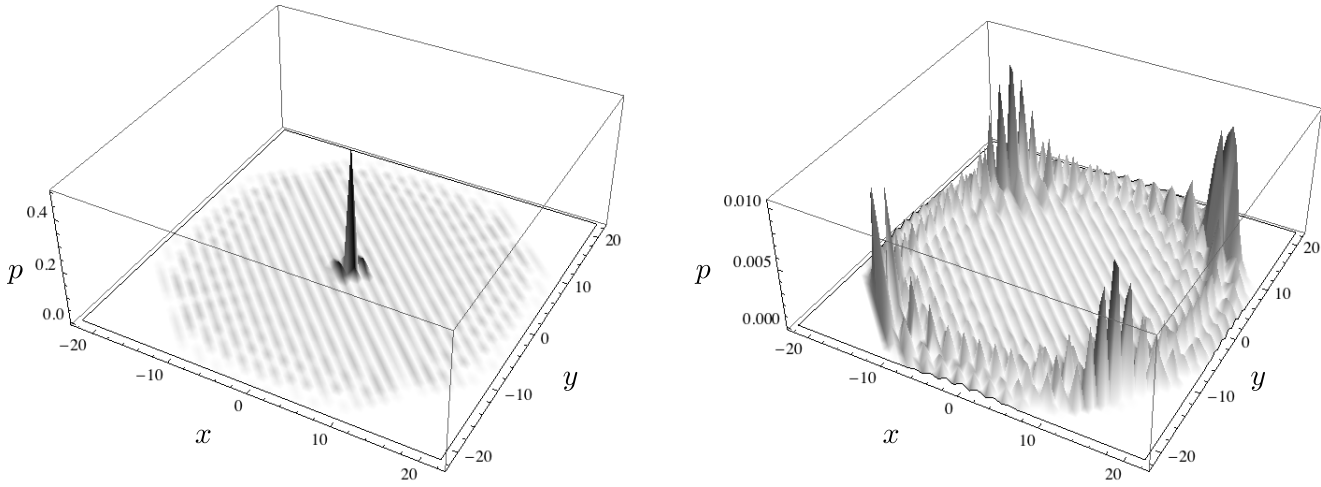


Figure 1:5. A typical position distributions of the Grover walk driven by the coin (1:26) on the Cartesian square lattice after 30 steps. The plot on the left shows the characteristic peak of the trapping phenomena: during the whole time evolution this peak never decays to zero. The initial state for the plot on the left was $|\psi\rangle = |0,0\rangle_P \otimes (|L\rangle + |D\rangle + |U\rangle + |R\rangle)/2$. The plot on the right shows the ring like distribution, which avoids the trapping effect for a single, well-defined initially localized state $|\psi\rangle = |0,0\rangle_P \otimes (|L\rangle - |D\rangle - |U\rangle + |R\rangle)/2$

can be achieved by using a quantum walk model, which translates into finding a marked vertex (or even more marked vertices in a generalized case) on a graph structure [47]. In the discrete time quantum walk model the “mark” on the element is given by a modified coin operator. Here, we briefly review a quantum walk based search performed on a torus [48–50]. We note that this particular algorithm does not provide the full quadratic quantum speedup, instead, it has a $O(\sqrt{N \log N})$ runtime. However, since it uses a simple two-dimensional graph structure, it is rather convenient to use it as an illustration for the quantum walk based searches.

Let us employ the definitions of the two-dimensional discrete time quantum walk model from the previous section. We choose the underlying graph to be a $\sqrt{N} \times \sqrt{N}$ torus, *i.e.* a Cartesian lattice with N sites (database elements) and periodic boundary conditions. The coin operator of the walk is a slightly modified version of the Grover coin:

$$C_S = C_G(\sigma_x \otimes \sigma_x) = \frac{1}{2} \begin{pmatrix} 1 & 1 & 1 & -1 \\ 1 & 1 & -1 & 1 \\ 1 & -1 & 1 & 1 \\ -1 & 1 & 1 & 1 \end{pmatrix}. \quad (1:27)$$

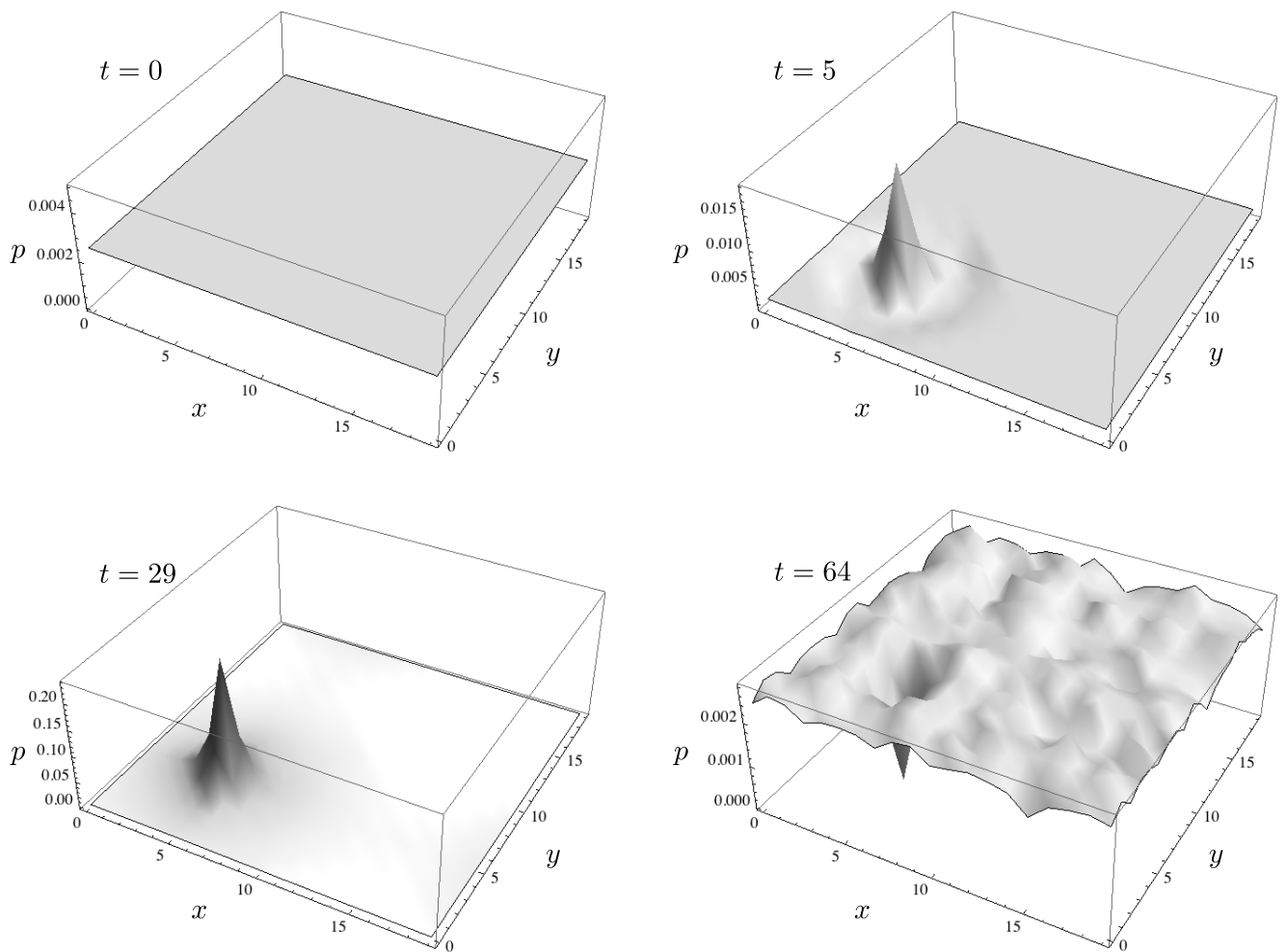


Figure 1:6. Search on a 20×20 ($N = 400$) torus. The plots show the probability distribution at different time steps. The data is illustrated with a joined 3D mesh (texture) to guide the eye. The marked state is the $|5, 5\rangle_P$. At the beginning ($t = 0$) the initial state is a uniform superposition of all states. During the walking process, constructive interference forms at the marked vertex ($t = 5$), and it reaches its peak for the first time at step $t = 29 \approx \sqrt{2N}$. Following that, the peak decreases, and even drops below the probability value of any unmarked peaks, reaching its minimum around $t = 64$.

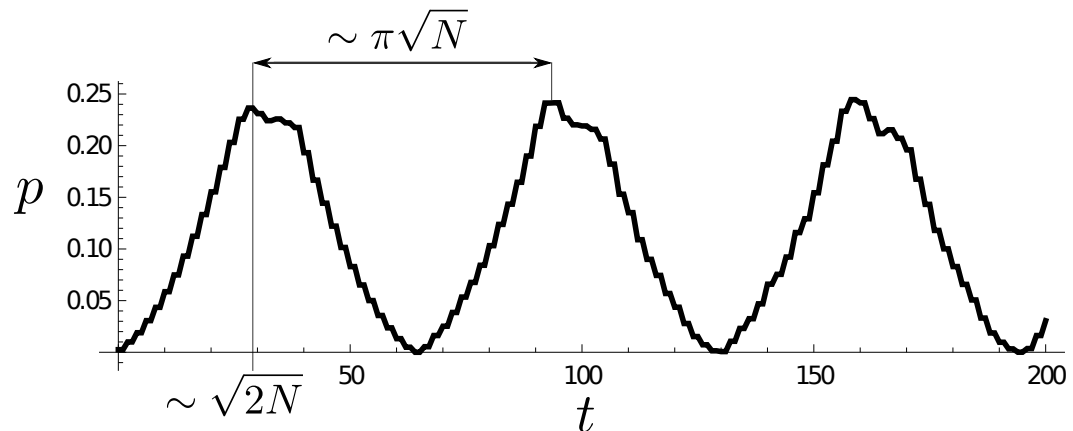


Figure 1:7. The probability of finding the single marked vertex on a 20×20 ($N = 400$) torus. The first peak appears after $\sqrt{2N}$ steps, *i.e.*, that is the optimal time to perform the measurement. The height of the peak is $O(1/\log N)$. The data points are joined to emphasize the periodicity. The length of a period is $\sim \pi\sqrt{N}$ steps.

In search algorithms we mark vertices by using a special coin. In this case the marker coin is

$$C_M = -\sigma_x \otimes \sigma_x = \begin{pmatrix} 0 & 0 & 0 & -1 \\ 0 & 0 & -1 & 0 \\ 0 & -1 & 0 & 0 \\ -1 & 0 & 0 & 0 \end{pmatrix}. \quad (1:28)$$

Thus, the full coin toss operation is given as:

$$\Gamma = \sum_{x \notin M} |x\rangle_P \langle x|_P \otimes C_S + \sum_{x \in M} |x\rangle_P \langle x|_P \otimes C_M, \quad (1:29)$$

where M is the set of marked vertices. Here we consider only a single marked vertex, thus $|M| = 1$. The initial state of the search is:

$$|\psi_S\rangle = \frac{1}{2\sqrt{N}} \sum_{x,y=0}^{\sqrt{N}-1} \sum_{c=\{L,D,U,R\}} |x, y, c\rangle. \quad (1:30)$$

It is proven [49, 50] that after $\sqrt{2N}$ steps the probability of finding the walker at the marked vertex reaches a peak. However, we have to note that the probability of finding the particle at the marked vertex is not high enough. In fact, scales as $O(1/\log N)$ with the number of total elements (vertices). In order to achieve the practically useful probability of $O(1)$ one can employ the amplitude amplification method [160]. Thus, after $O(\sqrt{\log N})$ repetitions the probability of finding the marked vertex is raised to $O(1)$. In summary, the total runtime of the algorithm is $O(\sqrt{N \log N})$. We illustrate this search algorithm in a numerical example in FIG. 1:6 and FIG. 1:7.

1.2. Continuous time quantum walks

In discrete time walks there is a well-defined time instance, when the transition of the particle (hopping) happens instantaneously. However, in some physical processes this transition is not sharp or periodic. For example, only the rate of transitions are known, that is the number of transitions (steps) in a given period of time. In such cases a continuous time description is desirable. For classical walks there is a straightforward connection between the discrete time and the continuous time version. The key is to take the limiting case of the discrete time model by simultaneously going with the number of steps and with the length of steps (in space), to infinity and to zero, respectively. The result is a diffusion process, where, from a single initial δ distribution a Gaussian distribution emerges, which spreads with the square root of time. However, there are two key differences compared to the discrete time version: First, after

even infinitesimally small time the particle will have an exponentially low, but finite probability to “jump” far from its initial position. Second, the positions are not discrete anymore. We note that the method outlined above — taking the simultaneous limit, *i.e.* by going with the number of steps to infinity, and with the length of steps to zero — can be performed on discrete time quantum walks, and will result in a so-called *weak limit* [161–163].

Continuous time quantum walks [31, 34] have a different approach. The simple discrete graph structure is kept, but the transition time is not sharp like in its discrete time counterpart — the time evolution is continuous, not stroboscopic. Let us give the formal definition in the following. The Hilbert space of continuous time quantum walks on a given $G(V, E)$ undirected graph is spanned by vectors corresponding to the vertices of the graph

$$\mathcal{H} = \text{Span} \{ |v\rangle \mid v \in \mathbb{Z} \}, \quad (1:31)$$

i.e. it coincides with the position space of discrete time quantum walks. The time evolution is governed by a Hamiltonian given by its elements as

$$\langle i|H|j\rangle = \begin{cases} -\gamma & \text{if there is an edge between vertices } i \text{ and } j \\ d\gamma & \text{if } i = j \text{ where } d \text{ is the degree of the vertex} \\ 0 & \text{otherwise.} \end{cases} \quad (1:32)$$

Here, $\gamma \in \mathbb{R}$, $\gamma > 0$ is the rate of the continuous time quantum walk. We note that the off-diagonal elements of the Hamiltonian is the adjacency matrix of the graph $G(V, E)$ (up to the rate γ). Also, one can view the Hamiltonian as a discrete Laplacian. The time evolution is given as the formal solution of the time-independent Schrödinger equation, *i.e.* as the exponential of the Hamiltonian:

$$|\psi(t)\rangle = \exp(-iHt) |\psi(0)\rangle. \quad (1:33)$$

We note that similarly to the classical case the walker has a finite, exponentially small probability to appear far from the origin. If we consider a continuous time quantum walk as a cellular automaton by restricting it to discrete time steps, we can see that it breaks the locality in Meyer’s no-go lemma. This non-locality shows that there are some important differences in the definitions of the discrete time and continuous time models. In the discrete time case only the unitary form of the time evolution operator is defined, and the graph structure is encoded through the displacement operator S (see Eq.(1:6)). In the continuous time case, the Hamiltonian reflects the underlying graph structure. Consequently, should one construct any unitaries from such a Hamiltonian, it would contain non-nearest neighbor interactions (jumps). In fact, a similar analogy holds for the discrete time case too: should one deduce

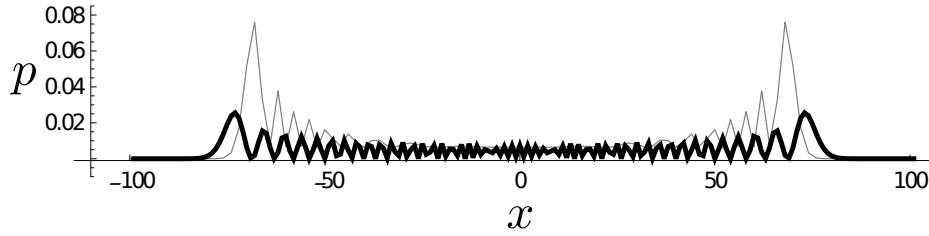


Figure 1:8. Comparison of the position distribution of a continuous time quantum walk (thick line) with a discrete time quantum walk (thin line) on a one-dimensional integer lattice at $t = 100$. Both models exhibit ballistic spreading. We have chosen $\gamma = 0.3827$ as for this rate the variance of the two distributions coincide. For the discrete time model, only the even sites are plotted, because for even number of steps the probabilities at all the odd labeled sites are zero. The plotted data are represented by connected lines to guide the eye, and to emphasize the interference fringes.

a quasi-Hamiltonian from the unitary time evolution operator, one would find that the Hamiltonian contains non-nearest neighbor interactions, too. The resolution of the apparent contradiction is that the exponential “tail” of the wavefunction vanishes due to destructive interference.

Another difference is that the discrete time variant inherently contains the additional coin degree of freedom, whereas continuous time quantum walks are defined without a coin. Connection between discrete time quantum walks and continuous time quantum walks exists, albeit it is non-trivial [164–166].

The continuous time quantum walk model has similar properties as its discrete time counterpart. In fact, it also exhibits ballistic spreading on regular lattices, and is suitable for designing quantum algorithms, *e.g.* searches [167, 168]. For comparison, we illustrate both models on the line in FIG. 1:8. By design, continuous time quantum walks are suitable for modeling transport of single excitations on undirected graphs [39–41, 44]. Also, by adding imaginary terms to the diagonal of the Hamiltonian, sources and absorbers (detectors for a continuous weak measurement) can be added in a straightforward manner [169].

1.3. Scattering quantum walks

Quantum walks naturally represent the spreading of a wave packet on a quantum network. In most of the cases the graph $G(V, E)$ corresponding to a quantum network is viewed as vertices and edges representing the positions where the walker can reside and the possible unitary transitions (movement) between such sites, respectively. However, there is another approach for quantum walks where the role of these two sets are reversed: the so-called *scattering quantum walks* [32, 170, 171]. In this section we briefly review this model.

Given a $G(V, E)$ undirected graph, the Hilbert space of the walk is spanned by:

$$\mathcal{H} = \text{Span} \{ |i, j\rangle \mid i, j \in V \text{ where } (i, j) \in E \}, \quad (1:34)$$

i.e. by pairs of vertices connected with an edge. Note that a single undirected edge connecting two sites a and b gives two basis states: $|a, b\rangle$ and $|b, a\rangle$. That is, an undirected edge is viewed as two directed edges connecting a pair of sites. We note that like in the discrete time quantum walk model, this model breaks the scalarity in Meyer's no-go lemma. The action of a single discrete time evolution step on a state is defined as:

$$U|a, b\rangle = r^{(a,b)}|b, a\rangle + \sum_{c \in V \text{ where } (b,c) \in E} t^{(a,b)(b,c)}|b, c\rangle, \quad (1:35)$$

that is, the particle suffers a backscattering with amplitude $r^{(a,b)}$, and it is scattered forward with amplitudes $t^{(a,b)(b,c)}$. Unitarity is ensured by selecting proper complex r and t coefficients.

The whole process can be understood more clearly using an interferometric analogy. The vertices represent optical multiports while the edges are the paths connecting them. The two quantum basis states corresponding to an (undirected) edge represent the two directions: $|a, b\rangle$ means that a photon propagates towards multiport b , while $|b, a\rangle$ represents a photon flying towards multiport a on the same path. Naturally, these two photons cannot interfere (scatter) with each other. To summarize, the quantum walk process describes a single photon passing through the network of optical multiports. The advantage of this approach is that it can be applied to any undirected graph structure, and even to some special directed ones. Like all quantum walk models, this scattering approach is viable for constructing quantum algorithms [52, 172].

Let us illustrate this model on a one-dimensional integer lattice. The Hilbert space can be given in a simple form

$$\mathcal{H} = \text{Span} \{|i, i+1\rangle, |i+1, i\rangle \mid i \in \mathbb{Z}\}. \quad (1:36)$$

The most straightforward multiport between two neighboring edges is a 50/50 beamsplitter, described by the Hadamard matrix:

$$B = \frac{1}{\sqrt{2}} \begin{pmatrix} 1 & -1 \\ 1 & 1 \end{pmatrix}. \quad (1:37)$$

Thus, the unitary time evolution operator has the form:

$$U = \sum_{i \in \mathbb{Z}} \frac{1}{\sqrt{2}} (|i+1, i+2\rangle\langle i, i+1| + |i+1, i\rangle\langle i, i+1| + |i, i-1\rangle\langle i+1, i| - |i, i+1\rangle\langle i+1, i|). \quad (1:38)$$

We illustrate the probability distribution of this scattering walk example in FIG. 1:9. We note here that on regular graphs the scattering walk is unitarily equivalent with a well constructed discrete time quantum

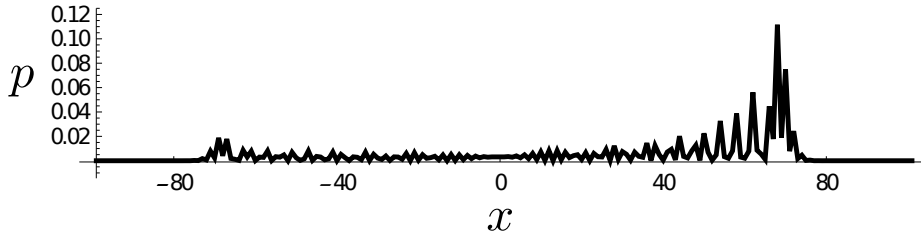


Figure 1:9. The position distribution of a scattering quantum walk on a network of 50/50 beamsplitters, described by the matrix B of Eq. (1:37). The walker took 100 steps and started from the state $|0, 1\rangle$, *i.e.* a photon flying to the right. The data points in the plot are joined with a line to guide the eye and to emphasize the interference fringes.

walk. It is easy to illustrate this equivalence on the current one-dimensional example by relabeling the states as

$$\begin{aligned} |i, i + 1\rangle &\rightarrow |i + 1, R\rangle \\ |i + 1, i\rangle &\rightarrow |i, L\rangle, \end{aligned} \tag{1:39}$$

for all $i \in \mathbb{Z}$ and using the transpose of B as the coin operator: The resulting walk is the one-dimensional discrete time Hadamard walk of Section 1.1.1. One of the major differences between the two approaches is the position measurement process: although in Eq. (1:39) the states of the scattering walk $|i, i + 1\rangle, |i + 1, i\rangle$ represent the same edge, thus the same position, the corresponding discrete time quantum walk states $|i + 1, R\rangle, |i, L\rangle$ are at different position (vertex). Consequently, measuring the edges as positions in the scattering model and measuring the vertices as positions in the discrete time model will produce a different probability distribution, albeit there is a unitary equivalence between them.

1.4. Szegedy's quantum walk

A Markov chain is a discrete time stochastic process without a memory. All Markov chains can be viewed as classical walks. In fact, time invariant Markov chains can be described through stochastic matrices P , whose elements satisfy $\sum_m P_{n,m} = 1$. This matrix can also be viewed as an adjacency matrix of a directed weighted graph, which is the underlying position graph of a classical walker. Then, a single step of time evolution is given by the application of P to the probability distribution (classical state) on the vertices.

The quantization of such classical walks (Markov chains) is not trivial. However, Szegedy provided [33] a robust mathematical construction for quantizing such systems. Such walks are called *Szegedy's quantum walks*. In this thesis we show a simplified way to construct such walks, and we stress that consequently this approach is not as general as the original definition given by Szegedy in [33].

The first idea comes from the construction of discrete time quantum walks: to successfully construct a discrete time (nearest neighbor) unitary process some non-trivial add-ons are needed. In the case of discrete time quantum walks that add-on is the coin space. However, in Szegedy's walk the position space is doubled, thus once again, the scalarity is broken in Meyer's no-go lemma. Secondly, the time evolution somehow resembles the reflection in the Grover search. In fact, the time evolution of Szegedy's walk consists of reflections between these doubled position spaces. Lastly, the position measurement involves tracing out one of the position spaces.

Let us present the definition. The single position space is spanned by the states corresponding to the vertices V of the graph $G(V, E)$ which are from the index set for $P_{n,m}$. Thus the full (doubled) Hilbert space is given by

$$\mathcal{H} = \text{Span} \{ |n, m\rangle \mid n, m \in V \} . \quad (1:40)$$

Note that this Hilbert space can be viewed as the composite Hilbert space of two single particles with state vectors $|n\rangle_1 \otimes |m\rangle_2 = |n, m\rangle$. For better understanding we will use this two-particle picture. To give the time evolution, first we define quantum states that encode the elements of P :

$$|\phi(n)\rangle = \sum_{m \in V} \sqrt{P_{n,m}} |n, m\rangle . \quad (1:41)$$

Next, a reflection is defined on these states

$$F = 2 \sum_{n \in V} |\phi(n)\rangle \langle \phi(n)| - I . \quad (1:42)$$

It is straightforward to see that F is unitary, and its act on the first part (first particle) of the position space is identity:

$$\text{Tr}_2(F) = \sum_{n, n', m} (\langle n, m | F | n', m \rangle) \cdot |n\rangle \langle n'| = I_1 , \quad (1:43)$$

that is, it only affects the second abstract particle. To complete the time evolution, an additional step is needed: a reflection representing a P which acts on the first particle. This can be achieved by swapping the two particles through a generalized swap operation:

$$W = \sum_{m, n} |m, n\rangle \langle n, m| . \quad (1:44)$$

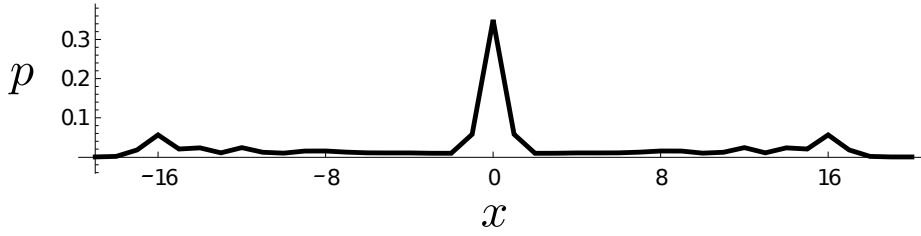


Figure 1:10. The position distribution of Szegedy's walk on the line after 20 steps. The corresponding classical Markov chain is given by a matrix with elements $P_{m,m+1} = P_{m,m} = P_{m,m-1} = 1/3$ for all $m \in \mathbb{Z}$, *i.e.* the walker would step to the left, to the right or stay at its current position with the same probability. The two small outward propagating peaks at sites ± 16 are responsible for the ballistic spreading of the quantum particle. The discrete data points in the plot are connected to guide the eye.

Finally, the complete form of the unitary single step time evolution operator is:

$$U = FW . \quad (1:45)$$

We illustrate this walk in FIG. 1:10.

Szegedy's walk is a very powerful mathematical tool suitable for quantizing general classical Markov chains. In contrast, constructing quantum walks on directed or weighted graphs using the models discussed in the previous sections are not straightforward, and might be possible only with radical changes in their definition. Due to the very general definition Szegedy's walk is a handy mathematical model used mainly in quantum information theory for designing quantum algorithms, and proving their efficiency. Like all other types of quantum walks, Szegedy's walk is also capable of performing a quadratically faster search [33]. However, we note that due to the doubling of the position space, and the rather abstract reflection concept included in the time evolution operator, Szegedy's walk is quite hard to realize experimentally and up to date there are no known experiments focusing on this very model.

1.5. Optical realizations

The optical realization of quantum walks were always appealing, since they consist of a straightforward way to illustrate and construct physical systems (experiments) simulating quantum walks. The most straightforward concept is the optical Galton board [94, 119, 120], which is an interferometric analog of the mechanical Galton board: the spikes are replaced with beamsplitters, and photons propagate instead of balls. A single photon running through the Galton board goes through constant splitting and re-joining *i.e.* self-interference, and in the end it realizes a discrete time quantum walk. The very drawback of using optical Galton boards is that the number of optical elements (beamsplitters) needed scales exponentially

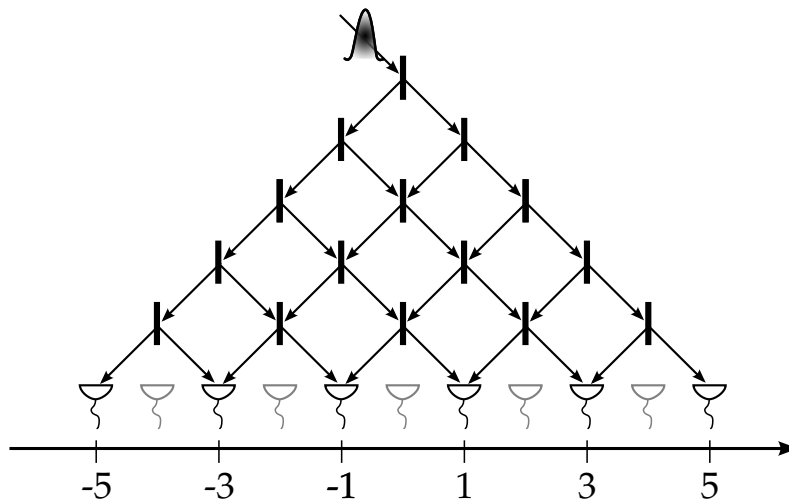


Figure 1:11. The optical Galton board implementation of quantum walks on the line. The thick lines represent beamsplitters. The advantage of this setup is that it is easy to understand, and also it is easy to tune the individual parameters of the walk, *i.e.* the coins (beamsplitters) can be different in space and time. In this scenario the number of steps is fixed — the arrangement in the figure shows a 5 step quantum walk. With the number of steps, the number of needed optical elements (thus, resources) increases exponentially, thus this implementation is not really practical.

with the number of steps the quantum walker takes³. We illustrate this arrangement in FIG. 1:11.

A more promising approach comes from scattering quantum walks (See Section 1.3): a photon propagating through a one-dimensional array of beamsplitters would make a suitable experimental scenario [94], where the number of optical elements only scale linearly with the number of steps. However, here the detection of the photon is not trivial: a possible solution is to weakly couple the photon out from the interferometer at every positions, and detect it there. However, the static outcoupling introduces further uncertainty when it comes to the number of steps taken, the measurement (which disrupts the walk process, since the photon is absorbed) might happen after any number of unitary steps and cannot be fixed like in the Galton board scenario. We illustrate this possible experimental configuration in FIG. 1:12.

Schreiber *et al.* [122] have given an approach, which circumvents the need for more and more optical elements with growing number of steps. Let us shortly review this experimental scenario here. The first idea is that the position of the walker is encoded in the time of arrival of a single photon. That is, a single detector detects the photon and the time of the detection gives the position value of the walker. The coin state of the particle is encoded in the polarization of the photon: vertical polarization corresponds to the coin state $|L\rangle$ and horizontal to $|R\rangle$. First, the photon flies through a half-wave plate which carries out

³ Using exponential physical resources to simulate quantum walks is rather inefficient. Considering finite numerical precision, even just brute-force classical computer simulations would use resources that scales polynomially with the number of steps.

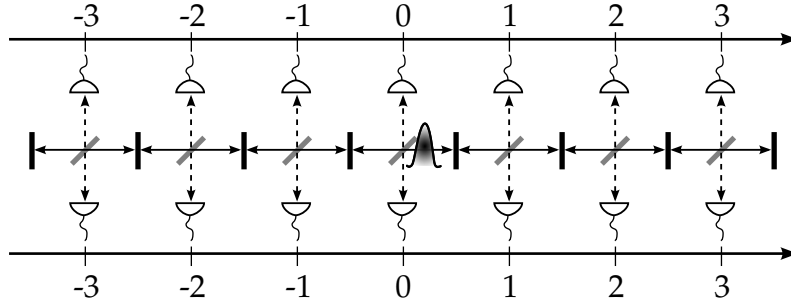


Figure 1:12. The scattering approach to the quantum walk on the line. The photon scatters through a linear system of beamsplitters (thick lines), while other beamsplitters with high transmittivity (gray thick lines) send the photon to detectors. In this arrangement the number of elements needed scales linearly with time. (However, one can consider reflective or periodic boundary conditions, where the number of elements might be kept fixed.) On the other hand, since the detectors are built-in elements of the arrangement and they perform a measurement at every time step, the time the photon spends in the interferometer is also not-fixed, *i.e.* measurement (detection) might happen after any number of steps.

the coin operation

$$C = \begin{pmatrix} \cos 2\theta & \sin 2\theta \\ \sin 2\theta & -\cos 2\theta \end{pmatrix}. \quad (1:46)$$

Here θ is the rotation angle of the half-wave plate relative to one of its optical axes. Next, the photon is split according to its polarization by a polarizing beamsplitter. The vertically polarized part ($|L\rangle_C$) enters a delay loop (a considerably longer optical path) that adds a time-delay, while the horizontal part ($|R\rangle_C$) flies through without the delay. The two parts of the wavefunction are eventually joined by a polarizing beamsplitter. This procedure corresponds to a single step of a quantum walk, where the time-of-arrival of the photon encodes a single step. We illustrate this in FIG. 1:13.

The key idea is that the repetition of a single step can be carried out by feeding back the output of the interferometer to its input. In this way the walker can take several steps without adding more optical elements. The feeding back is actually performed through a beamsplitter: One of the inputs and outputs of the beamsplitter are connected to the single-step interferometer, while the other input is the port where single photons enter the arrangement and the other output port is where the detector is placed. The complete arrangement scheme is given in FIG. 1:14. Like in the scattering example given above, the number of steps taken is not fixed, since the detection (outcoupling through the beamsplitter) is static, *i.e.* no one can guarantee that a photon entering the circuit will take a well defined number of steps before it is measured. This is the very drawback of this experimental setup. The time of detection (the amount of time that a photon spent in the interferometer) naturally corresponds to the number of steps taken through the walk, and on a finer timescale it gives the position of the walker.

The setup is quite flexible as the number of optical elements used are quite low, and it is remarkably

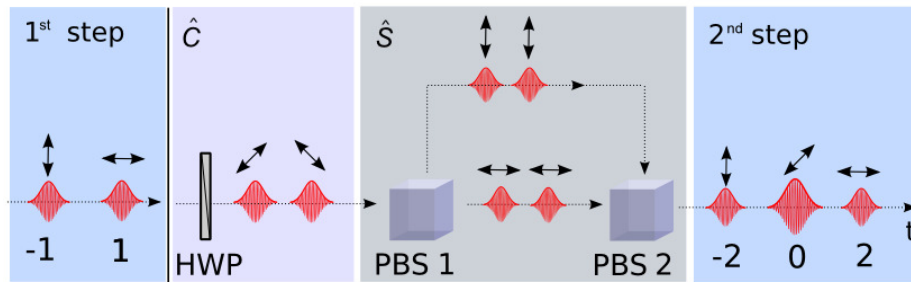


Figure 1:13. A single step of the delay-loop experiment. The superposed photon of the first step arrives from the left: its internal state (polarization) encodes the coins state, while the arrival time encodes the position. First, the half-wave plate realizes a rotation of the polarization, thus a coin operation (See Eq. (1:46)). Next, a polarizing beamsplitter splits the signal and the vertical $|L\rangle_C$ part suffers a delay which corresponds to a step to the left. (Consequently, the non-delayed flight of the horizontal $|R\rangle_C$ part corresponds to a step to the right.) The two parts are joined by a polarizing beamsplitter, and the step is finished. This figure is taken from [122].

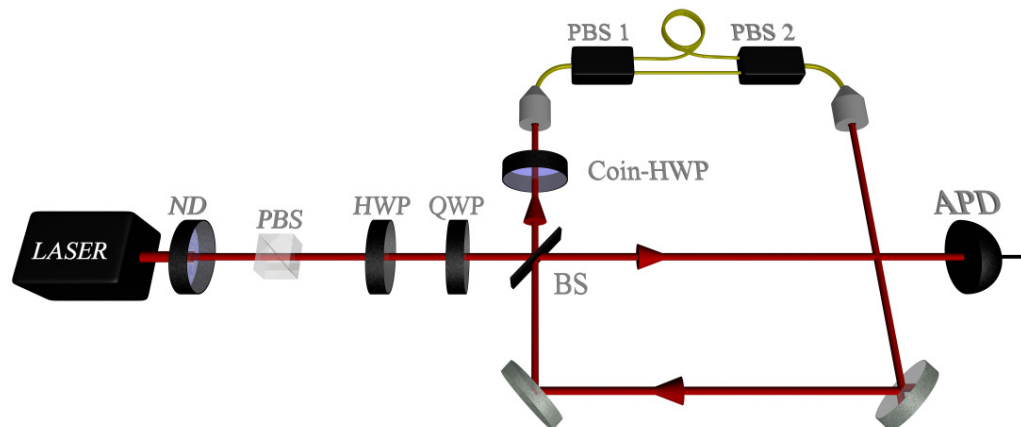


Figure 1:14. The setup of the delay-loop experiment. The pulse-operation laser is attenuated to a single-photon level via a neutral density filter (ND). It is followed by a polarizing beamsplitter (PBS), half-wave plate (HWP) and quarter-wave plate (QWP) which prepare the initial state of the system. The photon enters the quantum walk interferometer through a beamsplitter (BS). Also through the same beamsplitter the photon walking in the interferometer might exit and be detected at the avalanche photodiode (APD). This figure is taken from [122].

easy to change the coin operator. For example, with active optical elements, the coin can be changed throughout the walking process, thus even open quantum walks can be studied with this setup [123]. Also, by adding more delay loops, thus introducing new timescales at the detection, the setup can be extended to simulate higher dimensional walks [124].

Chapter 2

Entropy rates of stochastic processes

2.1. Definition of the entropy rate

It is well known [141] in information theory that the *Shannon entropy*

$$H(X) = - \sum_x p(x = X) \log_2 p(x = X) \quad (2:1)$$

quantifies the average information content of a random variable X . Here, by $p(x = X)$ we denote the probability that X takes the value x . For a sequence of independent and identically distributed (*i.i.d.*) random variables X_i the total information content grows linearly with the addition of new random variables, and equals $n \cdot H(X)$, where n is the total number of random variables. This statement is established by the asymptotic equipartition property. We stress that the Shannon entropy is only applicable for the special sequences satisfying the i.i.d. criteria.

In general, in an indexed sequence of random variables $\mathcal{X} = X_1 \dots, X_n$, — called a *stochastic process* — the random variables are not necessarily identically distributed and independent. In this case the *entropy rate*

$$H(\mathcal{X}) = \lim_{n \rightarrow \infty} \frac{1}{n} H(X_1, X_2, \dots, X_n) \quad (2:2)$$

replaces the entropy in the asymptotic equipartition property. In other words, it describes the average asymptotic information content of a stochastic process *per sample*. Here we note that usually the index of a stochastic process is viewed and referred to as *time*. One can expand the previous formula using the definition of the joint entropy

$$H(\mathcal{X}) = \lim_{n \rightarrow \infty} \frac{1}{n} \sum_{x_1, \dots, x_n} p(x_1 = X_1, \dots, x_n = X_n) \log_2 p(x_1 = X_1, \dots, x_n = X_n). \quad (2:3)$$

In its most general form the entropy rate can be quite hard to determine. However, for special, but still physically relevant cases, the definition can be simplified considerably.

A stochastic process is called *stationary* if any subset of the sequence of random variables it is invariant under time shift, that is

$$p(X_{n_1} = x_1, \dots, X_{n_k} = x_k) = p(X_{n_1+l} = x_1, \dots, X_{n_k+l} = x_k). \quad (2:4)$$

for all k, l -s and $n_1 < n_2 < \dots < n_k$. In physics, such stationary processes typically arise as solutions of time independent differential equations. A quantity related to the entropy rate can be defined as:

$$H'(\mathcal{X}) = \lim_{n \rightarrow \infty} H(X_n | X_{n-1}, \dots, X_1). \quad (2:5)$$

It can be proven for stationary processes [141] that if the latter limit exists, then the limit giving the entropy rate (2:2) also exists and $H'(\mathcal{X}) = H(\mathcal{X})$. Thus, for time stationary processes Eq. (2:5) can be used to compute the entropy rate.

A *Markov chain* is a stochastic process satisfying

$$p(X_{i+1} = x_{i+1} | X_i = x_i) = p(X_{i+1} = x_{i+1} | X_i = x_i, X_{i-1} = x_{i-1}, \dots, X_1 = x_1), \quad (2:6)$$

i.e. the next random variable of the process only depends on the current random variable — the system is memoryless. Since X_{i+1} only depends on the current random variable X_i , we can call it the *state* of the system at time i . The connection between two consecutive states can be described by a transition matrix

$$P_{jk}^{(i)} \equiv p(X_{i+1} = j | X_i = k), \quad (2:7)$$

which is a stochastic matrix by construction

$$\sum_j P_{jk}^{(i)} = \sum_j p(X_{i+1} = j | X_i = k) = 1. \quad (2:8)$$

If a Markov chain is described by a single transition matrix P , it is called *time-homogeneous*.

Let us calculate the partial entropy rate (*i.e.* Eq. (2:2) evaluated for finite n -s)

$$H(n, \mathcal{X}) = \frac{1}{n} H(X_n, \dots, X_1) \quad (2:9)$$

for time-homogeneous Markov chains.

$$\begin{aligned} H(n, \mathcal{X}) &= \frac{1}{n} \left[\sum_{k=2}^n H(X_k | X_{k-1}, \dots, X_1) + H(X_1) \right] = \frac{1}{n} \left[\sum_{k=2}^n H(X_k | X_{k-1}) + H(X_1) \right] \\ &= \frac{n-1}{n} H(X_n | X_{n-1}) + \frac{1}{n} H(X_1). \end{aligned} \quad (2:10)$$

Thus, the entropy rate is given as

$$H(\mathcal{X}) = \lim_{n \rightarrow \infty} H(n, \mathcal{X}) = \lim_{n \rightarrow \infty} H(X_n | X_{n-1}) = \lim_{n \rightarrow \infty} H(X_n | X_{n-1}, \dots, X_1) = H'(\mathcal{X}). \quad (2:11)$$

Hence, if either $H(\mathcal{X})$ or $H'(\mathcal{X})$ exists then the other exists, too. Consequently, one can calculate the entropy rate of time-homogeneous Markov chains by using Eq. (2:5).

A Markov chain is *irreducible* if all states are reached in finite time from any initial states. An irreducible and aperiodic stationary Markov chain has a unique stationary (asymptotic) state:

$$\mu P = \mu. \quad (2:12)$$

Note that in information theory the stochastic matrices are the transpose of the stochastic matrices used in statistical physics, that is the unique stationary distribution is a left eigenvector with eigenvalue one. One can see, that the entropy rate of irreducible time-homogeneous Markov chains can be calculated as

$$H(\mathcal{X}) = \lim_{n \rightarrow \infty} H(X_n | X_{n-1}) = - \sum_{i,j} \mu_i P_{ij} \log_2 P_{ij}. \quad (2:13)$$

In the following we review some basic textbook examples to give a better view on the concept of entropy rate.

2.2. Examples

The first example of the entropy rate is the one leading back to the Shannon entropy. Let us investigate the entropy rate of a stochastic process consisting of a sequence of i.i.d. random variables. In terms of the joint probability distribution: $p(X_1 = x_1, X_2 = x_2, \dots, X_n = x_n) = p(X_1 = x_1)p(X_2 = x_2) \cdots p(X_n = x_n)$. Employing the definition of Eq. (2:2)

$$H(\mathcal{X}) = \lim_{n \rightarrow \infty} \frac{1}{n} H(X_1, X_2, \dots, X_n) = \lim_{n \rightarrow \infty} \sum_n \frac{1}{n} H(X_1) = H(X_1). \quad (2:14)$$

This is where we have started: The entropy growth (entropy rate) of the sequence of i.i.d. random variables per new random variable is constant, and is given by the Shannon entropy of a single random variable.

The next typical textbook example is the random walk on a weighted simple graph. A weight $W_{i,j}$ between vertices i and j is proportional to the probability that the walker passes through it. First, a stochastic matrix must be defined using the weights:

$$P_{ij} = \frac{W_{ij}}{\sum_k W_{ik}}. \quad (2:15)$$

We again note that this matrix is the transpose of the stochastic matrices used in physics. Next, a stationary distribution μ satisfying $\mu P = \mu$ must be determined. We will assume that this distribution

is unique. Then, by using Eq. (2:13) the entropy rate can be calculated.

It is easy to see that in some cases the entropy rate can be calculated in a more straightforward manner using other symmetries of the system. Let us consider the unbiased one-dimensional discrete time classical walk. In this model, from every position, the particle will hop to the left or to the right with probability $1/2$. Since the system is infinite, the method we have described above is not straightforward to follow. However, one can see that the translational invariance of the system helps us: in terms of the stochastic process, it is wiser to encode the differences of subsequent positions (± 1) rather than the actual discrete positions. Exploiting this, we can easily derive the corresponding stochastic matrix

$$P = \frac{1}{2} \begin{pmatrix} 1 & 1 \\ 1 & 1 \end{pmatrix}. \quad (2:16)$$

It is easy to see that this stochastic process has the entropy rate of 1 bit. Alternatively, one could argue that the random drive of an unbiased homogeneous discrete time classical walk is a toss of a fair coin. Consequently the entropy rate of the walk is the same as the coin toss, thus 1 bit.

Chapter 3

Asymptotics of random unitary operations

3.1. Random unitary evolution of quantum Markov chains

Quantum operations represent a versatile approach to describe general time evolution of quantum states living on a Hilbert space \mathcal{H} . That is, they can describe open system time evolution (decoherence, dephasing, decay through environmental noise) and also can include measurements. A common way to mathematically specify a quantum operation $\mathcal{M} : B(\mathcal{H}) \rightarrow B(\mathcal{H})$ is through the so-called Kraus representation:

$$\mathcal{M}(\rho) = \sum_i A_i \rho A_i^\dagger, \quad (3:1)$$

where

$$\sum_i A_i^\dagger A_i \leq I. \quad (3:2)$$

By $B(\mathcal{H})$ we denote the space of bounded operators acting on the Hilbert space \mathcal{H} . Note that such evolution of quantum states happens without any memories, thus it describes a quantum Markov chain: a quantum evolution, where the next state depends only on the previous. These quantum operations are widely used in various fields of quantum information theory, *e.g.* describing quantum communication channels, entanglement witnesses or probabilistic cloning. The most notable property of such operations is the complete positivity, *i.e.* the joined density operator of the system in question with any environment (ancilla) must remain positive under the quantum operation.

A special case of quantum operations is the *random unitary operation (RUO map)* [138–140]. RUO maps describe a norm (trace) preserving open system time evolution: from a set of unitaries some inherently classical random process chooses a single unitary which evolves the system. Since the inherent random nature of the process, the expected outcome is an incoherent mixture of the states corresponding to all possible selections weighted with the probability of choosing the given unitary. Described formally, RUO maps are given as:

$$\mathcal{R}(\rho) = \sum_i p_i U_i \rho U_i^\dagger, \quad (3:3)$$

where $\sum_i p_i = 1$. It is straightforward to see that RUO maps are trace preserving and their Kraus

operators can be defined as $A_i = \sqrt{p_i}U_i$.

RUO maps are quite useful to describe the open evolution of quantum states where some unpredictable classical process is present. For example, one can imagine the random interaction of quantum particles (gas) in a box [138]: the collision of particles is described by a unitary, however the particles suffer frequent and unpredictable collisions. Thus their time evolution is best described by a RUO map.

3.2. Properties and asymptotics of RUO maps

In this section we review the most important properties of, and the asymptotic method for RUO maps [138–140] on which we will later rely. By construction RUO maps incoherently mix different quantum states. When one considers a time evolution driven by a single RUO map, the purity of the quantum state cannot increase. Therefore, the von Neumann entropy of subsequent states cannot decrease. In finite systems the maximally mixed state (which is proportional to the identity operator) represents a lower bound for purity and an upper bound for the von Neumann entropy. Consequently, under the repeated application of a RUO map, asymptotically a set of *isentropic* quantum states is achieved⁴.

Thus, any quantum state ρ_{as} from this set satisfies:

$$S(\rho_{as}) = S(\mathcal{R}(\rho_{as})) , \quad (3:4)$$

where S is the von Neumann entropy. Employing the definition of Eq. (3:3) and also the property that the von Neumann entropy does not change under unitary operations we get, that:

$$\sum p_i S(U_i \rho_{as} U_i^\dagger) = S(\rho_{as}) = S(\mathcal{R}(\rho_{as})) = S\left(\sum_i p_i U_i \rho_{as} U_i^\dagger\right) . \quad (3:5)$$

Let us use the concavity of the von Neumann entropy S ; which says that the entropy of a mixture is greater than or equal to the entropy of the parts:

$$S(p_1 \rho_1 + p_2 \rho_2 + \cdots + p_n \rho_n) \geq p_1 S(\rho_1) + p_2 S(\rho_2) + \cdots + p_n S(\rho_n) . \quad (3:6)$$

Here, equality only holds when all ρ_i -s are the same. Therefore, in Eq. (3:5) all $U_i \rho_{as} U_i^\dagger$ must be equal:

$$U_i \rho_{as} U_i^\dagger = U_j \rho_{as} U_j^\dagger \quad \text{for all } i, j\text{-s} . \quad (3:7)$$

⁴ This entropic argument is already known to be a suitable tool for finding asymptotics of open systems [173].

Consequently, any quantum state ρ_{as} from the set of asymptotic states must evolve unitarily:

$$\mathcal{R}(\rho_{as}) = U_i \rho_{as} U_i^\dagger \quad \text{for all } i\text{-s.} \quad (3:8)$$

The importance of this observation is unquestionable: Unitary time evolutions are normal, *i.e.* they can be diagonalized by unitary operators. We employ this property to determine the asymptotic subspace of RUO maps. We note that, however, the total RUO map \mathcal{R} is usually not normal: $[\mathcal{R}, \mathcal{R}^\dagger] \neq 0$, thus cannot be diagonalized by unitaries.

Let us formally diagonalize the asymptotic subspace. The eigenvectors found during the diagonalization are operators (X) satisfying

$$U_i X U_i^\dagger = \lambda X \quad \text{for all } i\text{-s, with } |\lambda| = 1. \quad (3:9)$$

We call such X operators *attractors*. We note that Eq. (3:9) determines both X and the corresponding λ eigenvalue of unit magnitude⁵. As attractors are eigenvectors in the asymptotic subspace, they also span this space and form an orthonormal basis if they are orthonormalized through the Hilbert-Schmidt scalar product:

$$\text{Tr} \left(X_i X_j^\dagger \right) = \delta_{i,j}. \quad (3:10)$$

We call this asymptotic subspace

$$\mathbf{A} = \text{Span}(\{X_i\}) \quad (3:11)$$

attractor space. We note that there is a trivial attractor which is always available (*i.e.* satisfies (3:9)), that is proportional to identity:

$$Z = \frac{1}{\sqrt{\dim I}} I, \quad (3:12)$$

which is due to the construction of RUO maps: RUO maps are unital. However, this observation has an immediate consequence. All other attractors forming the asymptotic subspace basis X_i are of zero trace

$$\text{Tr} \left(Z X_i^\dagger \right) = \frac{1}{\sqrt{\dim I}} \text{Tr} \left(X_i^\dagger \right) = 0, \quad (3:13)$$

thus are not necessarily valid density matrices. In other words, the convex space of all possible physical asymptotic density operators is a smaller subspace in the linear attractor space.

⁵ All λ eigenvalues in the asymptotic subspace are of unit magnitude, since the asymptotic subspace evolves unitarily (3:8).

Finally, the attractors can be used to give the asymptotic evolution of RUO maps as

$$\rho_{as}(t \gg 1) = \sum_{i, |\lambda|=1} \lambda^t X_i \cdot \text{Tr} \left(\rho(0) X_i^\dagger \right). \quad (3:14)$$

Note that the last equation is simply a reformulation of the projector expansion. We stress that this expression holds true only if attractors X_i form an orthonormal basis according to (3:10). Another interesting property of the last formula is that it is independent of the probabilities p_i forming the RUO map (*cf.* Eq. (3:3)), as long as $0 < p_i < 1$ for all i -s. That is, the asymptotics are determined only by the set of unitaries U_i : The selection of p_i -s merely scales and affects the initial dynamics. We would also like to bring focus on the appearance of the unit magnitude eigenvalues λ in Eq. (3:14): They indicate that the asymptotic dynamics could possibly contain not just stationary states but also periodic and quasi-periodic limit cycles.

In summary, the asymptotic dynamics of RUO maps are determined in the following way: First, one should find the subspace of attractors X_i -s and the corresponding unit magnitude eigenvalues λ using Eq. (3:9). Next, by using the Hilbert-Schmidt scalar product of Eq. (3:10) one constructs an orthonormal basis. Lastly, by employing Eq. (3:14) these attractors can be used to determine asymptotic dynamics of the RUO map with respect to an initial state $\rho(0)$.

3.3. Example

In this section we illustrate RUO maps and the asymptotic method reviewed above through a simplistic example. Our model consists of a pair of spin- $\frac{1}{2}$ particles in magnetic field that are allowed to collide. We assume that due to a β magnetic field in the z direction a single spin undergoes the following rotation during a unit of time:

$$S(\beta) = \exp(-i\beta\sigma_z) = \begin{pmatrix} \exp(-i\beta) & 0 \\ 0 & \exp(i\beta) \end{pmatrix}. \quad (3:15)$$

We assume that the particles are far away from each other (weakly interacting) most of the time, thus they are not coupled to each other. Consequently, their evolution is independent:

$$S_{12} = S(\beta) \otimes S(\beta). \quad (3:16)$$

Now, let us consider the following collision model. We assume that during a unit time step, there is a small probability p , that the two particles will collide, in which case they exchange their quantum states

through a swap operation:

$$C = \begin{pmatrix} 1 & 0 & 0 & 0 \\ 0 & 0 & 1 & 0 \\ 0 & 1 & 0 & 0 \\ 0 & 0 & 0 & 1 \end{pmatrix}. \quad (3:17)$$

We assume that the particles are far from each other most of the time, thus the probability of collision is small, and we neglect the probability that multiple collisions can happen during a unit step of time.

Let us build the RUO of the model using the building blocks given above. First, with probability $1 - p$ the particles evolve without any disturbance

$$U_1 = S_{12} \quad \text{with } p_1 = 1 - p. \quad (3:18)$$

Next, with probability p the particles collide during a unit step of time. That is described by:

$$U_2 = CS_{12} \quad \text{with } p_2 = p. \quad (3:19)$$

We note that the exact time of the collision during a single time step is not important since the swap operation commutes with the magnetic precession unitary, *i.e.*

$$S_{12}^\tau CS_{12}^{(1-\tau)} = CS_{12}. \quad (3:20)$$

Finally, the RUO \mathcal{R} is given by

$$\mathcal{R}(\cdot) = (1 - p)S_{12}(\cdot)S_{12}^\dagger + pCS_{12}(\cdot)S_{12}^\dagger C^\dagger. \quad (3:21)$$

Now, we find the asymptotic dynamics by finding the attractors X and the corresponding eigenvalues of unit magnitude using Eq. (3:9).

Since this is a 4×4 problem it can be explicitly solved by hand without difficulty. The attractors

spanning the asymptotic space \mathbf{A} has the closed form:

$$\left. \begin{aligned} X_1 &= \begin{pmatrix} 1 & 0 & 0 & 0 \\ 0 & 0 & 0 & 0 \\ 0 & 0 & 0 & 0 \\ 0 & 0 & 0 & 0 \end{pmatrix} & X_2 &= \begin{pmatrix} 0 & 0 & 0 & 0 \\ 0 & 0 & 0 & 0 \\ 0 & 0 & 0 & 0 \\ 0 & 0 & 0 & 1 \end{pmatrix} \\ X_3 &= \frac{1}{\sqrt{2}} \begin{pmatrix} 0 & 0 & 0 & 0 \\ 0 & 1 & 0 & 0 \\ 0 & 0 & 1 & 0 \\ 0 & 0 & 0 & 0 \end{pmatrix} & X_4 &= \frac{1}{\sqrt{2}} \begin{pmatrix} 0 & 0 & 0 & 0 \\ 0 & 0 & 1 & 0 \\ 0 & 1 & 0 & 0 \\ 0 & 0 & 0 & 0 \end{pmatrix} \end{aligned} \right\} \text{with } \lambda = 1 \quad (3:22)$$

corresponding to stationary asymptotics;

$$\left. \begin{aligned} Y_1 &= \frac{1}{\sqrt{2}} \begin{pmatrix} 0 & 1 & 1 & 0 \\ 0 & 0 & 0 & 0 \\ 0 & 0 & 0 & 0 \\ 0 & 0 & 0 & 0 \end{pmatrix} & Y_2 &= \frac{1}{\sqrt{2}} \begin{pmatrix} 0 & 0 & 0 & 0 \\ 0 & 0 & 0 & 1 \\ 0 & 0 & 0 & 1 \\ 0 & 0 & 0 & 0 \end{pmatrix} \end{aligned} \right\} \text{with } \lambda = \exp(-2i\beta) \\ \left. \begin{aligned} Y'_1 &= Y_1^\dagger \\ Y'_2 &= Y_2^\dagger \end{aligned} \right\} \text{with } \lambda = \exp(2i\beta) \quad (3:23)$$

and

$$\left. \begin{aligned} Z_1 &= \begin{pmatrix} 0 & 0 & 0 & 1 \\ 0 & 0 & 0 & 0 \\ 0 & 0 & 0 & 0 \\ 0 & 0 & 0 & 0 \end{pmatrix} \end{aligned} \right\} \text{with } \lambda = \exp(-4i\beta) \\ \left. \begin{aligned} Z'_1 &= Z_1^\dagger \end{aligned} \right\} \text{with } \lambda = \exp(4i\beta) \quad (3:24)$$

which are responsible for limit cycles. From these attractors the asymptotics are readily determined via Eq. (3:14).

Let us show the asymptotics for a class of initial states. We prepare a separable state where both of our spins are pointing in the x direction:

$$\rho_0 = \frac{1}{2}(I + a\sigma_x) \otimes \frac{1}{2}(I + b\sigma_x) = \frac{1}{4} \begin{pmatrix} 1 & b & a & ab \\ b & 1 & ab & a \\ a & ab & 1 & b \\ ab & a & b & 1 \end{pmatrix}, \quad (3:25)$$

where $a, b \in [-1..1]$. By employing Eq. (3:14) the asymptotic density operator is readily constructed:

$$\rho_{as}(t \gg 1) = \frac{1}{4} \begin{pmatrix} 1 & \frac{1}{2}(a+b)e^{-2i\beta t} & \frac{1}{2}(a+b)e^{-2i\beta t} & abe^{-4i\beta t} \\ \frac{1}{2}(a+b)e^{2i\beta t} & 1 & ab & \frac{1}{2}(a+b)e^{-2i\beta t} \\ \frac{1}{2}(a+b)e^{2i\beta t} & ab & 1 & \frac{1}{2}(a+b)e^{-2i\beta t} \\ abe^{4i\beta t} & \frac{1}{2}(a+b)e^{2i\beta t} & \frac{1}{2}(a+b)e^{2i\beta t} & 1 \end{pmatrix}. \quad (3:26)$$

Note that the magnetic precession can still be observed on the off-diagonal elements of the density operator despite the decoherence effect of collisions — thus, the asymptotic state of the spins has a limit cycle, controlled by the external magnetic field.

These small discrete time weakly interacting systems are important models used for studying the thermalization and other thermodynamical phenomena and quantities in quantum mechanical systems [174, 175]. The asymptotic method reviewed here is particularly suitable for such studies. We will also see later in this thesis that this approach is also very fruitful in percolation quantum walks.

Chapter 4

Walks on percolation graphs

4.1. Definition and some properties of percolation graphs

The word *percolation* usually refers to the movement of fluid through a porous material. A common way to describe this motion is by a random walk on a graph with randomly broken connections, that is missing edges or vertices [128, 129]. Such graphs are called percolation graphs. There are two major approaches to the description of a percolation graph. According to the first approach, all edges have the identical $1 - p$ probability to be broken independently from each other, where broken means, that they are missing (erased) from the graph $G(V, E)$. This model is called bond (edge) percolation since the imperfectness affects the edges. In the second approach the graph vertices can be missing with the same $1 - p$ probability, independently from each other. Naturally, when a vertex of a graph is erased all connecting edges are also erased. This approach is called site percolation. Both the bond and site percolation are useful for modeling natural processes, *e.g.* the filtering of liquids, cracks in wood, and even the robustness of man-made infrastructure — computer and electrical networks.

One of the most interesting properties of percolation graphs is the phase transition they can exhibit: Someone can ask the question whether in an infinite graph or lattice an infinite cluster (connected component) exists. The probability of the occurrence of such a cluster is either 0 or 1 due to Kolmogorov's zero-one law. It is straightforward to see that the existence of the cluster depends on the value of p . Under a critical p_c the probability of an infinite cluster is zero, while above the critical threshold the probability jumps to one. We illustrate this property on FIG. 4:1. Determining the critical probability is quite hard mathematically, even for very simple regular lattices — most of the known results up to date are numerical. To give an example, the bond percolation threshold for a square lattice is exactly $1/2$, however the exact value of the site percolation threshold is yet to be found analytically: its approximate value is $p_c \approx 0.5927$ [176, 177].

The mathematical properties of percolation graphs are strongly connected with the behavior of walks on them. For example the probability of a walker passing through an infinite percolation graph (thus actually performing percolation) corresponds to the probability of the existence of an infinite cluster. Moreover, discrete time walkers provide a natural time scale — the duration of a unit step — which allows one to consider a dynamically changing percolation graph. In this case the probability p describes the probability that an edge (vertex) is present on the graph during unit time step. Before (or after) every single step of the walker, one randomly draws a new percolation graph (a new configuration of the

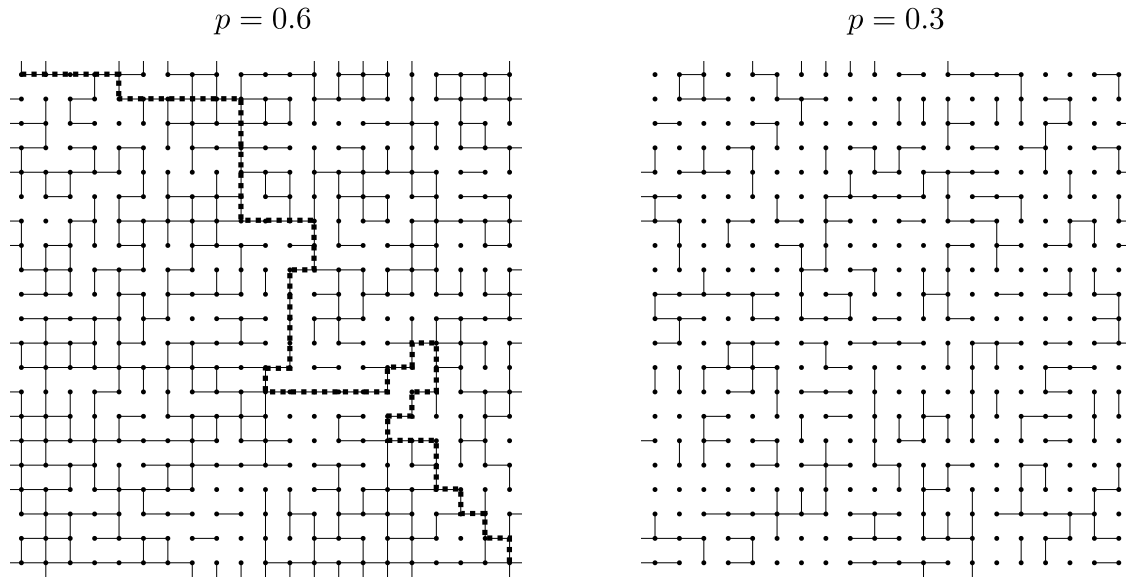


Figure 4:1. Two bond percolation square lattices. The plot on the left shows a lattice where the probability of each edge being present is identical, independent from each other and its value is $p = 0.6$. The plot on the right shows a lattice where this probability is $p = 0.3$. In square lattices the critical bond percolation threshold is $p_c = 0.5$, *i.e.* above this threshold the probability of finding an infinite connected cluster is 1, while below the threshold, this probability is zero. We illustrate this property by showing that on the plot on the left there is a path connecting the upper left corner with the lower right corner, whereas on the plot on the right there is no path between them.

edges). This generalized approach is called *dynamical percolation* [130].

4.2. Overview of quantum walks on percolation graphs

Classical walks on percolation graphs are suitable for modeling systems where random errors affect the classical transport. On the other hand, transport can follow the rules of quantum mechanics. In this case quantum walks on percolation graphs might give a suitable description. Since quantum walks have an inherently deterministic nature, the effect of the random percolation inevitably disturbs the coherence of the walker. Moreover, even just to describe quantum walks on percolation graphs is rather non-trivial. In this section we briefly review the most influential works from the literature of quantum walks on percolation graphs.

The first work on quantum walks on graphs with percolation is, to our knowledge, by Romanelli *et al.* [131]. The authors investigated the one-dimensional discrete time Hadamard quantum walk (see Section 1.1.1) on the line under the decoherence effect of dynamical percolation — which they call *broken links*. Their model has a single parameter corresponding to errors of the graph: p , which is the probability that a link between any two adjacent sites is missing during a unit time step. In this model the time evolution

is kept unitary:

$$U(t) = U_{\mathcal{K}}^{(t)} U_{\mathcal{K}}^{(t-1)} \dots U_{\mathcal{K}}^{(1)}, \quad (4:1)$$

with

$$U_{\mathcal{K}} = S_{\mathcal{K}} \cdot (I_P \otimes C) \quad (4:2)$$

where $S_{\mathcal{K}}$ is the step operator on the percolation line, *i.e.* it realizes a step for a concrete configuration $\mathcal{K} \subseteq E$ of the edges. An important question is to define $S_{\mathcal{K}}$ unitarily. The authors have given

$$\begin{aligned} S_{\mathcal{K}} = & \sum_{(x,x+1) \in \mathcal{K}} |x+1, R\rangle\langle x, R| + \sum_{(x,x-1) \in \mathcal{K}} |x-1, L\rangle\langle x, L| + \\ & \sum_{(x,x+1) \notin \mathcal{K}} |x, L\rangle\langle x, R| + \sum_{(x,x-1) \notin \mathcal{K}} |x, R\rangle\langle x, L|. \end{aligned} \quad (4:3)$$

that is, the walker facing a broken edge (*i.e.* not in \mathcal{K}) has its internal coin state reflected without changing position. Although between steps the configuration of the underlying graph might change, statistical averaging is not defined in the model, thus, the effect of broken links is considered as a unitary noise. The question the authors have addressed was how the dynamically changing graph affects the variance (spreading) of the quantum walk. They found numerically that a transition between the two-peaked quantum (ballistically spreading) and classical (diffusively spreading) Gaussian distributions happens after a critical number of steps, which can be expressed as

$$t_c = \frac{1}{p\sqrt{2}}. \quad (4:4)$$

A simple argument behind this result can be given as follows: At the beginning, the wave-function is confined to a small region. Consequently, it is not disturbed by the dynamical percolation of the graph, thus, the walk can spread ballistically. At time t , the walk covers $t/\sqrt{2}$ sites, and about $pt/\sqrt{2}$ links are broken in that area. As the proportion of broken links grows to the order of 1, the disturbance becomes relevant, and the quantum walk will lose its quadratic speedup, reverting to the classical diffusive spreading. This behavior is illustrated in FIG. 4:2. The diffusion coefficient is estimated to be $D \simeq 0.4 \frac{(1-p)}{p}$ by linear regression. The authors also determined a critical value for p which is approximately 0.44, when the diffusion coefficient is 1/2, which corresponds to that of the classical unbiased random walk.

The two-dimensional extension of the above dynamical percolation model was first considered by Oliveira *et al.* [132]. The two-dimensional Hadamard, Grover and Fourier walks (*cf.* Section 1.1.2) were

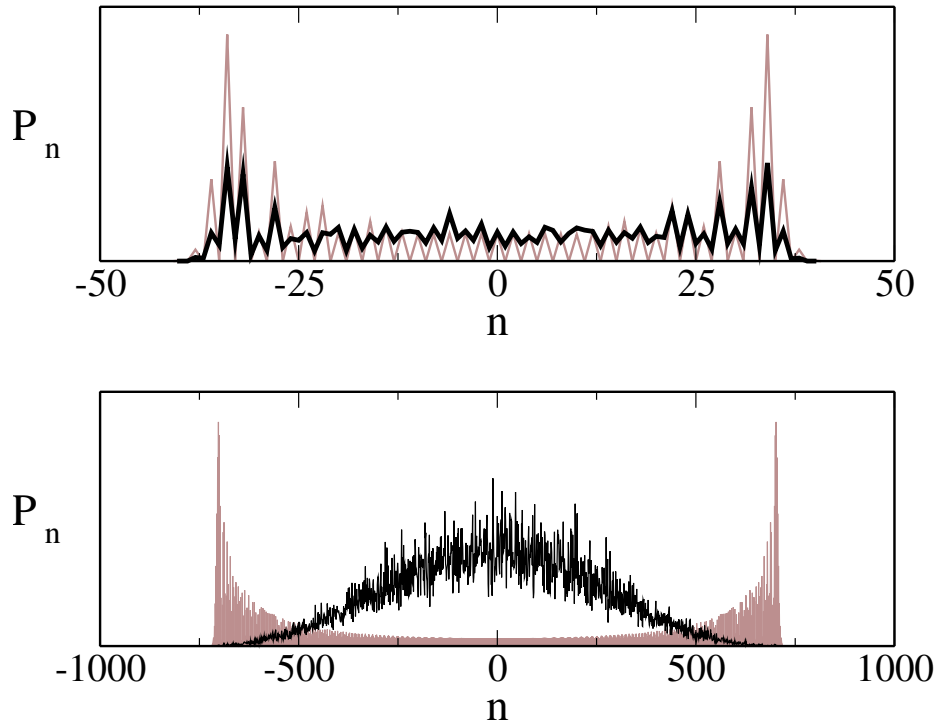


Figure 4:2. Dynamical percolation as unitary noise in a one-dimensional quantum walk. The position distribution P_n of a quantum walk on the percolation line is shown, for $p = 0.01$ (which is the probability that a given edge is missing) at two different time instances. For small number of steps, the walk is only slightly affected by the decoherence effect of the percolation, albeit the spreading is still ballistic at $t = 50$, as seen in the upper plot. After the critical number of steps [see Eq.(4:4)], the decoherence becomes significant and the walker spreads diffusively, exhibiting a Gaussian distribution as illustrated in the lower plot which corresponds to $t = 1000$. The distributions corresponding to the undisturbed (unitary) case of $p = 0$ are shown in the background. This figure is taken from [131].

studied in terms of the diffusion coefficient. The authors showed that if the percolation probabilities can be tuned independently on the diagonal line, the walker can become confined to that one-dimensional region. This confinement can lead to increased coherence (and thus, ballistic spreading). Hence, at the extreme cases of low $p \ll 1$ and high $p \approx 1$ the system behaves as a ballistically spreading coherent wave, whereas in the regime in-between the decoherence is significant and the walk is diffusive.

Abal *et al.* [133] investigated the one-dimensional infinite line with broken links using a single-parameter coin class

$$U_C = \begin{pmatrix} \cos \theta & \sin \theta \\ \sin \theta & -\cos \theta \end{pmatrix} \quad (4:5)$$

They have introduced a translation-invariant type of the dynamical percolation: With probability p^2 the walker stays, with probability $(1-p)p$ the walker is not displaced to the left (or to the right). Finally, with probability $(1-p)^2$, the walker is free to move (performs an undisturbed step). The translational invariance allowed the authors to use Fourier transformation to analyze the system. The dependence of

the diffusion coefficient on the parameter of the coin was determined numerically.

In the work of Leung *et al.*, [134] the one-dimensional lattice with dynamically broken links is investigated using the statistical mixture of the unitary trajectories.

$$\rho(t) = \sum_{\mathcal{K} \in E} p_{\mathcal{K}} U_{\mathcal{K}}^t \rho(0) \left(U_{\mathcal{K}}^\dagger \right)^t \quad (4:6)$$

Their results about the one-dimensional system agree with the results of Romanelli *et al* reviewed above. Furthermore, they claimed that the transition from ballistic to diffusive motion happens slowly in certain cases, thus the quantum speedup could still be exploited for small number of steps. For larger systems they found that the spreading is diffusive. However, the pre-factor of the spreading of the quantum walk can be still higher than its classical counterpart, *i.e.* its motion is diffusive but faster. The authors also studied the effect of random phases on spreading. In the same work the Grover walk on a two-dimensional Cartesian lattice (*cf.* Section 1.1.2) with static bond and the site percolation was analyzed using the same statistical mixing as in (4:6). The authors numerically determined the spreading (variance) of the system. Their results show that below the critical bond (site) percolation threshold $p \approx 0.5$ ($p \approx 0.6$) the quantum walk — like a classical walk — can not spread. However, above the threshold the spreading of the system shows a fractional scaling, *i.e.* sub-diffusive motion. This is illustrated on Fig. 4:3. In the limit when small number of links are broken the quantum walk surpasses the classical diffusive spreading and exhibits sub-ballistic fractional spreading. The authors employed mostly numerical simulations to obtain their results. We note that since the number of configurations grows exponentially in Eq. (4:6) these simulations become exponentially hard to compute.

In a related article Lovett *et al.* [135] numerically investigated percolation graphs as a factor affecting the efficiency of a quantum walk based search (*cf.* Section 1.1.3) on two- and three-dimensional lattices. They found that below the percolation threshold the search fails naturally, since with high probability the graph is not connected. Consequently, the probability amplitude cannot be concentrated (interfere constructively) on the marked vertices. However, the authors found that just above the critical percolation threshold the walk exhibits the speed, $\mathcal{O}(N)$, of a classical search. The reason behind this effect is that in the percolation graph with parameter around the percolation threshold the remaining connected structure resembles a one-dimensional graph. Furthermore, above this regime the speed of search rapidly converges to the quantum value⁶. Surprisingly, the quantum scaling is reached around $p = 0.7$ — where p is the probability of an edge being in the graph.

Marquezino *et al.* [136] investigated discrete time quantum walk on an n -dimensional hypercube. The

⁶ The quantum walk based search needs $\mathcal{O}(\sqrt{N \log N})$ oracle queries in two-dimensions, and $\mathcal{O}(\sqrt{N})$ queries in three or more dimensions [47–50].

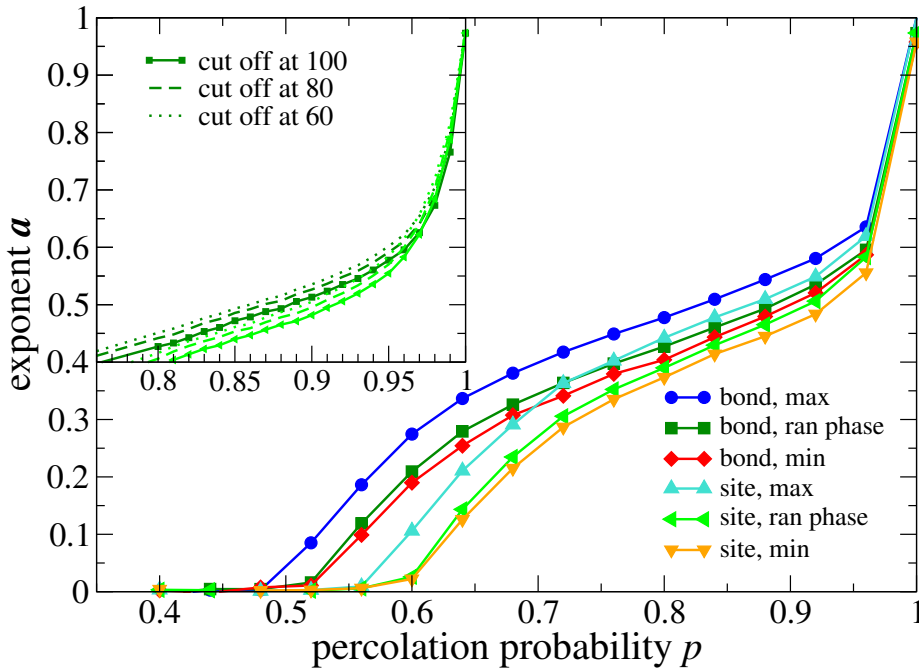


Figure 4.3: Fractional scaling exponent α for two-dimensional percolation lattices derived from numerical data for $t = 100$ to 140 steps. The inset shows more detail for $0.8 < p < 1.0$ in case of random phases, and using different lower cut-off-s. This figure is taken from [134].

average limiting distribution

$$\pi(x) = \lim_{T \rightarrow \infty} \frac{1}{T} \sum_{t=0}^{T-1} P(x, t),$$

was considered in their work, where $P(x, t)$ is the position distribution of the walk at time t . The authors employed the dynamical percolation (broken links) as a type of unitary noise — *i.e.* no averaging over different percolation lattices was performed (*cf.* Eq. (4:1)). In the unperturbed ($p = 0$, no broken links) Grover operator driven case the average limiting distribution is not necessarily uniform. It depends on the initial state. However, in the percolation case even a small noise will cause the system to reach the uniform limiting position distribution. The authors used mixing time to characterize the speed of convergence. They found that it depends on the probability p , and the numerical results imply that the fastest mixing happens around $p_c \approx 0.1$. Consequently, even a small decoherence can aid the mixing procedure.

In continuous time quantum walks (CTQWs), the static percolation (where the disorder does not change through the evolution) was considered in the works of Mülken *et al.* [40, 41] and Anishchenko *et al.* [44]. Also, the case of dynamical percolation with CTQWs has been studied by Darázs *et al.* [137]. The authors showed that the dynamical percolation acts as a rescaling of time evolution when the changes occur with a high enough frequency. The return probability was also investigated in detail. It is shown

that although the system suffers a strong decoherence due to the rapid changes of the underlying lattice, the return probability still shows an oscillatory behavior in time, which is a characteristic property of the undisturbed quantum evolution.

Part II

Chapter 5

Asymptotics of quantum walks on percolation graphs

Discrete time quantum walks (*cf.* Section 1.1) obey unitary dynamics by design. Thus, they are closed quantum systems. Percolation (See Chapter 4), that is the removal of edges from the underlying graph controlled by some classically random process, naturally makes this time evolution open. Recently, these kind of systems gained some interest (See Sec. 4.2), but most actual results are either numerical or phenomenological, mostly due to the “size” of the problem: A quantum walk spread on a bigger graph means a bigger territory for percolation, and the number of actual percolation graphs (configurations) grows exponentially with the size of the graph. Thus, even purely numerical results are hard to obtain due to the required computational power.

This section is devoted to study general discrete quantum walks on finite graphs (lattices) under the decoherence effects of dynamical percolation. Employing the asymptotic theory of RUO maps (*cf.* Chapter 3) we present a method for finding the asymptotics of such open walks, which is based on separation of time evolution. We also show that on regular graphs the superoperator corresponding to the open system evolution can be constructed using polynomial resources.

This chapter is organized as follows: First, in section 5.1 we define the model of discrete time quantum walks on percolation graphs. Next, we formally solve the asymptotics of this model and also reveal a polynomial construction that aids the numerical studies. In section 5.3 we present a general analytical method for obtaining the asymptotics. Following that, we show that on regular lattices the presented method becomes considerably simpler. Finally, we draw some conclusions.

5.1. Definitions

We repeat (see section 1.1) that discrete time (coined) quantum walks are described on a composite Hilbert space

$$\mathcal{H} = \mathcal{H}_P \otimes \mathcal{H}_C, \tag{5:1}$$

where \mathcal{H}_P is the position space corresponding to the vertices of some underlying graph or lattice $G(V, E)$, whereas \mathcal{H}_C is the coin space corresponding to the directions of nearest neighbor hops. The single step of the closed time evolution is given by a unitary operation (See Eq. (1:7)) which corresponds to two essential phases. First, the internal coin degree of freedom of the particle is rotated unitarily — this corresponds to the coin toss. Second, according to this coin state, the particle is coherently shifted to its

new position.

Suppose that due to some errors in the hopping mechanism the particle cannot pass through an edge during a unit time interval (discrete step). We consider such an edge *broken* during that unit time step. Naturally, otherwise the particle is free to pass through the same edge. We call such an edge *perfect*. We assign a probability p_ℓ to each edge $\ell \in E$ of the graph representing the probability of the edge being perfect during a unit time step. In this way $1 - p_\ell$ is the probability of the edge being broken during the same unit time step. We assume that all these events are independent. A natural way to describe a system with such imperfections is to introduce dynamical percolation into the underlying graph: Before every discrete time step we choose an edge configuration $\mathcal{K} \subseteq E$ randomly (according to the probabilities p_ℓ), which describes the failures in the hopping mechanism. Broken edges are simply missing from the percolation graph, *i.e.* they are not in configuration \mathcal{K} .

We now give the time evolution of such systems. Through the dynamical percolation (randomly changing edge configuration) classical randomness enters the model. Thus, we describe the state of the system using density operator formalism. A unit step of the stochastic time evolution reflects our lack of knowledge about the actual (random) edge configuration \mathcal{K} , that is a unit step is an incoherent mixture of different coherent time evolutions:

$$\rho(n+1) = \sum_{\mathcal{K}} \pi_{\mathcal{K}} U_{\mathcal{K}} \rho(n) U_{\mathcal{K}}^\dagger \equiv \Phi(\rho(n)), \quad (5:2)$$

where Φ is a linear *superoperator*. $\pi_{\mathcal{K}}$ represents the probability that a given edge configuration \mathcal{K} occurs:

$$\pi_{\mathcal{K}} = \left\{ \prod_{\ell \in \mathcal{K}} p_\ell \right\} \left\{ \prod_{\ell \notin \mathcal{K}} (1 - p_\ell) \right\}. \quad (5:3)$$

By $U_{\mathcal{K}}$ we denote the unitary time evolution operator of the QW on the percolation graph with configuration \mathcal{K} . The superoperator Φ by construction belongs to the class of random unitary operations — RUO maps (See Chapter 3).

We define the unitary $U_{\mathcal{K}}$, that depends on the configuration $\mathcal{K} \subseteq E$, in the following. Whenever the particle faces a broken (missing) edge, which it cannot pass, it stays at its current place, but suffers a reflection in its internal coin degree of freedom. We describe this reflection by an off-diagonal unitary matrix R . Naturally, the walker can pass through a perfect edge like in the case of the time evolution of a closed system. The formal mathematical definition is given as:

$$U_{\mathcal{K}} = S_{\mathcal{K}}(I_P \otimes C), \quad (5:4)$$

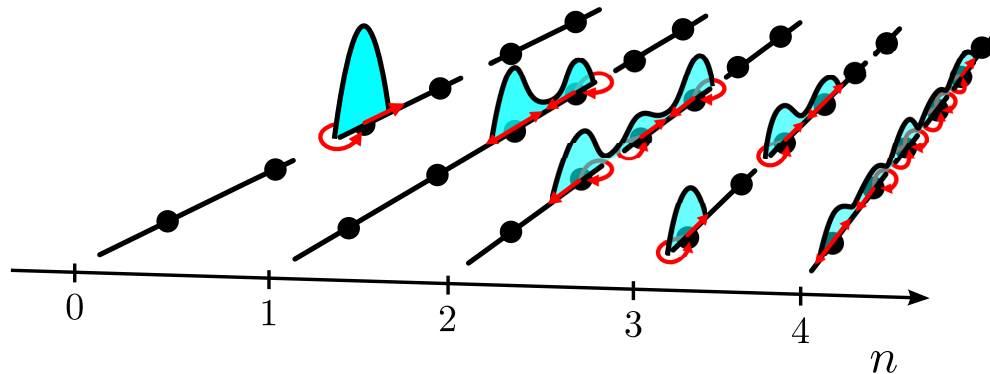


Figure 5:1. Illustration of a discrete time quantum walk on a one-dimensional graph with dynamical percolation. In the figure we show a single possible unitary trajectory of the system — time is labeled by n . The quantum state of the walk is pure in every step. We stress that the lack of knowledge about the actual edge configuration (percolation graph) makes the system open, so the time evolution is not unitary. The arrows show the directions where the wave packet can spread (hop) in the next step, while the loops correspond to the case when the wave packet cannot pass through a missing (broken) edge — as a consequence its internal coin degree of freedom will suffer a reflection.

where

$$S_{\mathcal{K}} = \sum_{(x,x\oplus c)\in\mathcal{K}} |x\oplus c\rangle_P \langle x|_P \otimes |c\rangle_C \langle c|_C + \sum_{(x,x\oplus c)\notin\mathcal{K}} |x\rangle_P \langle x|_P \otimes |c\rangle_C \langle c|_C R, \quad (5:5)$$

is the step operator on configuration $\mathcal{K} \subseteq E$. The first term describes the coin dependent shift (hopping) when the edge is perfect (*cf.* Eq. (1:6)): with $x \oplus c$ we denote the nearest neighbor of x in the direction c . The second term corresponds to the case when the actual edge is broken: the internal coin degree of freedom suffers a reflection by operator R but the particle stays at its current place. C denotes the unitary coin operator. We note that in equation (5:4) operator $I_P \otimes C$ is spatially homogeneous, but $S_{\mathcal{K}}$ breaks any translational invariance. We illustrate a single unitary trajectory of this system in FIG. 5:1.

To summarize, the discrete evolution of the quantum walker on a dynamical percolation graph is described by repeated application of the single step Φ of Eq. (5:2). After the n -th step the walker, that was initially at the state ρ_0 , will be found in

$$\rho(n) = \Phi^n(\rho_0). \quad (5:6)$$

In the following we give the formal solution for the asymptotics.

5.2. Formal solution and a polynomial construction

Both the unitary and the percolative coined quantum walks can be viewed as repeated iterations of one single step. In the case of the percolative quantum walk, there is a random choice of broken

edges in each step. For such an open system, each step can be different in a certain realization of the process, nevertheless statistically speaking one can view the process as an iteration of the same step on the density operator of the system. This fact is expressed by the repeated application of the time-independent superoperator introduced in the previous section. The analysis of the dynamics for a percolative quantum walk is in general more involving than the analysis of the corresponding unperturbed unitary walk. In the latter case, the discrete evolution can be described by the iteration of a single unitary operator. There are two advantages of having a unitary generator at hand. First, it can be diagonalized and, second, we can always choose an orthonormal basis formed by its eigenvectors. In contrast, for the open system we have a generator Φ like Equation (5:2), a superoperator acting on density operators. Such a superoperator is not necessarily normal, *i.e.* it does not commute with its adjoint operator, therefore one may not be able to simply diagonalize it in some orthonormal basis. However, one can still find the solution for the asymptotic behaviour of an iterated random unitary dynamics. The theoretical background is reviewed in Chapter 3.

The key aspect is to find the attractor space \mathbf{A} (See Eq. (3:11)) which is spanned by attractors $X_{\lambda,i}$ (*cf.* Eq. (3:9)) satisfying

$$U_{\mathcal{K}}X_{\lambda,i} = \lambda X_{\lambda,i}U_{\mathcal{K}} \quad \forall \mathcal{K} \subseteq E, \quad |\lambda| = 1. \quad (5:7)$$

Then, the asymptotic dynamics can be readily determined with the help of the following formula (*cf.* Eq.(3:14))

$$\rho_{as}(n) = \Phi^n(\rho_0) = \sum_{|\lambda|=1,i} \lambda^n X_{\lambda,i} \cdot \text{Tr} \left(\rho_0 X_{\lambda,i}^\dagger \right) \quad \text{for } n \gg 1. \quad (5:8)$$

Here the phases of the λ eigenvalues of unit magnitude are responsible for the appearance of asymptotic dynamics which can be stationary asymptotics, periodic or quasi-periodic limit cycles. We note that in order for the latter formula to hold true, the orthonormality of attractors (*cf.* Eq.(3:10)) is needed:

$$\text{Tr} \left(X_{\lambda,i} X_{\lambda',j}^\dagger \right) = \delta_{\lambda,\lambda'} \delta_{i,j}. \quad (5:9)$$

It is important to stress that the attractors given in Eq. (5:7) do not depend on the probability distribution $\{\pi_{\mathcal{K}}\}$, thus, the asymptotic behavior of dynamics of Eq. (5:8) generated by RUO maps is insensitive to the actual p_ℓ probabilities of errors, except in the extremal cases when some $p_\ell = 1$ or 0. As we discussed in Chapter 4 in percolative systems sometimes there exists a critical value for the probability, at which a phase transition occurs in the system. Here, a direct consequence of the insensitivity of the asymptotic dynamics to the particular value of the parameter is that the asymptotic dynamics cannot

reflect signatures of such a phase transitions.

Although the solution is formally given, determining the attractor space matrices through Eq. (5:7) is a hard task. In fact, the number of configurations \mathcal{K} depends exponentially on the number of edges $|E|$, which is on regular lattices, proportional to the number of vertices $N \equiv |V|$. This last number is usually called the *size* of the system. This exponential dependence makes brute force numerical studies inefficient for larger systems. Moreover, the construction of Φ superoperator that we need to study the exact short time dynamics also requires resources that scale exponentially with the size of the system. However, we show that for regular graphs the problem of finding a numerical solution can be handled using only polynomial many resources. We rewrite Eq. (5:8) in terms of matrix elements $X_{t,d}^{s,c} = \langle s, c | X | t, d \rangle$. Thus,

$$\hat{\rho}_{t,d}^{s,c}(t+1) = \sum_{a,b,q,r} \hat{\rho}_{q,r}^{a,b}(t) \left(\sum_{\mathcal{K} \subseteq E} \pi_{\mathcal{K}}(p) U_{\mathcal{K},a,b}^{s,c} U_{\mathcal{K},q,r}^{*t,d} \right). \quad (5:10)$$

The second sum is taken over all possible configurations $K \subseteq E$. This latter summation is the one with exponential dependence on the size of the system (for regular lattices). However, by studying the elements of $S_{\mathcal{K}}$ one can see that only elements connecting neighboring vertices (a vertex is considered to be its own neighbor) can be nonzero. Thus, $S_{\mathcal{K}}$ is a sparse matrix. Consequently, the expensive second sum can be taken only over edges between neighboring sets of vertices ξ , thus $\subseteq \xi \mathcal{K} \subseteq E$. On a d -regular graph every vertex has d neighbors, thus a single run of the second sum, restricted to the set ξ , contains only $2^{2d} = 4^d$ additions in the worst case. As the first summation is $\mathcal{O}(N^2)$ (polynomial) with respect to the number of vertices, the total computation cost is reduced to the polynomial regime with respect to N . One can repeat the same line of thoughts to see that the superoperator Φ is also a sparse operator, and the cost of its construction by can be reduced to the polynomial regime as well. During our studies we performed numerical tests to confirm our analytical results and to generate figures, and we found a great use of this result.

In the following we move on to give a general analytic method for determining the asymptotics of a quantum walk on dynamical percolation lattices.

5.3. General method

In general, determining the attractor space is a demanding task. However, it can be simplified considerably with the use of symmetries (*e.g.* translation invariance) of the walk. We will use the translation invariance of the coin operator to separate the definition of the attractor space matrices of Eq. (5:7) into a coin and a graph dependent part. By using the time evolution definition of Eq. (5:4), Eq. (5:7) takes

the form

$$S_{\mathcal{K}}(I_P \otimes C) X (I_P \otimes C^\dagger) S_{\mathcal{K}}^\dagger = \lambda X, \quad (5:11)$$

which we immediately rewrite into

$$\lambda S_{\mathcal{K}}^\dagger X S_{\mathcal{K}} = (I_P \otimes C) X (I_P \otimes C^\dagger), \quad (5:12)$$

where $|\lambda| = 1$. This equation must be satisfied for all $\mathcal{K} \subseteq E$. A closer look at the latter formula reveals that the right hand side does not depend on edge configurations and the left hand side does not depend on the coin operator. Consequently, we can separate the equations collected in Eq. (5:12) into two sets of equations. The solution for the original problem should satisfy all the equations in these new collections, simultaneously. First, if we apply $S_{\mathcal{K}'}$ from the left and its adjoint from the right to Eq. (5:12) we get

$$S_{\mathcal{K}} S_{\mathcal{K}'}^\dagger X S_{\mathcal{K}'} S_{\mathcal{K}}^\dagger = X \quad \forall \mathcal{K}', \mathcal{K} \subseteq E \quad (5:13)$$

which we call the *shift conditions*. The second set consists of only equation

$$\lambda S_{\mathcal{K}'}^\dagger X S_{\mathcal{K}'} = (I_P \otimes C) X (I_P \otimes C^\dagger), \quad (5:14)$$

which must hold for a single given $\mathcal{K}' \subseteq E$. We note that in case of discrete time quantum walks the coin operation is local (*cf.* Eq. (5:4)). Also, the step operator Eq. (5:5) on percolation lattices is local on an isolated vertex. Consequently, the most straightforward configuration for Eq. (5:14) is the empty configuration $\mathcal{K}' = \{\}$, *i.e.* when all edges are broken. In this case Eq. (5:14) have the simple local form of

$$(I_P \otimes RC) X (I_P \otimes C^\dagger R^\dagger) = \lambda X, \quad (5:15)$$

which we call the *coin condition*. Using the coin block form of the operator $X = \sum_{s,t} |s\rangle\langle t| \otimes X^{(s,t)}$ one can realize that equation (5:15) is equivalent to the set of identical (local) *coin block* conditions

$$(RC) X^{(s,t)} (RC)^\dagger = \lambda X^{(s,t)} \quad (5:16)$$

for each coin block $X^{(s,t)}$. (We intentionally use the notion "coin block" because each matrix $X^{(s,t)}$ is defined on the coin Hilbert space \mathcal{H}_C .) Employing the isomorphism $\langle \mathbf{x}^{(s,t)} | c, d \rangle \equiv \langle c | X^{(s,t)} | d \rangle$ we can

turn Eq. (5:16) into an eigenvalue problem for the operator RC

$$(RC) \otimes (RC)^* \mathbf{x}^{(s,t)} = \lambda \mathbf{x}^{(s,t)}. \quad (5:17)$$

Let us give some physical meaning for the equations (5:13) and (5:16). The shift conditions Eq. (5:13) represent the underlying graph with the boundary conditions. Also, all attractors are contained in the space that satisfies the shift condition. On the other hand the coin block conditions Eq. (5:16) determine the possible members of the attractor spectrum, which are the eigenvalues of the superoperator Φ that have a unit magnitude ($|\lambda| = 1$). Also, through the coin block conditions the internal coin structure of attractors are given, and the actual attractors can be found in the space given by the shift conditions.

To summarize, we provided the following method. First, one should find a solution space spanned by the shift conditions of Eq. (5:13). This solution space is naturally determined by the underlying graph of the walk. Second, by employing the coin conditions (5:16) one can determine the unit magnitude eigenvalues λ and also restrict the space that satisfies the shift conditions to the actual attractors. Lastly, through Eq. (5:9) the attractors can be orthonormalized to form an orthonormal basis, and by using Eq. (5:8), the asymptotics are given readily. The presented method which is based on separation is generally applicable to general percolative quantum walks, with the only restriction that the coin operator has to be translation-invariant and local. This method is one of our main results. In the following we further simplify our method and illustrate it on a family of one-dimensional graphs.

5.4. Shift conditions on regular lattices

In the previous section we gave a general method for finding the asymptotics for percolative discrete time quantum walks. The given process can be simplified even further by studying regular, translation-invariant graphs (lattices). The translational invariance allows us to study whole graph families, where the number of lattice sites is not fixed, rather it is a parameter of the problem. In this section we consider simple translation-invariant one-dimensional lattices, which are the linear graph (line) and the circle graph (N-cycle), both consisting of $N = |V|$ vertices. These graphs represent two physically relevant situations: reflecting and periodic boundary conditions. We set the reflection operator $R = \sigma_x$. However, we note that the simplifications presented here are valid for higher dimensional and more general lattices too, since the only property we use is the translational invariance of the graph. We have chosen the one-dimensional graphs for the purpose of giving a straightforward example.

In this section we will use the one-dimensional notation of Section 1.1.1, *i.e.* the positions on the one-dimensional lattice are given by integers. In our case we consider non-negative integers to represent the vertices of the graph. Coin states $|L\rangle$ and $|R\rangle$ are corresponding to steps to the left and to the right,

respectively.

To begin with, we repeat the shift conditions of Eq. (5:13) here:

$$S_{\mathcal{K}} S_{\mathcal{K}'}^\dagger X_{\lambda,i} S_{\mathcal{K}'} S_{\mathcal{K}}^\dagger = X_{\lambda,i} \quad \forall \mathcal{K}', \mathcal{K} \subseteq E. \quad (5:18)$$

It is easy to see that $\mathcal{K} = \mathcal{K}'$ is a tautology, thus actual conditions (restrictions on the elements of $X_{\lambda,i}$) are given only when the configurations are different. For the system under consideration $S_{\mathcal{K}}$ matrices are always permutation matrices, thus for given configurations they define a one-to-one correspondence between matrix elements. Moreover, we deal with walks that make only nearest neighbor steps. These properties imply that a single matrix element determines three other matrix elements at most. We will denote a matrix element of a matrix from the attractor space with

$$\langle s_1, c_1 | X_{\lambda,i} | s_2, c_2 \rangle = W_{s_2, c_2}^{s_1, c_1}. \quad (5:19)$$

Naturally, we start with a matrix where all matrix elements are free parameters to chose. We now fix a matrix element $W_{q,L}^{p,L}$ for further investigation. When $p \neq q$, the edges $(p, p \oplus 1)$ and $(q, q \oplus 1)$ are different. Thus, application of Eq. (5:18) results in:

$$W_{q,L}^{p,L} = W_{q \oplus 1, R}^{p \oplus 1, R} = W_{q \oplus 1, R}^{p, L} = W_{q, L}^{p \oplus 1, R}. \quad (5:20)$$

On the other hand, when $p = q$, the edges $(p, p \oplus 1)$ and $(q, q \oplus 1)$ are the same and hence both indices of the matrix element "feel" the same configuration (shifts). In this case:

$$W_{p, L}^{p, L} = W_{p \oplus 1, R}^{p \oplus 1, R}. \quad (5:21)$$

One can repeat the process shown above to determine all the shift conditions for the elements of an attractor space matrix. Due to translation invariance of the underlying graph the conditions can be summarized in a concise way:

$$W_{s_2 \oplus 1, L}^{s_1 \oplus 1, L} = W_{s_2, R}^{s_1, R} = W_{s_2 \oplus 1, L}^{s_1, R} = W_{s_2, R}^{s_1 \oplus 1, L}, \quad (5:22)$$

when $s_1 \neq s_2$ is satisfied. If $s_1 = s_2 \equiv s$, the following conditions must hold:

$$W_{s \oplus 1, L}^{s \oplus 1, L} = W_{s, R}^{s, R} \quad (5:23)$$

$$W_{s \oplus 1, L}^{s, R} = W_{s, R}^{s \oplus 1, L}. \quad (5:24)$$

Furthermore, if $s_{1(2)} \ominus (\oplus) 1$ belongs to a reflecting boundary (in case of the linear graph), the correspond-

ing equations must be omitted from the set of equations defined above. This omission gives the difference between the reflecting and periodic boundary conditions. Note that position indices run through their corresponding abstract spaces, i. e. s, s_1, s_2 runs through the site labels of the underlying one-dimensional graph. Again, note that shift conditions do not connect elements that have different coin labels at the same position, i. e. shift conditions do not restrict the form of coin blocks available at a given position — this is a common property for all shift conditions.

In summary, the abstract shift condition subspace determined by Eq. (5:13) can be given by using the equations (5:22), (5:23), and (5:24). The translational invariance of the operations allow for such compression of solutions. The method can be applied to graphs with arbitrary number of vertices $N = |V|$. This allows for studying solutions which are out of the reach for the current numerical or experimental techniques.

5.5. Conclusions

Discrete time quantum walks on dynamical percolation graphs are special cases of open systems. Due to the exponential amount of computational resources needed to study such systems, finding proper analytical tools is essential. In this chapter we presented a general analytical tool for giving the asymptotic dynamics of quantum walks on finite graphs dynamically percolated graphs.

We first defined the random unitary operation (RUO) that gives the time evolution. This time evolution can also be viewed as a superoperator which is linear with respect to the density operator. For such superoperators the asymptotics can be determined through the construction of the so-called attractor space. We have given a general method based on the separation of the equation for the time evolution which formally gives the attractor space. This was done through two sets of equations called the shift conditions and coin condition. The shift conditions correspond to the graph structure, while the coin condition gives the coin structure of the attractors, and also determines the actual asymptotic dynamics through the phases of eigenvalues. Thus, the asymptotic dynamics is determined by the coin operator. This separation allows for studying whole classes of coins on the same graph in a straightforward way, since only the coin conditions corresponding to different coins must be applied to the same space determined by the shift conditions.

We also showed that on regular translational invariant graphs (lattices) the shift conditions can be simplified considerably, giving a concise form to the conditions. This allows for studying whole families of lattices where the number of vertices (the size of the system) is a free parameter, too. Through this, even numerically unreachable graphs can be studied.

Although the computational power required for the brute force construction of the asymptotics or

the superoperator for regular graphs is exponential in terms of the graph size, we showed that the computational need can be reduced to the polynomial regime for regular graphs. The corresponding polynomial construction is based on the observation that the time evolution operator of discrete time quantum walks is a sparse matrix.

Chapter 6

Determining asymptotics through pure states

The asymptotics of time evolutions given by RUO maps are given through the search of the attractor space (See Chapter 4). However, attractors are not restricted to proper density matrices. In fact, they just span a linear attractor space in which the convex space of the actual asymptotically available density operators reside. Consequently, attractors usually do not have an immediate physical meaning, thus it is hard to draw any physical properties of a system just given its attractor space. Naturally, one can address this problem: Is it possible to construct attractors in a way that they have a direct physical meaning? Is it possible to find some physically relevant part of the attractor space?

In this chapter we pursue the problem of giving an immediate physical meaning to attractors. We present a new, simpler method to give the asymptotics of RUO maps. This method is based on the search of pure common eigenstates, which are the fixed points of dynamics with actual physical meaning. Moreover, they can be found more easily in comparison with general attractors. The connection between the general attractor space approach and the pure state ansatz is discussed. We also apply this method on quantum walks with dynamical percolation.

This chapter is organized as follows. First, we present our ansatz based on finding pure fixed points of the dynamics. Next, we employ the ansatz on the model of quantum walks with dynamical percolation (which we described in the Chapter 5) to determine the asymptotics of the model. Finally, we draw conclusions.

6.1. Pure state ansatz

The asymptotics of RUO maps (See Chapter. 3) are given through finding the attractor space A (See Eq. (3:11)) which are spanned by attractors defined by Eq. (3:9). By construction these matrices are not guaranteed to be proper density matrices. Consequently, the attractor space is an abstract linear space containing the subspace of actual asymptotic density matrices. In this sense attractors do not necessarily carry a direct physical meaning.

We would like to use the fact that attractor matrices X evolve unitarily in the asymptotic regime as it is established by Eq. (3:9). Let us consider pure states $|\psi\rangle$ which are eigenstates of all the possible unitaries U_i used in the construction of the superoperator (*cf.* (3:3)):

$$U_i|\psi\rangle = \alpha|\psi\rangle \quad \text{for all } i\text{-s.} \quad (6:1)$$

We refer to these states simply as *common eigenstates*. We stress that a common eigenstate $|\psi\rangle$ takes the same α eigenvalue for all U_i unitaries. Surprisingly, as we will show below, the procedure based on finding these states can be very fruitful to construct a substantial part of the attractor space.

Such common eigenstates have an interesting property, namely they automatically form attractors as

$$U_i|\psi\rangle\langle\psi|U_i^\dagger = \alpha\alpha^*|\psi\rangle\langle\psi| = |\psi\rangle\langle\psi| = U_{i'}|\psi\rangle\langle\psi|U_{i'}^\dagger \quad (6:2)$$

for all i, i' -s. Let us choose an orthonormal basis of all common eigenstates $\{|\phi_{\alpha,i}\rangle\}$, where index i refers to possible degeneracies and α is the eigenvalue corresponding to $|\phi_{\alpha,i}\rangle$. It is apparent that any linear combination

$$Y = \sum_{\alpha\beta^*=\lambda,i,j} A_{\beta,j}^{\alpha,i} |\phi_{\alpha,i}\rangle\langle\phi_{\beta,j}|, \quad (6:3)$$

with a fixed eigenvalue product $\alpha\beta^* = \lambda$ constitutes an attractor corresponding to eigenvalue λ . Indeed, such attractors by their construction satisfy defining equation (3:9), which we repeat here for a moment:

$$U_i X U_i^\dagger = \lambda X \quad \text{for all } i\text{-s, with } |\lambda| = 1. \quad (6:4)$$

Interestingly, all these attractors satisfy even the stricter conditions (as it follows directly from the construction)

$$U_i X U_{i'}^\dagger = \lambda X \quad \text{for all } i, i'\text{-s, with } |\lambda| = 1. \quad (6:5)$$

We call these attractors *p-attractors*. In contrast with the condition on general attractors (6:4) the latter condition on p-attractors (5:7) is more restrictive, because in this case X must be invariant under the effect of any different pair of unitaries U_i and $U_{i'}$. Therefore, not all attractors can be constructed from pure common eigenstates in general. For example the trivial attractor proportional to identity is not a p-attractor, as it breaks the condition (6:5) (apart from the case of a purely unitary time evolution). Consequently, the attractor space must always contain the span of all p-attractors and identity, as a minimal subspace. In fact, for certain RUO based evolutions this minimal subspace case is actually the whole attractor space. In such case, the asymptotic time evolution simplifies considerably:

$$\rho(n) = U_i^n \mathcal{P} \rho_0 \mathcal{P} \left(U_i^\dagger \right)^n + \tilde{\mathcal{P}} \frac{\text{Tr} \{ \rho_0 \tilde{\mathcal{P}} \}}{\text{Tr} \tilde{\mathcal{P}}} \quad \text{where } n \gg 1. \quad (6:6)$$

Here, \mathcal{P} is a projection into the subspace of common eigenstates, and $\tilde{\mathcal{P}}$ is its orthogonal complement satisfying $\mathcal{P} + \tilde{\mathcal{P}} = I$. Let us discuss the meaning of (6:6) for a moment. In the minimal subspace case the

asymptotic state is an incoherent mixture of the common eigenstate subspace — evolving unitarily — and the completely mixed state projected on the orthogonal complement of the common eigenstate subspace. This formula also shows that the space spanned by common eigenstates is a decoherence free subspace. Thus, we have given a way to find decoherence free subspaces in RUO time evolutions. Such protected subspaces are always handy in quantum information, *e.g.* they can be employed for computation or information storage purposes.

Even when the attractor space is not the span of the trivial attractor and p-attractors, the pure state ansatz can aid the construction of the full attractor space. Practically speaking, even if there are some nontrivial non-p-attractors, it is convenient to first construct all p-attractors using the pure common eigenstates, which are naturally easy to calculate. Then, using the general method one can construct and add the non-p-attractors to complete the whole attractor space — the key idea is to elaborate the differences between (6:4) and (6:5). Another aspect of the pure state ansatz is that pure common eigenstates are much easier to calculate than regular attractor space matrices. In the following, we show a case study by employing the pure state ansatz for the case of the one-dimensional percolation quantum walks we studied in Chapter 5.

6.2. Percolation quantum walks

First, we start the analysis with searching for common eigenstates. According to Equations (5:4) and (6:1) they are defined by equations

$$S_{\mathcal{K}}(I_P \otimes C)|\psi\rangle = \alpha|\psi\rangle \quad \text{for all } \mathcal{K} \subseteq E. \quad (6:7)$$

This formula can be separated into a coin condition with one chosen edge configuration

$$S_{\mathcal{K}}(I_P \otimes C)|\psi\rangle = \alpha|\psi\rangle \quad (6:8)$$

and the set of shift conditions

$$S_{\mathcal{K}'}S_{\mathcal{K}}^\dagger|\psi\rangle = |\psi\rangle \quad \text{for all } \mathcal{K}, \mathcal{K}' \subseteq E. \quad (6:9)$$

The most straightforward configuration for Eq. (6:8) is the one with all edges broken $\mathcal{K} = \{\}$, which makes the coin condition local

$$(I_P \otimes RC)|\psi\rangle = \alpha|\psi\rangle. \quad (6:10)$$

Expanding an arbitrary pure quantum state as $|\psi\rangle = \sum_s |s\rangle \otimes |\psi^{(s)}\rangle_C$ we can rewrite Eq. (6:10) into the set of local and equivalent eigenvalue equations

$$RC|\psi^{(s)}\rangle_C = \alpha|\psi^{(s)}\rangle_C. \quad (6:11)$$

Equations (6:11) determine the possible candidates for eigenvalues α associated with common eigenstates (6:1) and also the general structure of internal coin states $|\psi^{(s)}\rangle$. These internal coin states are then bound to each other via shift conditions (6:9). This procedure provides us the whole subspace of common eigenstates (6:1) and via (6:3) we can easily construct all p-attractors.

Let us show here the difference between the parts of the attractor space formed by the p-attractors and the non-p-attractors. All p-attractors are determined by equations (6:5). Following the same separation steps as we performed earlier, equations (6:5) can be rewritten into the local condition for coin blocks and the set of shift conditions for p-attractors. The coin condition turns out to be the same as for general attractors (*cf.* Eq. (5:16)). However, the shift conditions (*cf.* Eq. (5:13)) differ:

$$S_{\mathcal{L}}S_{\mathcal{K}}^\dagger Y S_{\mathcal{K}'} S_{\mathcal{L}'}^\dagger = Y \quad \forall \mathcal{K}, \mathcal{K}', \mathcal{L}, \mathcal{L}' \subseteq E. \quad (6:12)$$

In fact, this is the only difference between general and p-attractors for percolation quantum walks. One can employ this knowledge to construct the whole attractor space. First, through the common eigenstates one can construct all p-attractors. Next, by allowing the less restrictive conditions on general attractors one can find the missing non-p attractors.

6.3. Conclusions

The general method developed for solving asymptotics of RUO maps (See Chapter 3) incorporates a key part, which is the construction of the so-called attractor space through finding attractors. These attractors are invariant fixed points of the open time evolution, albeit they are not restricted to valid density matrices. Consequently, attractors do not carry an immediate physical meaning. More importantly, if one cannot find all attractors, then there is only a very limited knowledge which can be obtained about the asymptotics of the system.

In this chapter we have given an ansatz which is based on the construction of attractors by using the pure fixed points of dynamics: common eigenstates. Naturally, these common eigenstates are much more easy to find, and all of them carry a direct physical meaning. The subspace formed by these eigenstates are decoherence free, thus are protected from the effects of the open system dynamics. Even without knowing the full attractor space this knowledge can be employed. We have also shown that the

attractors built from these eigenstates — which we call p-attractors — obey a stricter set of conditions in comparison with the general attractors. Thus, not all attractors can be constructed as p-attractors. A straightforward example for such non-p-attractor is the trivial attractor: the completely mixed state. However, in some cases the full attractor space is provided by the span of the trivial attractor and the p-attractors. We showed that in this case the asymptotic time evolution can be given in a nice concise form. We note here that this minimal subspace case will surface again later for some percolation quantum walks.

We have applied the proposed ansatz on discrete time percolation quantum walks. We saw that the separation of time evolution allows for finding common eigenstates easily. We also illustrated the difference between p- and non-p-attractors. The deeper understanding of this difference allows for finding asymptotics in a very economical way: First, one should construct all p-attractors through the easy to calculate common eigenstates. Second, by allowing the conditions of general attractors one can construct the missing p-attractors.

Chapter 7

One-dimensional quantum walks on percolation graphs — complete analysis

The problem of the discrete time quantum walks on one-dimensional percolation graphs represent the most simple scenario when one wishes to join these two areas of physics (See Chapter 4 for details). However, the problem was only partially addressed so far in the literature, and most studies were only numerical due to the complexity of the problem. Here our goal is to give a complete, closed form solution to the one-dimensional problem while leaving it as general as possible.

We employ our methods given in the previous chapters to solve the time evolution of the one-dimensional quantum walk on percolation graphs using general $SU(2)$ coins. We study two basic graph families: the circle and the linear graphs, corresponding to the periodic and reflective boundary conditions respectively. We derive the explicit closed form of the asymptotic states and find a rich variety of asymptotic solutions. We also discover the presence of the so-called edge states which are asymptotic states exponentially localized at the boundaries of the system.

This chapter is organized as follows. In the first section we explicitly derive the asymptotics of percolation walks on circles and lines. In section 7.2 we focus on the edge states. Finally, we draw conclusions.

7.1. Explicit solutions

In this section we explicitly solve the asymptotic time evolution of cycle and line graphs, both consisting of N vertices. We will rely on the notation used for one-dimensional walks of Sec. 1.1.1. Let us give the form of the time evolution operator of the one-dimensional percolation walk (*cf.* Eqs. (4:3), (5:4) and (5:5)) here:

$$U_{\mathcal{K}} = S_{\mathcal{K}}(I_P \otimes C), \quad (7:1)$$

where

$$S_{\mathcal{K}} = \sum_{(x,x+1) \in \mathcal{K}} |x+1, R\rangle\langle x, R| + \sum_{(x,x-1) \in \mathcal{K}} |x-1, L\rangle\langle x, L| + \sum_{(x,x+1) \notin \mathcal{K}} |x, L\rangle\langle x, R| + \sum_{(x,x-1) \notin \mathcal{K}} |x, R\rangle\langle x, L|. \quad (7:2)$$

Both definitions depend on the configuration of edges $\mathcal{K} \subseteq E$ and we set the reflection operator $R = \sigma_x$.

We start by employing the pure state ansatz of Chapter 6 to construct some part of the attractor space. For that we must search for common eigenstates of the dynamics, which is done by solving the local coin conditions (6:11) and shift conditions (6:9). We repeat that equations (6:11) determine the possible eigenvalues α corresponding to the common eigenstates (6:1) and also the structure of internal coin states. These internal coin states are then bound to each other via shift conditions (6:9).

To continue the analysis it is crucial to understand the difference between the shift conditions on p-attractors (6:12) and non-p-attractors (5:13) in our model. Let us denote a matrix element of p-attractor Y in the natural basis as

$$\langle s_1, c_1 | Y | s_2, c_2 \rangle = Y_{s_2, c_2}^{s_1, c_1}. \quad (7:3)$$

Using this notation we rewrite shift conditions (6:12) as

$$Y_{s_2 \oplus 1, L}^{s_1 \oplus 1, L} = Y_{s_2, R}^{s_1, R} = Y_{s_2 \oplus 1, L}^{s_1, R} = Y_{s_2, R}^{s_1 \oplus 1, L} \quad \forall s, s_1, s_2 \in V. \quad (7:4)$$

We repeat that the latter equation describes the shift condition requirements on the elements of p-attractors. On the other hand, general attractors for the same system have the shift conditions (5:22), (5:23) and (5:24). A closer second look reveals that (5:22) is the same condition as (7:4), thus the only difference is given by the less restrictive conditions (5:23) and (5:24).

In summary, the complete attractor space can be constructed as follows. First, using (6:11) one can determine the possible α eigenvalues and corresponding internal coin states. Second, employing the pure state shift conditions (6:9) all common pure eigenstates can be constructed. Using an orthogonalization process, a corresponding orthonormal basis must be formed from the eigenstates. Next, according to (6:3) all p-attractors can be constructed, along with the corresponding $|\lambda| = 1$ superoperator eigenvalues. Then, by allowing the general constraints (5:23) and (5:24), the attractor space must be extended to non p-attractors. In this way at least one additional attractor, proportional to identity, will be found, which is the trivial solution. We note that the different boundary conditions are handled by the shift conditions in all cases. Thus, if $s_{1(2)} \ominus (\oplus) 1$ belongs to a reflecting boundary (in a case of the line graph), the corresponding equations must be omitted from the set of shift condition equations.

Let us move on to solve the problem explicitly for the complete $SU(2)$ group of coins, and for arbitrary N number of vertices. We parametrize the coins as

$$C(\alpha, \beta, \gamma) = \begin{pmatrix} (e^{i(\alpha+\gamma)} - e^{i(\gamma-\alpha)}) \cos \beta \sin \beta & e^{-i\alpha} \cos^2 \beta + e^{i\alpha} \sin^2 \beta \\ e^{i\alpha} \cos^2 \beta + e^{-i\alpha} \sin^2 \beta & (e^{i(\alpha-\gamma)} - e^{-i(\alpha+\gamma)}) \cos \beta \sin \beta \end{pmatrix} \quad (7:5)$$

with $\beta \neq k \cdot \pi/2 \mid k \in \mathbb{Z}$ and $\alpha \neq k \cdot \pi \mid k \in \mathbb{Z}$. Thus we exclude coins leading to a trivial scenario in which the resulting dynamics merely relabels quantum states and does not invoke any interference effect. In fact, such special cases without any quantum interferences represent a purely classical process, thus can be solved using a classical stochastic description.

We solve (6:11) to gain the possible eigenvalues of common eigenstates and its associated local coin states: The spectrum of the matrix $\sigma_x C(\alpha, \beta, \gamma)$ is $\{e^{i\alpha}, e^{-i\alpha}\}$ with corresponding eigenvectors $|v_1\rangle_C = (\cos \beta, e^{i\gamma} \sin \beta)^T$, $|v_2\rangle_C = (\sin \beta, -e^{i\gamma} \cos \beta)^T$. Equipped with this knowledge, by employing (6:9) one can construct the following orthonormal basis of common eigenstates for a percolation chain

$$|\phi_1\rangle = \left(\frac{(\cot \beta)^2 - 1}{(\cot \beta)^{2N} - 1} \right)^{1/2} \left\{ \sum_{s=0}^{N-1} (\cot \beta)^s e^{-i\gamma s} |s\rangle_P \otimes |v_1\rangle_C \right\}, \quad (7:6)$$

$$|\phi_2\rangle = \left(\frac{(\tan \beta)^2 - 1}{(\tan \beta)^{2N} - 1} \right)^{1/2} \left\{ \sum_{s=0}^{N-1} (-\tan \beta)^s e^{-i\gamma s} |s\rangle_P \otimes |v_2\rangle_C \right\} \quad (7:7)$$

with respect to the spectrum $\{e^{i\alpha}, e^{-i\alpha}\}$. The proof is the following. Any common eigenstate corresponding to eigenvalue $e^{i\alpha}$ can be written in the form $|\phi\rangle = \sum_s a_s |s\rangle_P \otimes |v_1\rangle_C$. Using shift conditions (6:9) we get $a_{s+1} = e^{-i\gamma} a_s \cot \beta$. Normalization yields the single common eigenstate (7:6). Following the same steps one can show that (7:7) is the second common eigenstate, corresponding to the eigenvalue $e^{-i\alpha}$. We note that these eigenstates are exponentially localized at the boundaries of the system (considering the position distribution), for most of the coin operators. Thus, they can be termed as edge states. We discuss these states in more detail in Section 7.2.

In view of equation (6:3), all p-attractors can be constructed directly from common eigenstates (7:6) and (7:7). Thus the p-attractor subspace corresponding to eigenvalue $\lambda_1 = 1$ is two-dimensional with the orthonormal basis $\{|\phi_1\rangle\langle\phi_1|, |\phi_2\rangle\langle\phi_2|\}$ and p-attractor space corresponding to the eigenvalue $\lambda_2 = \exp(2i\alpha)$ (resp. eigenvalue $\lambda_3 = \exp(-2i\alpha)$) is one-dimensional with orthonormal basis $\{|\phi_1\rangle\langle\phi_2|\}$ (resp. $\{|\phi_2\rangle\langle\phi_1|\}$). In the special case $\alpha = \pi/2$, both eigenvalues λ_2 and λ_3 are equal to -1 and the corresponding p-attractor subspace is two-dimensional with orthonormal basis $\{|\phi_1\rangle\langle\phi_2|, |\phi_2\rangle\langle\phi_1|\}$.

We find ourselves at the position where we should sort out which attractors remained undiscovered by the pure state method, *i.e.* attractors which are non-p-attractors. In order to answer this question, we have to employ the general separation method. We first determine the dimension of each attractor subspace corresponding to a given eigenvalue λ .

This is straightforward for the attractors associated with $\lambda = \exp(2i\alpha)$ for $\alpha \neq \pi/2$. According to equations (5:16) and (5:17) the general structure of the corresponding coin blocks is one-dimensional

$$X^{(s,t)} = u^{(s,t)} \begin{pmatrix} \cos \beta \sin \beta & -e^{i\gamma} \cos^2 \beta \\ e^{i\gamma} \sin^2 \beta & -e^{2i\gamma} \cos \beta \sin \beta \end{pmatrix}. \quad (7:8)$$

Let us assume that the coin block $X^{(0,0)}$ is determined, *i.e.* the free parameter $u^{(0,0)}$ is set. Shift conditions for the general attractors (5:22), (5:23) and (5:24) determine all other coin blocks, thus all other $u^{(s,t)}$ -s are determined by the parameter $u^{(0,0)}$ which is then naturally fixed by normalization (5:9). Consequently, the general attractor subspace associated with eigenvalue $\lambda = \exp(2i\alpha)$ is one-dimensional, thus, equal to the subspace of p-attractors. Similarly, one can easily see the same equivalence among general attractors and p-attractors associated with eigenvalue $\lambda = \exp(-2i\alpha)$.

We repeat the same procedure, for the $\lambda = 1$ eigenvalue. It turns out that the structure of coin blocks is two-dimensional

$$X^{(s,t)} = \begin{pmatrix} v^{(s,t)} & c_1 u^{(s,t)} \\ c_1^* u^{(s,t)} & c_2 u^{(s,t)} + v^{(s,t)} \end{pmatrix} \quad (7:9)$$

with $c_1 = \exp(-i\gamma) \sin \beta \cos \beta$ and $c_2 = -\cos(2\beta)$. Each coin block is determined by two parameters $u^{(s,t)}$ and $v^{(s,t)}$. Let us fix the linear parameters $u^{(0,0)}$ and $v^{(0,0)}$ of the diagonal coin block $X^{(0,0)}$. The less restrictive shift conditions (5:23) and (5:24) of general attractors determine only the linear parameter $u^{(0,1)}$ leaving the parameter $v^{(0,1)}$ free. Once this remaining free parameter is fixed, no free parameters remain due to shift conditions (5:22), (5:23) and (5:24). Thus, the attractor subspace associated with eigenvalue $\lambda = 1$ is three-dimensional. In order to get all three elements of this subspace it is sufficient to take the p-attractors of eigenvalue $\lambda = 1$ and add the identity, *i.e.* the trivial solution.

The last difficulty arises in the degenerate case when coin parameter $\alpha = \pi/2$ which leads to the degenerate superoperator eigenvalue $\lambda = -1$. By employing (5:16) and (5:17) we find that the general structure of the coin blocks corresponding to attractors of $\lambda = -1$ is

$$X^{(s,t)} \equiv D \left(u^{(s,t)}, v^{(s,t)} \right) = \begin{pmatrix} d_1 (u^{(s,t)} + v^{(s,t)}) & d_2^* v^{(s,t)} \\ d_2 u^{(s,t)} & -d_1 (u^{(s,t)} + v^{(s,t)}) \end{pmatrix} \quad (7:10)$$

with $d_1 = -1/2 \tan(2\beta)$ and $d_2 = \exp(i\gamma)$. Repeating the same steps as above, one can find that the attractor subspace associated with $\lambda = -1$ is three-dimensional. As the subspace of p-attractors associated with eigenvalue $\lambda = -1$ is only two-dimensional, we miss one attractor. In order to construct such attractor we derive a recurrent formula for coin blocks of p-attractors and attractors. Assume that we know one of the coin blocks $X^{(s,t)}$. Then using shift conditions for p-attractors (7:4) one can show that neighboring coin blocks of p-attractors are determined by formulas

$$X^{(s,t+1)} = D \left(-\frac{d_2}{d_1} u^{(s,t)} - d_1 d_2 (u^{(s,t)} + v^{(s,t)}), d_1 d_2 (u^{(s,t)} + v^{(s,t)}) \right), \quad (7:11)$$

$$X^{(s+1,t)} = D \left(d_1 d_2^* (u^{(s,t)} + v^{(s,t)}), -\frac{d_2^*}{d_1} v^{(s,t)} - d_1 d_2^* (u^{(s,t)} + v^{(s,t)}) \right). \quad (7:12)$$

In the view of these relations we can immediately have two observations. First, all coin blocks of a p-attractor are determined by a single coin block only. Consequently, the subspace of p-attractors associated with $\lambda = -1$ is two-dimensional indeed. Second, if one coin block is zero, then all other coin blocks and the whole p-attractor is inevitably zero. In other words, p-attractors corresponding to $\lambda = -1$ cannot have a zero coin block. On the contrary, for general attractors shift conditions are less restrictive. Thus, formulas for the neighbors of the diagonal coin blocks $X^{(s,s)}$ read

$$\begin{aligned} X^{(s,s+1)} &= D \left(-\frac{d_2}{d_1} u^{(s,s)} - v^{(s,s+1)}, v^{(s,s+1)} \right), \\ X^{(s+1,s)} &= D \left(u^{(s+1,s)}, -\frac{d_2^*}{d_1} v^{(s,t)} - u^{(s+1,s)} \right). \end{aligned} \quad (7:13)$$

We observe that the linear parameters $v^{(s,s+1)}$ and $u^{(s+1,s)}$ are not determined by parameters of the coin block $X^{(s,s+1)}$. Coin blocks $X^{(s,s+1)}$ and $X^{(s+1,s)}$ are bound to each other by the shift condition (5:24) and thus only one of these two parameters is free in fact. In order to define an attractor X associated with $\lambda = -1$ we have to specify two parameters of its coin block $X^{(0,0)}$ and one parameter $v^{(s,s+1)}$. All other coin blocks are determined by shift conditions for attractors (5:22),(5:23) and (5:24). To construct the last missing independent attractor it is sufficient to choose coin block $X^{(0,0)}$ as zero matrix ($u^{(0,0)} = v^{(0,0)} = 0$) and set the linear parameter $v^{(s,s+1)} = 1$. All other coin blocks are defined by shift conditions (5:22),(5:23) and (5:24). Apparently, the attractor constructed in this recurrent way cannot be a p-attractor.

An elegant analytical form of this recurrently constructed missing attractor for $\lambda = -1$ is not known so far. Using the numerical simulation data, by induction we found that the missing attractor can be written in the closed analytical form

$$X_{\pi/2} = X_{-1} F^\dagger E F, \quad (7:14)$$

where

$$X_{-1} = \sum_{s=0}^{N-1} \frac{(-1)^s}{\sqrt{2N}} |s\rangle_P \langle s|_P \otimes \begin{pmatrix} 1 & 0 \\ 0 & -1 \end{pmatrix}_C. \quad (7:15)$$

F is the discrete Fourier transformation operator acting on position states

$$F = \sum_{s,t=0}^{N-1} e^{i2\pi st/N} |s\rangle_P \langle t|_P \otimes I_C. \quad (7:16)$$

E is the block diagonal matrix

$$E = \bigoplus_{g=0}^{N-1} \frac{1}{i \sin\left(\frac{2g\pi}{N} - \gamma\right) - \cot 2\beta} \begin{pmatrix} i \sin\left(\frac{2g\pi}{N} - \gamma\right) & e^{-i2\pi g/N} \cot 2\beta \\ e^{i2\pi g/N} \cot 2\beta & i \sin\left(\frac{2g\pi}{N} - \gamma\right) \end{pmatrix}. \quad (7:17)$$

Let us summarize the complete list of attractors. First, we consider the case with coin parameter $\alpha \neq \pi/2$. For the percolation line the attractor space is five-dimensional.

$$\left. \begin{aligned} Z_1 &= |\phi_1\rangle\langle\phi_1|, \\ Z_2 &= |\phi_2\rangle\langle\phi_2|, \\ Z_3 &= \frac{1}{\sqrt{2N-2}} (I_P \otimes I_C - Z_1 - Z_2) \end{aligned} \right\} \text{ for } \lambda_1 = 1$$

$$X = |\phi_1\rangle\langle\phi_2|, \text{ for } \lambda_2 = e^{2i\alpha}$$

$$\tilde{X} = |\phi_2\rangle\langle\phi_1|, \text{ for } \lambda_3 = e^{-2i\alpha}. \quad (7:18)$$

On the percolation cycle graph the pure eigenstates of the line graph ($|\phi_1\rangle$ and $|\phi_2\rangle$) vanish if they are not translation-invariant. Consequently, $|\phi_1\rangle$ is a common eigenstate on cycles if $(\cot \beta)^N e^{-i\gamma N} = 1$ is satisfied. Likewise, for $|\phi_2\rangle$ the equation $(-\tan \beta)^N e^{-i\gamma N} = 1$ needs to be true. We note that only on cycles with even number of edges both eigenstates might be available. For $(\cot \beta)^N e^{-i\gamma N} = 1$ the attractor space of the cycle consists $\{Z_1, Z_3\}$, and when $(-\tan \beta)^N e^{-i\gamma N} = 1$ the attractor space is spanned by $\{Z_2, Z_3\}$. When both conditions are met, the attractor space of the QW on the percolation cycle is the same as on the percolation line (7:18). We note that satisfying the above conditions allowing states $|\phi_1\rangle$ and $|\phi_2\rangle$ will result a flat position distribution. That is, they will not localize exponentially at the boundaries of the graph. This property is clearly understandable as the cycle graph has no dedicated boundaries due to the translation invariance.

For the degenerate case $\alpha = \pi/2$ the additional attractor $X_{\pi/2}$ (7:14) is always present on the percolation line. The shift conditions require translation invariance for the attractors on the percolation cycle. X_{-1} is the only building block in the definition of $X_{\pi/2}$ (*i.e.* equation (7:14)), which might restrict such translational invariance, hence $X_{\pi/2}$ appears in the attractors space of cycles with an even number of vertices only.

The explicit form of attractors given above confirms two important properties of studied asymptotic dynamics. First, coin blocks of attractors corresponding to $\lambda \neq 1$ (while $|\lambda| = 1$) are strictly traceless, *i.e.* should one trace out the coin degree of freedom, the remaining position density matrix strictly depend on just the $\lambda = 1$ attractors. Consequently, if one is interested in the position density operator (*e.g.* want to calculate the position distribution), only attractors corresponding to $\lambda = 1$, *i.e.* Z_1, Z_2 and Z_3 are

needed for the calculation. Second, all position density operators are stationary in time,

$$\rho_P(n) = \text{Tr}_C \rho(n) = \text{Tr}_C \rho(n+1) = \rho_P(n+1) \quad \text{where } n \gg 1 \quad (7:19)$$

Consequently, limit cycles or other non-stationary asymptotic dynamics might be observable only in the coin degree of freedom.

7.2. Edge states

It is well known that the position distribution of a classical walk on a connected undirected graph converge to the uniform distribution. This result is independent of the choice of a graph and from the initial distribution of the walk. In contrast, we found that the asymptotic position distribution can be nonuniform on the percolative quantum walks we study, despite the strong decoherence. Moreover, one can observe the existence of the so-called edge states with exponentially decaying position distributions. Indeed, both common eigenstates (7:6) and (7:7) exhibit this behavior. We stress that this interesting effect in one-dimension only arises on the line graph — on the cycle graph such states cannot be observed since they do not fulfill the translation invariance required by the periodic boundary conditions.

In order to study this behavior in more details, let us denote the initial state of the walker by ρ_0 . After sufficiently many iterations we reach the asymptotic evolution, which according to (5:8) can be written as

$$\rho(n) = O_1 Z_1 + O_2 Z_2 + \frac{1 - O_1 - O_2}{\sqrt{2N - 2}} Z_3 + \mathcal{R} \quad \text{where } n \gg 1. \quad (7:20)$$

Here, O_i denotes the overlap of the initial state ρ_0 with common eigenstate (7:6) and (7:7), *i.e.* $O_i = \text{Tr}\{Z_i \rho_0\}$. They satisfy relation $O_1 + O_2 \leq 1$. The traceless operator \mathcal{R} refers to the overlap of the initial state ρ_0 with attractors X , \tilde{X} and $X_{\pi/2}$. However, this part does not contribute to the asymptotic position distribution of the walker, which reads

$$P(s) = \langle s | \text{Tr}_C \rho(n) | s \rangle = \mathcal{N} (O_1 q^{N-1-s} + O_2 q^s) + \frac{1 - O_1 - O_2}{2N} \quad \text{where } n \gg 1. \quad (7:21)$$

We defined $\mathcal{N} = (q-1)/(q^N-1)$ and $q = \tan(\beta)$. The first term in (7:21) clearly displays the exponentially decreasing behavior from the left edge to the right, and then from a certain minimum an exponentially increasing probability towards to the right edge. The minimum depends on initial overlaps O_i . If one of these overlaps is zero one can observe a monotonous exponential behavior. The second term of the position distribution (7:21) is constant and might dampen the exponential behavior slightly.

One can ask the following question: which coins result in the most prominent edge states, *i.e.* where

the exponential localization is the most significant. One can easily infer that this occurs if β is close to the values $k \cdot \pi/2 | k \in \mathbb{Z}$. That is, the coin is almost a permutation matrix. Surprisingly, the exponential localization behavior of the asymptotic position distribution is also available for unbiased coins, *i.e.* whose matrix elements have the same amplitude. A short calculation reveals that these are coins $\mathcal{C}(\alpha, \beta, \gamma)$ which follow condition $|\sin(\alpha) \sin(2\beta)| = 1/\sqrt{2}$. From this condition one can see that the most significant behavior is obtained for $\beta = \pi/8$ and $\alpha = \pi/2$, which corresponds to the coin

$$\mathcal{C}(\alpha = \pi/2, \beta = \pi/8, \gamma) = \frac{i}{\sqrt{2}} \begin{pmatrix} e^{i\gamma} & -1 \\ 1 & e^{-i\gamma} \end{pmatrix}. \quad (7:22)$$

Thus, even for unbiased coins we can get strong exponential behavior of the position distribution (7:21) with $q = (\tan(\beta))^2 = 3 - 2\sqrt{2} \approx 0.1716$.

7.3. Conclusions

The refined methods given in the previous sections — the separation technique for general attractors and the pure state ansatz — provide a useful toolset for investigating the asymptotic properties of discrete time quantum walks on percolation graphs, even when the addressed problem is rather general. In this chapter we have successfully employed these tools and explicitly solved the problem for one-dimensional percolation graphs.

First, we used the pure state ansatz and constructed the pure common eigenstates explicitly. From these states the corresponding p-attractors are built. In the following we employed the general formalism for percolation walks, to extract the missing non-p-attractors. We obtained closed form solutions using the general $SU(2)$ coin classes while also keeping the number of vertices of the underlying graph (N) as a free parameter.

We observed that these one-dimensional systems can exhibit a rich variety of asymptotic behaviors. Apart from stationary asymptotics keeping some quantum coherence of the initial state, periodic and quasi periodic limit cycles can occur due to the appearance of the $\lambda = \exp(\pm 2i\alpha)$ superoperator eigenvalue. However, the attractor subspace corresponding to such limit cycles are strictly composed from attractors with zero trace in all coin sub-blocks. Consequently, limit cycles are not observable in the position density operator (position distribution), *i.e.* actual asymptotic *dynamics* is restricted to the coin degree of freedom only.

By studying the walk on the line graph we discovered that the pure eigenstates in most cases have the form of edge states, which are exponentially localized at the dedicated boundaries of the system. These states also demonstrate the usefulness of the attractor space formalism: the exponent of the localization

for edge states and also coins leading to the most pronounced effect are obtained easily.

The results presented in this chapter are amongst the first closed form analytical results which showed the long time dynamics of quantum walks on percolation graphs. The appearance of any forms of coherence in such systems in the asymptotic limit were first discussed here.

Chapter 8

Two-dimensional quantum walks on percolation graphs

The natural step following the solution of the general one-dimensional problem of percolation quantum walks is to move to higher dimensions. Two-dimensional quantum walks (See Sec. 1.1.2) are straightforward generalizations of one-dimensional quantum walks, extending the basic definitions to two-dimensional graph. However, due to the much broader selection of coins available, *i.e.* $SU(4)$ for 4-regular two-dimensional lattices, these walks exhibit a richer variety of effects. In fact, the complete map of behaviors and effects under the total $SU(4)$ family of coins are yet to be explored.

The percolation theory of two-dimensional graph structures is much richer compared to the one-dimensional percolation graphs. The most interesting effect is undoubtedly the appearance of the non-trivial phase transition (See Chapter 4). For example, on a two-dimensional Cartesian lattice if the probability of the edges to be missing is higher than 1/2 the probability for finding an infinite connected component is exactly zero.

In this chapter we join these two interesting areas and through concrete cases we reveal some unexpected effects. We extend and employ the methods we developed for studying quantum walks on percolation graphs to the two-dimensional case. We reveal that albeit dynamical percolation is a homogeneous noise, it can break a certain rotational symmetry in walks. Moreover, we show that the trapping effect of the Grover-walk surprisingly survives the decoherence of the dynamical percolation. Finally, we draw conclusions.

8.1. Description and asymptotics

The Hilbert space of the two-dimensional QWs is a composite one: $\mathcal{H} = \mathcal{H}_P \otimes \mathcal{H}_C$, where the position space \mathcal{H}_P is spanned by states corresponding to the vertices of a two-dimensional Cartesian lattice with $M \otimes N$ sites, and the coin space \mathcal{H}_C is spanned by vectors corresponding to nearest neighbor steps: $|L\rangle, |D\rangle, |U\rangle, |R\rangle$ — we expand all 4-by-4 matrices in this basis respectively. A single step of the time evolution on a percolation graph is given by equations (5:4) and (5:5). We define the reflection operator as $R = \sigma_x \otimes \sigma_x$.

To solve the asymptotic dynamics of such a system, first one have to find all p-attractors — in analogy with the one-dimensional case (*cf.* Chapter 7) . This can be done by employing equation (6:1) as

$$S_{\mathcal{K}}(I_P \otimes C) |\psi\rangle = \alpha |\psi\rangle. \tag{8:1}$$

We separate this equation into a local coin condition with one chosen edge configuration

$$S_{\mathcal{K}}(I_P \otimes C)|\psi\rangle = \alpha|\psi\rangle \quad (8:2)$$

and to a set of shift conditions

$$S_{\mathcal{K}'}S_{\mathcal{K}}^{\dagger}|\psi\rangle = |\psi\rangle \quad \forall \mathcal{K}, \mathcal{K}' \subseteq E. \quad (8:3)$$

Let us expand a pure state in the natural basis $|\psi\rangle = \sum_{s,t,c} \psi_{s,t,c} |s,t\rangle_P \otimes |c\rangle$. Employing this notation, we can rewrite the shift conditions (8:3) as

$$\left. \begin{aligned} \psi_{s,t,R} &= \psi_{s\ominus 1,t,L} \\ \psi_{s,t,U} &= \psi_{s,t\ominus 1,D} \end{aligned} \right\} \quad \forall (s,t) \in V. \quad (8:4)$$

Here we note that in the shift conditions the boundary conditions must be taken into account: The equations corresponding to the amplitudes where the wavefunction is outside of the graph with reflective boundaries (carpet graph) should be omitted. The periodic boundary conditions (torus graph) are taken into account by using modulo $M(N)$ operations.

After one successfully constructed all pure common eigenstates, by employing (6:3) all p-attractors can be built in a straightforward way. As in the one-dimensional case, all such p-attractors satisfy the shift condition

$$S_{\mathcal{L}}S_{\mathcal{K}}^{\dagger}YS_{\mathcal{K}'}S_{\mathcal{L}'}^{\dagger} = Y \quad \forall \mathcal{K}, \mathcal{K}', \mathcal{L}, \mathcal{L}' \subseteq E. \quad (8:5)$$

However, one can see that general attractors must satisfy a less strict condition

$$S_{\mathcal{K}'}S_{\mathcal{K}}^{\dagger}YS_{\mathcal{K}}S_{\mathcal{K}'}^{\dagger} = Y \quad \forall \mathcal{K}, \mathcal{K}' \subseteq E. \quad (8:6)$$

Consequently, one can investigate the differences between the two latter sets of shift conditions, and construct all missing non-p-attractors. The whole process is analogous to the method we give in Chapter 7. However, since the dimension and the possible degeneracies in the system are higher, the analysis is much more involving. In fact, the vast number of special (*e.g.* degenerate) sub-cases makes the most general problem using $SU(4)$ coins practically unsolvable in a closed form. However, as we show in the following, investigating just some special cases can lead to unexpected results.

8.2. The two-dimensional Hadamard walk: breaking the directional symmetry

The two-dimensional Hadamard walk (*cf.* Section 1.1.2) is a direct generalization of the one-dimensional Hadamard walk, using the tensor product form coin

$$H^{(2D)} = H \otimes H = \frac{1}{2} \begin{pmatrix} 1 & 1 & 1 & 1 \\ 1 & -1 & 1 & -1 \\ 1 & 1 & -1 & -1 \\ 1 & -1 & -1 & 1 \end{pmatrix}, \quad (8:7)$$

where

$$H = \frac{1}{\sqrt{2}} \begin{pmatrix} 1 & 1 \\ 1 & -1 \end{pmatrix}, \quad (8:8)$$

is the well known coin operator of the one-dimensional Hadamard walk (*cf.* Section 1.1.1). In the undisturbed case this coin exhibits a spreading behavior, which is characterized by peaks propagating from the origin at a constant velocity. In the percolation case first we solve (6:11) to obtain the spectrum of common eigenstates resulting in the set of eigenvalues $\{i, -i, 1, 1\}$. The corresponding eigenvectors of the $RH^{(2D)}$ operator are $|v_1\rangle_C = \frac{1}{2}(1, -i, -i, -1)^T$, $|v_2\rangle_C = \frac{1}{2}(1, i, i, -1)^T$, $|v_3\rangle_C = \frac{1}{\sqrt{2}}(1, 0, 0, 1)^T$ and $|v_4\rangle_C = \frac{1}{\sqrt{2}}(0, 1, -1, 0)^T$, respectively. We find the following orthonormal basis of common pure eigenstates on the percolation $M \times N$ carpet

$$|\phi_1\rangle = \sum_{s=0}^{M-1} \sum_{t=0}^{N-1} \frac{(-1)^s}{\sqrt{MN}} |s, t\rangle_P \otimes |v_1\rangle_C, \quad (8:9)$$

$$|\phi_2\rangle = \sum_{s=0}^{M-1} \sum_{t=0}^{N-1} \frac{(-1)^s}{\sqrt{MN}} |s, t\rangle_P \otimes |v_2\rangle_C, \quad (8:10)$$

$$|\phi_3(t)\rangle = \sum_{s=0}^{M-1} \frac{1}{\sqrt{M}} |s, t\rangle_P \otimes |v_3\rangle_C, \quad (8:11)$$

$$|\phi_4(s)\rangle = \sum_{t=0}^{N-1} \frac{(-1)^t}{\sqrt{N}} |s, t\rangle_P \otimes |v_4\rangle_C. \quad (8:12)$$

The next step is to prove the completeness, *i.e.* that these are indeed all pure common eigenstates available. For that we apply shift conditions (8:4) on the coin eigenstates $|v_i\rangle_C$. In the case of the $\alpha = i$ eigenvalue a general common eigenstate must have the form $|\phi\rangle = \sum_{s,t} a_{s,t} |s, t\rangle_P \otimes |v_1\rangle_C$. Thus, we get $a_{s+1,t} = -a_{s,t}$ and $a_{s,t+1} = a_{s,t}$, thus a single eigenvector is found and it takes the form (8:9).

Similarly, for $\alpha = -i$ a single vector (8:10) is found. For $\alpha = 1$ the general form of a common eigenstate is $|\phi\rangle = \sum_{s,t} |s, t\rangle_P \otimes (a_{s,t}|v_3\rangle_C + b_{s,t}|v_4\rangle_C)$. Applying the shift conditions we find $a_{s,t} = a_{s-1,t}$ and $b_{s,t} = -b_{s,t-1}$. This means $M + N$ free parameters, thus an $M + N$ dimensional subspace of common eigenstates with basis vectors (8:11) and (8:12).

Now, we have to determine the remaining attractors which cannot be constructed from common eigenstates. Like in the one-dimensional case, non p-attractors can be searched in a diagonal form. Thus, solving the local equation (5:15) for a diagonal coin block for $\lambda = 1$ imposes

$$\mathbf{B} = \begin{pmatrix} a & c & C & A \\ d & b & B & D \\ -D & B & b & -d \\ A & -C & -c & a \end{pmatrix}, \quad (8:13)$$

where $a - A = b + B$ and $D - d = c + C$. As we require only diagonal coin blocks to be nonzero, and also for them $A = B = C = D = c = d = 0$, thus $a = b$. This means that all diagonal coin blocks are proportional to identity $X_{s,t}^{s,t} = a_{s,t}I$. Due to shift conditions all $a_{s,t}$ are equal, thus a single attractor is revealed to be proportional to the identity, i. e. we found the trivial attractor as the only additional non-p attractor. Similarly, one can show that for the other possible attractor eigenvalues there are no additional non p-attractors. In summary, all attractors can be constructed employing (6:3) and adding the trivial attractor proportional to identity. Thus, the solution presented here is complete.

Let us have a look on the influence of boundary conditions on the available eigenvectors. It should be noted that $|\phi_1\rangle$ and $|\phi_2\rangle$ are not available for periodic boundary condition in the s -direction with odd M . In a similar way $|\phi_4\rangle$ is not a common eigenstate for periodic boundary condition in the t -direction with odd N . From the $\alpha = \{i, -i, 1, 1\}$ pure state eigenvalues the possible attractor space eigenvalues are $\lambda = \{1, -1, i, -i\}$. For the $\lambda = 1$ eigenvalue, for all boundary conditions

$$X_0 = I \quad (8:14)$$

$$X_1(t_1, t_2) = |\phi_3(t_1)\rangle\langle\phi_3(t_2)| \quad (8:15)$$

are valid attractors, spanning a $1 + N^2$ dimensional space. For even M -s on periodic boundary conditions in the s direction or open boundaries in the s direction additional attractors

$$X_2 = |\phi_1\rangle\langle\phi_1| \quad (8:16)$$

$$X_3 = |\phi_2\rangle\langle\phi_2| \quad (8:17)$$

form a two-dimensional space. When in the t direction the system is open or periodic with even N -s the

additional

$$X_4(s_1, s_2) = |\phi_4(s_1)\rangle\langle\phi_4(s_2)| \quad (8:18)$$

$$X_5(s_1, t_2) = |\phi_4(s_1)\rangle\langle\phi_3(t_2)| \quad (8:19)$$

$$X_6(t_1, s_2) = |\phi_3(t_1)\rangle\langle\phi_4(s_2)| \quad (8:20)$$

attractors become available, forming an $M^2 + 2MN$ dimensional space.

For the superoperator eigenvalue $\lambda = i$, for even M -s in the s direction or open boundaries in the s direction

$$Y_1(t_2) = |\phi_1\rangle\langle\phi_3(t_2)| \quad (8:21)$$

$$Y_2(t_1) = |\phi_3(t_1)\rangle\langle\phi_2| \quad (8:22)$$

attractors are available spanning a $2N$ dimensional space. The following attractors appear in addition if either we have open boundary condition in the direction t or we have periodic boundary condition for t with even N :

$$Y_3(s_2) = |\phi_1\rangle\langle\phi_4(s_2)| \quad (8:23)$$

$$Y_4(s_1) = |\phi_4(s_1)\rangle\langle\phi_2|. \quad (8:24)$$

In that case the dimension of the attractor space is increased by $2M$. The form of definition (5:7) implies, that the attractors corresponding to the conjugate $\lambda = -i$ eigenvalue are simply the hermitian conjugate of the attractor space matrices corresponding to $\lambda = i$.

The last possible superoperator eigenvalue is $\lambda = -1$, with the attractors

$$Z_1 = |\phi_1\rangle\langle\phi_2| \quad (8:25)$$

$$Z_2 = |\phi_2\rangle\langle\phi_1| \quad (8:26)$$

available when direction s is open or periodic with even M , adding a two-dimensional space to the attractor space. Altogether, the maximal number of attractors for carpet (open boundaries) or for an even-times-even torus (periodic boundaries) are $(M + N + 2)^2 + 1$.

Let us now analyze the consequences one can draw from the explicit form of the eigenvectors (8:9) - (8:12) for the asymptotic behavior of the walks. The common eigenvectors $|\phi_1\rangle$ and $|\phi_2\rangle$ in (8:9), (8:10) are uniform in position. When the asymptotic state can be expanded by these, then the asymptotics will be uniform in position. In contrast, the other two families of eigenvectors $|\phi_3(t)\rangle$ and $|\phi_4(s)\rangle$ in (8:11), (8:12) are spatially non-uniform. The asymptotic states built by them will have ridge like stripes.

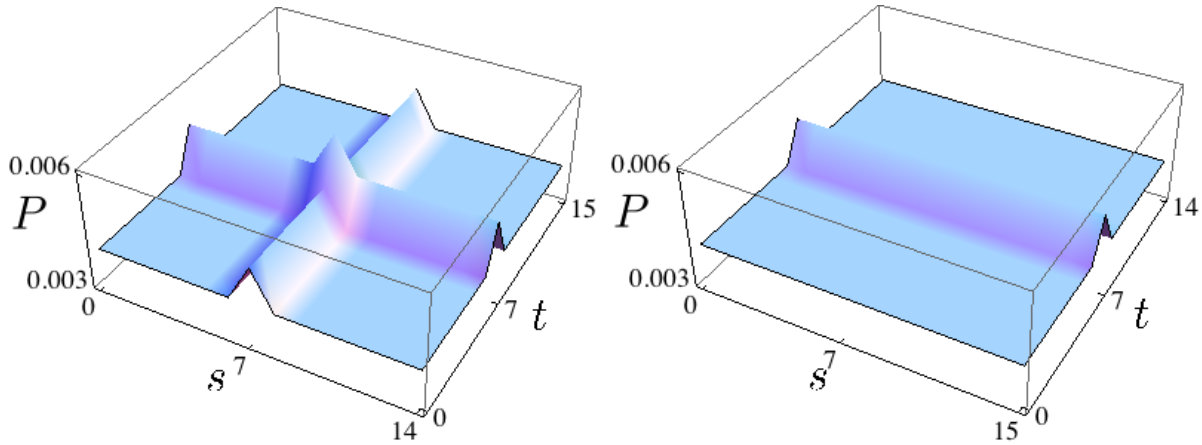


Figure 8:1. Asymptotic position probability distributions P of the two-dimensional Hadamard walk on the torus graphs, starting from the initial state: $|7, 7\rangle_P \otimes \frac{1}{\sqrt{2}}(|L\rangle_C + |D\rangle_C)$. The plot on the left corresponds to the 15×16 percolation torus and the plot on the right corresponds to the 16×15 percolation torus. Due to the 90 degree rotation of the underlying graph (and the initial state), the position distribution changes considerably. For the unitary (percolation-less) case the symmetry breaking is not observable within numerical precision.

Therefore, the boundary conditions for which $|\phi_3(t)\rangle$ or $|\phi_4(s)\rangle$ are allowed can lead to a non-uniform asymptotic position distribution. While dynamical percolation means a spatially homogeneous source of decoherence, it may result in a spatially inhomogeneous asymptotic distribution. However, these states are not edge states like in the non-uniform one-dimensional walks. In contrast with the two-dimensional counterpart the Hadamard walk on a one-dimensional percolation lattice always results in a uniform distribution in position.

Further analyzing the asymptotically inhomogeneous solutions we find that percolation can cause the breaking of the directional symmetry, in the following sense. Taking a certain initial state the undisturbed (unitary) two-dimensional Hadamard walk may show a directional symmetry for the position distribution: if both the graph and the initial state are rotated by 90 degrees the resulting position distribution will also be a rotated version of the original position distribution at all times. In a numerical example we demonstrate that introducing percolation in this system can break the above directional symmetry.

Let us consider the example of a torus with size even-times-odd. A quantum walk with percolation on such a torus will have an attractor space with dimension $(N + 2)^2 + 1$. In contrast, if we rotate the graph (odd-times-even torus) while keeping the coin operator the same, we find an attractor space with dimension $(N + M)^2 + 1$. This change in the dimension of the attractor space clearly demonstrates the symmetry breaking. Furthermore, by examining the corresponding eigenvalues we find that in the second case (odd-times-even torus) only the $\lambda = 1$ eigenvalue occurs, leading to stationary asymptotic states. Whereas in the first case (even-times-odd torus) also the $\lambda = \{-1, \pm i\}$ eigenvalues will be included in the solution possibly allowing for oscillations in the asymptotic state of the system. In figure 8:1. we plot the asymptotic position distributions for the two cases. Numerical simulations of a Hadamard walk on

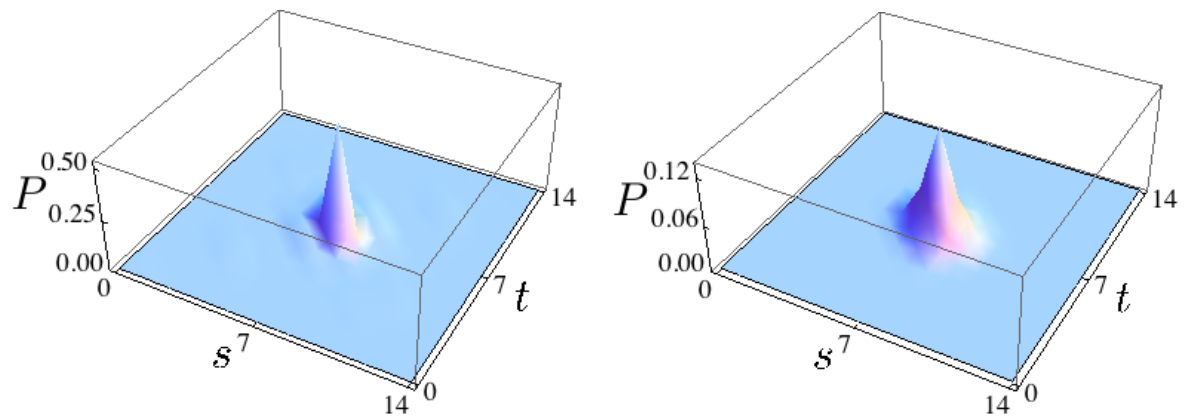


Figure 8:2. Trapping (localization) of Grover walks (see section 8.3) on the 15×15 torus (periodic boundaries). The plot on the left shows the distribution after 1000 steps if unitary time evolution on a perfect graph. The plot on the right shows an asymptotic position distribution of the Grover walk on a percolation graph. Both walks are started from the initial state $|7, 7\rangle_P \otimes \frac{1}{2}(|L\rangle + |D\rangle + |U\rangle + |R\rangle)$. The localization property is observed both for the closed and open system dynamics. This effect is due to the common eigenstates of the system with finite support (*cf.* equation (8:28)). We note that in the percolation (plot on the right) case the peak is not as high as for the unperturbed walk.

tori without percolation show no difference between even-times-odd and rotated odd-times-even systems within numerical precision. Thus, we conclude that the directional symmetry breaking is induced by percolation. This is a new effect which was not reported before.

8.3. The Grover-walk: preserving trapping on percolation lattice

Two-dimensional quantum walks driven by the Grover coin (*cf.* Section 1.1.2)

$$G = \frac{1}{2} \begin{pmatrix} -1 & 1 & 1 & 1 \\ 1 & -1 & 1 & 1 \\ 1 & 1 & -1 & 1 \\ 1 & 1 & 1 & -1 \end{pmatrix} \quad (8:27)$$

gained a considerable interest in the literature, due to their use in quantum search (See Section 1.1.3) and also by exhibiting the property of trapping (localization). This latter phenomenon is the inability of some part of the wave function to leave its initial position due to destructive interference of the outgoing waves. That is, a walker started from a localized initial state can be always found at its initial position with a finite probability, except for a single well-defined initial state.

In the following, we show the attractor space of the Grover walk. The common eigenstates defined

via equation (8:1) have the explicit form of

$$|\phi_1\rangle = \frac{1}{\sqrt{4MN}} \sum_{s=0}^{M-1} \sum_{t=0}^{N-1} |s, t\rangle_P \otimes |v_1\rangle_C, \quad (8:28)$$

$$\begin{aligned} |\phi_2(s, t)\rangle = \frac{1}{\sqrt{8}} \{ & |s, t\rangle_P \otimes |v_2\rangle_C + |s, t \oplus 1\rangle_P \otimes (|v_2\rangle_C + |v_3\rangle_C) \\ & + |s \oplus 1, t\rangle_P \otimes (|v_2\rangle_C + |v_4\rangle_C) \\ & + |s \oplus 1, t \oplus 1\rangle_P \otimes (|v_2\rangle_C + |v_3\rangle_C + |v_4\rangle_C) \}, \end{aligned} \quad (8:29)$$

$$|\phi_3(s)\rangle = \sum_{t=0}^{N-1} \frac{(-1)^t}{\sqrt{2N}} |s, t\rangle_P \otimes |v_3\rangle_C, \quad (8:30)$$

$$|\phi_4(t)\rangle = \sum_{s=0}^{M-1} \frac{(-1)^s}{\sqrt{2N}} |s, t\rangle_P \otimes |v_4\rangle_C, \quad (8:31)$$

where $|v_1\rangle_C = (1, -1, -1, 1)^T$, $|v_2\rangle_C = (1, 1, 0, 0)^T$, $|v_3\rangle_C = (0, -1, 1, 0)^T$ and $|v_4\rangle_C = (-1, 0, 0, 1)^T$. These eigenstates correspond to the eigenvalues $\alpha = \{-1, 1, 1, 1\}$, respectively. The addition denoted by \oplus takes the boundary conditions into account: for reflecting boundary conditions (*e.g.* carpet) the part of the states leaning over the boundary of the graph should be omitted (its amplitude is zero and the corresponding superposition state is normalized accordingly), and for periodic boundary conditions (*e.g.* torus) the addition \oplus corresponds to modulo operations with respect to the graph size.

Using these common eigenstates all p-attractors can be constructed by employing equation (6:3). Performing the general analysis results that the only non-p-attractor is the trivial one, which is proportional to identity. Thus, the total number of attractors is $(MN + M + N + 1)^2 + 1$ for all carpets, and $(MN + 1)^2 + 1$ for tori if M or N are odd. However, in the latter case (8:30) and (8:31) are restricted by the periodic boundary conditions — they cannot be used to construct attractors. When M and N are both even in the case of tori, a single additional state from (8:30) or (8:31) can be chosen as an additional common eigenstate. This results in an attractor space with total number of attractors $(MN + 2)^2 + 1$.

Analyzing the structure of the eigenstates reveals their connection with the effect of trapping. The common eigenstates $|\phi_2(s, t)\rangle$ have finite support. Consequently, these states cannot be sensitive to boundary conditions, thus one can expect that they remain common eigenstates even on an infinite system. Moreover, these states are responsible for the trapping (localization) effect: An initially localized state overlapping with a $|\phi_2(s, t)\rangle$ state can always be found at its initial position with finite probability. The trapping effect for the percolation graph is illustrated in figure 8:2. In addition, the family of pure localized eigenstates $|\phi_2(s, t)\rangle$ form a subspace which is free from the decoherence effects of the dynamical percolation. Such decoherence-free subspace might be quite useful, *e.g.* serve as a quantum memory.

We have to make one more remark about these trapping eigenstates. In the literature of quantum walks localization (trapping) is a phenomena corresponding to the behavior of the system, namely that at the origin the probability of finding the particle is non-vanishing. However, this definition is not really suitable

for all systems, *e.g.* on finite systems, where naturally the wavefunction cannot escape. At the same time, as we have shown in this very section, trapping is due to the appearance of exponentially localized eigenstates. Consequently, we point out that the phenomena called "trapping (localization)" in quantum walks might be more general when it would refer to exponentially localized stationary eigenstates, instead of a recurrence property only meaningful on infinite graphs.

8.4. Conclusions

Moving from one- to two-dimensional quantum walks introduces a lot of new and interesting effects. Similarly, the problem of percolation is much more diverse for two-dimensional lattices. In this Chapter we studied two-dimensional quantum walk models on percolation graphs with different boundaries: the torus and the carpet, corresponding to the periodic and reflective boundary conditions.

The first walk we studied is the two dimensional generalization of the Hadamard walk. We have constructed the attractor space explicitly and pointed out the important differences in contrast with the one-dimensional counterpart: First, the asymptotic distribution of the two-dimensional Hadamard walk can be non-uniform. Second, the percolation can induce a rotational symmetry breaking to the system, which is not observable in the closed system dynamics.

The second model is the Grover walk. Here, we found that the trapping behavior of the closed system surprisingly survives the decoherence effect of the percolation. This is apparent from the common pure eigenstates with finite support. These states are fixed points of the dynamics, moreover they span a decoherence free subspace. Thus they might be used to preserve quantum information. We also have to note that these eigenstates point out that the "trapping (localization)" property of quantum walks can be tied to eigenstates, thus can be generalized to finite graphs, whereas the original definition of localization is only suitable for infinite graphs.

The general problem of two-dimensional walks on percolation lattices requests the solution of the complete $SU(4)$ problem. Practically, this problem would be very cumbersome to solve, and the number of special sub-cases induced by degeneracy would deny any closed form solutions. Nevertheless, subsets of the $SU(4)$ with lower number of parameters might be explored using the methods we showed here.

Chapter 9

Entropy rate of quantum walks

Quantum mechanical systems can be disturbed in several ways. Like in the case of percolation quantum walks, one can couple the system to a noisy environment, making the system open. Another approach is naturally given through quantum mechanics: measurement. One could raise the question: How much quantumness a system can keep if it is frequently measured? Our goal is to connect the answer to this question to the information content of the data obtained from the frequent measurements using the entropy rate.

Entropy rate quantifies the asymptotic per symbol information content of a discrete time stochastic process (which can be a frequently measured quantum system), as we reviewed it in Chapter 2. of Part I. For such stochastic processes the entropy rate replaces the entropy in the asymptotic equipartition property. Classical walks, which are classical Markov chains, are the typical textbook examples for the entropy rate. One can address the previous question from approaching from this direction too: What is the entropy rate of the quantum generalization of the classical walk? Does its entropy rate reflects some of its quantum properties? In this chapter we study these questions in detail. We develop analytical methods to calculate and approximate the entropy rate of periodically measured quantum walks. Through this we intend to investigate the classical-quantum transition in terms of classical information theory.

This chapter is organized as follows: First, we sketch the model we wish to study in Sec. 9.1. Next, to give a reference point, we calculate the entropy rate of certain periodically measured classical random walks. Then, in Sec. 9.3 we define a scenario in which the quantum walks serve as a signal sources. In Sec. 9.4 we give an explicit method to calculate the exact entropy rate of this model. In the following, we explicitly calculate the entropy rate of the one-dimensional Hadamard walk for frequent measurements. Due to the computational complexity of the method giving the exact rate, we give an upper bound protocol through the hidden Markov model, and we determine the scaling of the entropy rates in Sec. 9.6. In Sections 9.7 and 9.8 we discuss two other approaches for calculating the entropy rate: the “most quantum” scenario and the “quantum entropy rate”. Finally, we draw conclusions.

9.1. Periodically measured walks in a black box

We consider the following scenario. Let us assume that we have a source of information in a *black box*. We know that there is a physical process inside, which generates classical messages. However, this process might be either a classical random walk or some quantum process generating classical information. We

post that the quantum process has a well defined classical counterpart: If decoherence is significant, it becomes a classical random walk. A suitable choice is the discrete time quantum walk (QW) (See Chapter 1.1). Assuming such black box, we can utilize the apparatus of classical information theory to compare the classical random walk model with one of its quantum generalizations. There are two reasons behind the usage of the black box terminology: First, we want to hide the quantum or classical walk inside. Second, we restrict the number of tools available: the black box performs all quantum and classical measurements, the only information available is the position measurement outcome. We stress that we do not go beyond the concepts of classical information theory. Instead, we utilize them in order to learn more about the classical-quantum transition: What is the difference between a classical and quantum walk driven black box from the point of view of entropy rates? Does the periodically measured quantum walk keep some of its coherence?

The first problem we encounter is due to the measurement which disturbs a quantum system, thus the measurement protocol should be defined properly. We choose to periodically measure the same quantum walk over and over again. (Another approach would be to perform every measurements on a new, undisturbed system: we address this most-quantum scenario later.) The next problem is due to the correspondence of quantum walks with classical walks: Frequent position measurements, mean a strong decoherence for QWs, thus a classical walk. We overcome this problem by making the measurements less frequent, *i.e.* the walker residing in the black box are not measured after every single steps, but we let it evolve for more steps. In this way we hope that some of the characteristic quantum behaviors of the system can be observed in the entropy rate. In the following we determine the entropy rate of periodically measured classical walks to give a reference point for the quantum case.

9.2. Entropy rate of some classical random walks

We remark here that for a general classical walk as a stationary Markov process, the entropy rate, according to Eq. (2:13), is the average of the entropy of the rows of the probability transition matrix taken with the stationary probability of each vertex ⁷. In particular, if the stationary distribution is uniform and, for some symmetry reason, the rows are permutations of each other (thus having the same entropy), the entropy rate is simply the entropy of a row. That is, in the graph picture, the process is equivalent to a sequence of independent identically distributed random variables describing the random decision taken by the walker in each step. This reasoning will be applicable in some of the cases we discuss here. An unbiased (isotropic) classical random walk (CW) on a d -regular simple graph, for instance, has the entropy rate of $\log_2 d$: wherever we find the walker, it has d equal-probability edges to follow (isotropy),

⁷ As each row corresponds to a vertex where the walker may stand in a step, and each column to an edge pointing to a possible vertex it can jump to.

and the stationary distribution is obviously uniform. Hence, in this model, for every step we need $\log_2 d$ classical bits to encode the direction where the walker has moved randomly.

Now let us consider a simple one-dimensional walk on a finite cycle with M vertices, *i.e.* the walker in every steps moves one step to the left or to the right with the same $1/2$ probability. Suppose, that we intend to encode the position only at every w -th step of the walk. That is, the position of the walker is measured at every w -th steps. We call the parameter w as *waiting time*, which will also be the time we wait between two subsequent quantum measurements in the corresponding quantum protocol. The system under consideration is translation-invariant (homogeneous in space): The transfer probabilities $P_{x \rightarrow x+\delta}$ between arbitrary lattice sites x and $x + \delta$ depend only on the difference (distance) δ of the two sites. Thus, we can introduce the probability of a δ length step

$$p(\delta) \equiv P_{x \rightarrow x+\delta}. \quad (9:1)$$

In systems obeying this symmetry, it is common to encode the difference δ of the actual random position outcome from the previous random outcome, leading to the usage of at most $w + 1$ symbols, thus a finite alphabet. It is straightforward to see that the two encoding methods — encoding the absolute position outcomes and encoding the relative position differences — are equivalent. From (2:13) and (9:1) one can readily give the entropy rate as

$$H_w^{\text{CW}} = - \sum_{\delta=-w}^w p(\delta) \log_2 p(\delta), \quad (9:2)$$

which after a short calculation results in

$$\begin{aligned} H_w^{\text{CW}} &= 2^{-w} \sum_{i=0}^w \binom{w}{i} \left\{ w - \log_2 \binom{w}{i} \right\} \\ &\approx \frac{1}{2} (-1 + \log_2 \pi e w), \end{aligned} \quad (9:3)$$

which is the Shannon entropy of the binomial distribution and the Gaussian distribution respectively. Note that the $1/2$ pre-factor is a consequence of the diffusive spreading of the CW. Note that Eq. (9:3) is valid for both infinite and finite systems, as long as $w \ll M$. For finite M and rates that are high enough (in one-dimensional cycle graphs, for instance, this occurs for $w > M/2$), the walker mixes with itself, making the rate given by Eq. (9:3) inaccurate. In this case the sequence becomes a series of independent random variables with a uniform distribution over the accessible positions, thus the entropy rate becomes

the upper bound of the possible entropy rates,

$$H_{\text{limit}} = \begin{cases} \log_2 M & \text{for odd } M \\ -1 + \log_2 M & \text{for even } M \end{cases}. \quad (9:4)$$

The difference caused by the parity is due to the fact that the positions accessible for the walker may be restricted. In a one-dimensional cycle graph with even number of sites (M), the walker, from a given position, can reach either the even or the odd labeled sites only, depending on the waiting time w . Therefore, even for the limiting $w \gg M$, only half of the sites can be reached by the walker. For cycles with an odd number of sites, this restriction does not hold. Naturally, for an infinite line ($M \rightarrow \infty$) the upper limit of Eq. (9:4) does not exist and the entropy rate is always given by (9:3).

We can conclude that the entropy rate of a process arising from a one-dimensional classical walk with waiting time w is simply the Shannon entropy of the distribution of the shifts. Note that for the sake of readability the sum in Eq. (9:2) is taken between $-w$ and w ; however, since the classical walker leaves its position in every step, there is a parity correspondence between w and $p(\delta)$, thus we have $w + 1$ symbols to encode at most. In the next section we extend the concept of entropy rate to sources driven by quantum walks by closely following the procedure presented in this section.

9.3. Discrete time quantum walks as stochastic processes

We consider discrete time quantum walks (QWs), as defined in Section 1.1.1, thus, following the time evolution in Eq. (1:7). We repeat here that quantum walks are unitary, thus deterministic processes. However, we wish to use them as the source of messages (classical random variables). Thus, we have to introduce measurement into the system. We closely follow the procedure we employed for the classical case in the previous section: We let the walker evolve unitarily for w steps and we measure its position afterwards. This is the definition of a single iteration step in our process. Following that, we repeat this iteration step over and over on the same system. Should someone measure the position of the walker, she will get a random position x with probability

$$p(X_k = x) \equiv \sum_{c'} |\langle x, c' | \psi_k \rangle|^2, \quad (9:5)$$

where $|\psi_k\rangle = U^w |\psi_{k-1}\rangle$ is the Hilbert vector corresponding to the quantum state of the QW at the k th iteration step. The corresponding X_k is the random variable describing the position outcome at the k th iteration. From now on, we consider the sequence of X_k random variables as the stochastic process generating the message we wish to encode efficiently — *i.e.* X_k realizes (describes) the output of the

quantum walk equipped black box.

As it is given in Eq. (1:7), the QWs considered here are translation-invariant (homogeneous):

$$\langle y, c|U^t|x, c\rangle \equiv \langle y \oplus \delta, c|U^t|x \oplus \delta, c\rangle \quad \text{for all } x, y, t, \delta, c. \quad (9:6)$$

Consequently, in place of encoding the x_k measurement outcomes, one can encode position differences $\delta = x_k - x_{k-1}$. Note that this encoding simplification does not affect the value of the entropy rates. In fact, it is the standard notation for systems with translation invariance⁸.

The proposed definition of a QW-driven message source has a well-defined classical connection: Should one consider an unbiased coin matrix C (with all complex elements having the same absolute value in the natural (computational) basis), a quantum walk measured in every single step (waiting time $w = 1$) behaves exactly like a classical unbiased (isotropic) walk.

Throughout this chapter we will use the 2×2 Hadamard matrix (*cf.* Eq. (1:15))

$$C_H = \frac{1}{\sqrt{2}} \begin{pmatrix} 1 & -1 \\ 1 & 1 \end{pmatrix}, \quad (9:7)$$

driven one-dimensional quantum walks as our concrete example, unless stated otherwise. We use the Hadamard coin since it is unbiased, thus we have a very well controlled quantum-classical transition at our hands: measuring the walk after every steps ($w = 1$) results a classical walk.

9.4. Solution — employing the quantum Markov property

This section is dedicated to derive an explicit formula giving the entropy rate of periodically measured QWs in the black box. To achieve this we will use the quantum Markov chain nature of discrete time quantum walks, and employ the coin state as a key encoding aid while doing so. We will formally address the one-dimensional problem, but we stress that the results we give here could be generalized for higher dimensional QWs in easily.

To begin, we calculate the joint probability distribution $p(x_N, x_{N-1}, \dots, x_1)$ of the possible black box outputs (position measurement outcomes). Employing Eq. (9:5), the joint probability distribution of the random variable sequence X_k is given by

$$p(x_N, x_{N-1}, \dots, x_1) = \text{Tr} \left(S_{x_N} U^w S_{x_{N-1}} U^w \dots S_{x_1} U^w \rho_0 (U^w)^\dagger S_{x_1} \dots (U^w)^\dagger S_{x_{N-1}} (U^w)^\dagger S_{x_N} \right), \quad (9:8)$$

⁸ Equivalently, the original problem can be rephrased so the black box outputs the relative position differences δ instead of absolute positions. This rephrasing does not change the entropy rate of the system.

where

$$S_x = |x, R\rangle\langle x, R| + |x, L\rangle\langle x, L| \quad (9:9)$$

is the projector of the von Neumann measurement corresponding to the position $|x\rangle_P$ (*cf.* Eq. (1:9)) and $\rho_0 = |0, c_0\rangle\langle 0, c_0|$ is the initial state of the one-dimensional QW in the black box. Next we employ the definition in Eq. (2:2) to obtain the entropy rate. We stress that we have to use the original definition as we are not considering a classical Markovian process here — in contrast with classical walks which are always Markovian processes.

Calculating (9:8) and therefore the actual entropy rate in the asymptotic limit is demanding. In fact, if one would wish to calculate it using brute force methods, one would encounter an exponential usage of resources. In the following, we present a method to make the calculation manageable. It is based on the fact that the transition probabilities between subsequent measurement outcomes depend on a parameter which in fact can be taken into account: It is the internal quantum coin state, which carries additional information in the following sense.

After every position measurement, the wave function collapses to a single position site, but the information carried in the coin degree of freedom that particular site survives the process: It serves as the initial coin state in the following iteration. After acquiring any position measurement outcome (a black box output) $X_k = x$, since the evolution of QW is unitary (deterministic) until the position measurement, the full quantum state of the actual collapsed QW can be reconstructed with the knowledge of the full quantum state of the preceding (initial) iteration. In summary, the coin degree of freedom serves as a memory, carrying some information about the previous steps. The importance of this observation is twofold: First, the information carried in this internal memory can be used to improve our encoding method. Second, we use the coin to aid our calculation of the joint probability distribution, thus the entropy rate.

One can argue that all unitary quantum walks are quantum Markov chains by construction, thus the coin is not really a memory but it describes the *state* (as in information theory) of the quantum system in the actual iteration step. However, here we consider a function of the original quantum Markov chain (the quantum walk), *i.e.* we just gather the position measurement outcomes. With this respect the black box outputs can be described with a hidden Markov model, where the original (underlying) Markov chain is a quantum Markov chain: the two are connected with the nonlinear function of the position measurement process. However, as we have described above, this function can be inverted, *i.e.* the coin state can be determined, and used to predict outcomes, making the output encoding efficient. In this sense, our encoding might be considered as the actual efficient encoding of the periodically measured quantum Markov chain, since all quantum states of the time evolution can be reconstructed from the

classical data. This observation is one of our main results.

Let us employ this knowledge to solve the entropy rate problem. We intend to use the coin as the hidden continuous parameter of the model, by introducing an extended, $P_{x,\alpha \rightarrow y}$ stochastic transition matrix, where α is an abstract continuous parameter representing the internal coin state. The definition of the transition matrix is

$$P_{x,\alpha \rightarrow y} \equiv \text{Tr} \left\{ S_y U^w |x, \alpha\rangle \langle x, \alpha| (U^w)^\dagger \right\}. \quad (9:10)$$

Suppose that we know the initial (previous) quantum state of the system. The quantum state of the next iteration step can be calculated as follows:

$$|y\rangle_P \otimes |\mathcal{C}(x, y, \alpha)\rangle_C \equiv \frac{S_y U^w |x, \alpha\rangle}{\sqrt{\text{Tr} \{ S_y U^w |x, \alpha\rangle \langle x, \alpha| (U^w)^\dagger \}}}, \quad (9:11)$$

where we defined function $\mathcal{C}(x, y, \alpha)$ giving the unambiguous coin state. By employing these definitions in Eqs. (9:8) and (9:9) we arrive to

$$p(x_N, x_{N-1}, \dots, x_1) = P_{0, c_0 \rightarrow x_1} P_{x_1, c_1 \rightarrow x_2} P_{x_2, c_2 \rightarrow x_3} \dots P_{x_{N-1}, c_{N-1} \rightarrow x_N}, \quad (9:12)$$

where $c_i = \mathcal{C}(x_{i-1}, x_i, c_{i-1})$ and c_0 corresponds to the initial coin state.

Let us use the translation invariance (9:6) of the system. We shall see that

$$p_c(\delta) \equiv P_{x, c \rightarrow x+\delta} = P_{y, c \rightarrow y+\delta} \quad (9:13)$$

and

$$\mathcal{C}(\delta, c) \equiv \mathcal{C}(x, x + \delta, c) = \mathcal{C}(y, y + \delta, c) \quad (9:14)$$

for all values of x , y , and δ . Thus

$$p(x_N, x_{N-1}, \dots, x_1) = p \left(\sum_{i=1}^N \delta_i, \sum_{i=1}^{N-1} \delta_i, \dots, \delta_1 \right) = p_{c_0}(\delta_1) p_{c_1}(\delta_2) \dots p_{c_{N-1}}(\delta_N), \quad (9:15)$$

where $c_i = \mathcal{C}(\delta_i, c_{i-1})$ and $\delta_i = x_i - x_{i-1}$ with $x_0 = 0$. Note that the product form of the probability indicates the true Markov chain like nature of the system: The probability of any outcome can only depend on the previous quantum state of the system, that is, the internal coin state and its position (which is

in the δ difference picture is neglected due to translation invariance). Moreover, this description reveals that the system in question is time invariant, in the sense that the defining matrices $P_{x,\alpha \rightarrow y}$ are time independent. Formulated in other way, the solutions of the system are invariant under shifting of the time (see Eq. (2:4)). This will allow us to employ the definition of entropy rate for time stationary processes in Eq. (2:5).

The Shannon entropy of the joint distribution (9:15) can be calculated readily using the chain rule as

$$\begin{aligned} H(X_N, X_{N-1}, \dots, X_1) &= \sum_{i=1}^N H(X_i | X_{i-1}, \dots, X_1) \\ &= - \sum_{i=1}^N \sum_{\alpha \in \text{CS}} \nu_{i-1}(\alpha) \sum_{\delta=-w}^w p_\alpha(\delta) \log_2 p_\alpha(\delta), \end{aligned} \quad (9:16)$$

where

$$\nu_i(\alpha) = \sum_{\delta=-w}^w \sum_{\beta \in C^{-1}(\delta, \alpha)} \nu_{i-1}(\beta) p_\beta(\delta), \quad (9:17)$$

gives the distribution of coin states at the i th iteration step. Here,

$$C^{-1}(\delta, \alpha) \equiv \{ \beta \in \text{CS} \mid \mathcal{C}(\delta, \beta) = \alpha \}, \quad (9:18)$$

and

$$\nu_0(\alpha) \equiv \delta_{\alpha, c_0}. \quad (9:19)$$

In our notation, the δ symbol with two indices (δ_{α, c_0}) is the Kronecker δ . By CS we denote the continuous set of all abstract coin states. The entropy rate is then given by taking the limit as in Eq. (2:2),

$$\begin{aligned} H(\mathbf{X}) &= \lim_{N \rightarrow \infty} \frac{1}{N} H(X_N, X_{N-1}, \dots, X_1) \\ &= - \lim_{N \rightarrow \infty} \frac{1}{N} \sum_{i=1}^N \sum_{\alpha \in \text{CS}} \nu_{i-1}(\alpha) \sum_{\delta=-w}^w p_\alpha(\delta) \log_2 p_\alpha(\delta). \end{aligned} \quad (9:20)$$

Since we discovered the time invariant (quantum) Markov chain nature of the system, we can employ the

alternative definition (2:5) of the entropy rate. Thus,

$$\begin{aligned}
 H(\mathbf{X}) &= H'(\mathbf{X}) = \lim_{N \rightarrow \infty} H(X_N | X_{N-1}, \dots, X_1) \\
 &= - \lim_{N \rightarrow \infty} \sum_{\alpha \in \text{CS}} \nu_{N-1}(\alpha) \sum_{\delta=-w}^w p_\alpha(\delta) \log_2 p_\alpha(\delta) \\
 &= \sum_{\alpha \in \text{CS}} \mu(\alpha) \cdot H(p_\alpha(\delta)),
 \end{aligned} \tag{9:21}$$

where $\mu(\alpha) = \lim_{N \rightarrow \infty} \nu_N(\alpha)$ is the asymptotic distribution of coin states ⁹.

In summary, the method of calculating the entropy rate is the following: First, one should determine the asymptotic coin distribution $\mu(\alpha)$. Then $p_\alpha(\delta)$ shift probabilities can be determined easily using formulas in Eqs. (9:10) and (9:13). Finally, the entropy rate can be obtained using (9:21). Note that the method proposed here can be applied directly for both finite or infinite systems. Also it can be extended in a straightforward way to higher dimensional quantum walks, as we have not used the dimensionality of the walk. The remaining task at hand is to determine the asymptotic coin state distribution $\mu(\alpha)$, which we address in the following section.

9.5. Calculating the entropy rate of one-dimensional QWs

So far we have found that the quantum Markov chain nature of QWs can be employed to formally determine the entropy rate of the periodically measured system in the black box. However, we are yet to obtain any exact values for the entropy rate. Only one step is missing, which is to calculate the asymptotic coin distribution $\mu(\alpha)$. In this section we show a way to determine the asymptotic coin distribution, and also explicitly calculate the entropy rate of some QWs.

The asymptotic coin distribution $\mu(\alpha)$ can be calculated by defining a stochastic matrix,

$$P_{\alpha \rightarrow \beta} = \sum_{\delta=-w}^w \sum_{\chi \in C^{-1}(\delta, \beta)} \delta_{\alpha, \chi} p_\chi(\delta), \tag{9:22}$$

which gives the probability that from an α coin state after applying U^w the walker is found in the β coin state after the position measurement. It is straightforward to see that $P_{\alpha \rightarrow \beta}$ is indeed a stochastic

⁹ Coins states CS does not form a continuous set due to the discrete rotation of the coin operator, thus a summation symbol in Eq. (9:21) is sufficient.

matrix,

$$\begin{aligned} \sum_{\beta \in \text{CS}} P_{\alpha \rightarrow \beta} &= \sum_{\beta \in \text{CS}} \sum_{\delta=-w}^w \sum_{\chi \in C^{-1}(\delta, \beta)} \delta_{\alpha, \chi} p_{\chi}(\delta) \\ &= \sum_{\delta=-w}^w p_{\alpha}(\delta) = 1. \end{aligned} \quad (9:23)$$

After constructing the complete $P_{\alpha \rightarrow \beta}$ transition matrix, the $\mu(\alpha)$ asymptotic coin distribution can be readily found as the stationary state of the stochastic matrix $P_{\alpha \rightarrow \beta}$. One can see that the number of coin state “touched” during the time evolution can be infinite. That would yield an infinite stochastic matrix. We will address this problem later in the current section.

One-dimensional QWs have some symmetries which can be employed to make the calculation of the transition matrix more efficient. First, one-dimensional QWs have a spin-flip symmetry. This symmetry implies that, compared to the general initial coin state $l|L\rangle_C + r|R\rangle_C$, the orthogonal $r^*|L\rangle_C - l^*|R\rangle_C$ produces a mirrored position probability distribution. We use a single important consequence of this property: A walk started from $|L\rangle_C$ produces the exact same amount of entropy for any w waiting times as the walk started from $|R\rangle_C$, *i.e.*

$$H(p_L(\delta)) = H(p_R(\delta)) . \quad (9:24)$$

Second, for one-dimensional Hadamard QWs,

$$P_{\alpha \rightarrow L} + P_{\alpha \rightarrow R} \geq 2^{(1-w)} \quad \text{for all } \alpha \in \text{CS} . \quad (9:25)$$

Moreover, for arbitrary mixing coins of one-dimensional QWs using the coin operator

$$C = \begin{pmatrix} e & -f \\ f^* & e^* \end{pmatrix} \quad (9:26)$$

with $|f|^2 + |e|^2 = 1$ and $e, f \neq 0$

$$P_{\alpha \rightarrow LR} \equiv P_{\alpha \rightarrow L} + P_{\alpha \rightarrow R} \geq |e|^{2(w-1)} \quad \text{for all } \alpha \in \text{CS} . \quad (9:27)$$

Here, we defined the summarized transition probability for the abstract “joined” coin state LR . This property has an immediate consequence: The black box based on a QW always forgets its initial state. Since from an arbitrary coin state a transition to LR happens according to Eq. (9:27) the part carrying information about the initial state c_0 at the iteration step k is proportional to $(1 - |e|^{2(w-1)})^k$, which in the asymptotic $k \rightarrow \infty$ limit tends to 0. This observation is one of our main results.

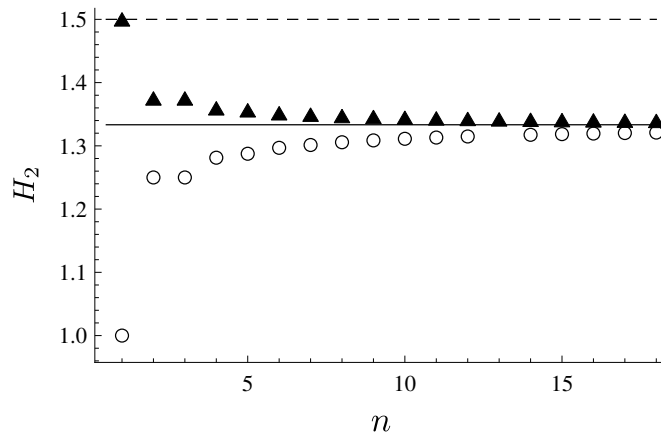


Figure 9:1. Convergence of the numerically calculated partial entropy rate [*cf.* Eq. (2:9)] H_2 for $w = 2$ waiting time. We have evaluated the definition of Eq. (2:2) for the first n iteration steps, using the joint probability distribution in Eq. (9:8). We used the one-dimensional QW with Hadamard coin (see Eq. (9:7)); the triangles and circles correspond to the walk started from initial states $|\psi_0\rangle = |0, L\rangle$ and $|\psi_0\rangle = \frac{1}{\sqrt{2}}(|0, L\rangle + |0, R\rangle)$, respectively. The continuous line corresponds to the analytically determined rate for the simulated model: $H_2^{\text{QW}} = 4/3$ bits. The dashed line corresponds to the rate of the CW: $H_2^{\text{CW}} = 3/2$ bits.

Using the method we have given above it is straightforward to determine the entropy rate of the QW with $w = 2$ as the simplest, nontrivial case,

$$H_2^{\text{QW}} = \frac{4}{3} \text{ bits.} \quad (9:28)$$

The details of the exact calculation using this approach can be seen in Appendix A. For reference, the entropy rate of the classical walk for $w = 2$ is $3/2$ bits as given by Eq. (9:3). We numerically approximated the entropy rate using the original definition of Eq. (2:2), for finite n 's [*cf.* Eq. (2:9)]. We illustrate the results in FIG. 9:1. The $4/3$ bits rate associated with QWs contradicts the assumption that due to ballistic spreading the entropy rate should be higher. In fact, revealing the coin as a carrier of information, thus extracting more information from simple position measurement outcomes, allows for a more efficient prediction of the next step, essentially leading us to a more efficient source coding method — and a lower entropy rate. However, it should be noted that for higher w waiting times the ballistic spreading will eventually dominate the scaling of the entropy rate, *i.e.* the rate of the QW will surpass the rate of the CW. We discuss this question in the next section.

The above given process is adequate when $\mu(\alpha)$ is nonzero for only a finite number of α coin states, *i.e.*, the number of coin states arising under the full time evolution is finite. In this case, the size of $P_{\alpha \rightarrow \beta}$ is finite too. However, depending on the coin operator and the waiting time we choose, the $P_{\alpha \rightarrow \beta}$ matrix can grow to infinite size. This issue can be solved by introducing a truncated (finite) basis. This will cause an uncertainty in the entropy rate. Let us introduce the set of unknown coin states: $|\text{?}\rangle_C$, which we use when we do not wish to consider (calculate) the elements of $P_{\alpha \rightarrow \beta}$ further. In other words, the

abstract set “?” collects all the coin states which the system does not touch up to the iteration step k , i. e.,

$$? = \{\alpha \in CS \mid \nu_i(\alpha) = 0 \text{ for all } i \in [0, k]\}, \quad (9:29)$$

where $\nu_i(\alpha)$ is the coin state distribution at the i th iteration step as given in Eq. (9:17). It is important to note that the rule of Eq. (9:27) applies to “?” as well, and it should be employed to make the truncated $P_{\alpha \rightarrow \beta}$ matrix a proper stochastic matrix.

Since the value $H(p_?(\delta))$ is unknown, Eq. (9:21) cannot be used. Fortunately, bounds for $H(p_?(\delta))$ can be calculated in a straightforward manner as

$$H_{\max} = \max_{\alpha \in CS} H(p_\alpha(\delta)) \quad (9:30)$$

and

$$H_{\min} = \min_{\alpha \in CS} H(p_\alpha(\delta)). \quad (9:31)$$

Considering this, the value of the exact entropy rate (9:21) are in the interval

$$H(\mathbf{X}) = \sum_{\alpha \notin ?} \mu(\alpha) \cdot H(p_\alpha(\delta)) + \frac{\mu(?)}{2} (H_{\max} + H_{\min} \pm \{H_{\max} - H_{\min}\}). \quad (9:32)$$

We use the compact form with a \pm sign to denote the interval where the exact entropy rate resides.

The now proposed truncating method can be applied to approximate the entropy rates for arbitrary w 's. We note that by increasing w the size of stochastic matrices grows rapidly:

$$\dim(P_{\alpha \rightarrow \beta}) \approx \frac{1}{w-2} \left[(w-1)^{k+1} - 1 \right] + 1, \quad (9:33)$$

where k is the number of iterations of the procedure we take during the calculation of the matrix ($P_{\alpha \rightarrow \beta}$) — and is also in the definition (9:29). Similarly, the scaling of $\mu(?)$ can be approximated as it is proportional to the relative error of the calculated entropy rate. After a lengthy, but straightforward calculation this turns out to be

$$\mu(?) \approx (1 - |e|^{2(w-1)})^{k+1}, \quad (9:34)$$

where we used $|e|^{2(w-1)}$ from Eq. (9:27). If we fix the precision (the value of $\mu(?)$) and the coin (parameter e) in the last expression, we find that with the increase of w the number of iterations k needed to achieve a fixed precision increases exponentially. Despite the problem blows up exponentially with the increase

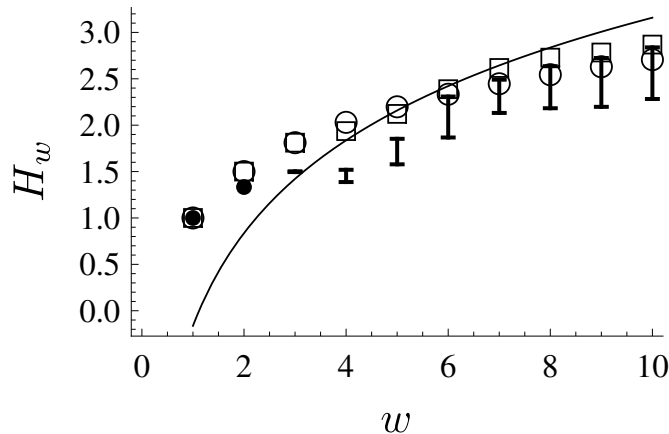


Figure 9:2. Entropy rates H_w of the periodically measured walks on a one-dimensional line as functions of waiting time w . The circles correspond to the entropy rate H_w^{CW} (see Eq. (9:3)) of the classical walk. We used the Hadamard coin of Eq. (9:7) for the quantum walk. The black disks correspond to the exactly calculated entropy rate H_w^{QW} given by Eq. (9:21), while the vertical line segments correspond to the interval defined by the lower and upper bound on the entropy rate in Eq. (9:32). The number of iterations is given in Table I. The rectangles correspond to the upper bound entropy rate H_w^{bound} defined in Section 9.6, while the continuous line represents the analytic approximation H_w^{approx} of Eq (9:41).

of w , we found that our method converges much faster than mere brute force simulation. This is due to the fact that the approximations (9:33) and (9:34) are based on a worst-case scenario, while as it can be seen in the explicit calculations, the convergence of the $\mu(\alpha)$ distribution is much better. Also, we have to note that our method aimed to calculate the entropy rate only, whereas in brute force simulations one would calculate the total joint probability distribution and then employ the basic definition — which is naturally much more resource consuming. To achieve an even lower computational cost in our method, one can extend the proposed simplifications — by use of the spin flip symmetry — in order to find further isentropic states like the ones in Eq. (9:24).

We have also determined the entropy rate of $w = 3$ walks using the given methods. For the one-dimensional Hadamard QW the approximative calculation resulted

$$H_3^{\text{QW}} = 1.499 \pm 0.004 \approx 3/2 \text{ bits}. \quad (9:35)$$

In comparison, the CW walk has the entropy rate of $H_3^{\text{CW}} = 3 - (3 \log_2 6)/(8 \log_2 2) \approx 2.031$ bits. The details of the calculation can be seen in Appendix B. We illustrate our results in Fig. 9:2 and Table I.

In the following we give an upper bound for the now determined entropy rate which is easier to measure or compute. We will also discuss the scaling of the entropy rate of QWs with respect to the waiting time w .

| w | Number of iterations |
|-------|----------------------|
| 3 | 11 |
| 4 | 10 |
| 5 | 10 |
| 6 | 4 |
| 7 | 4 |
| > 7 | 3 |

Table I. Number of iterations used to calculate entropy rate for the periodically measured quantum walk illustrated in Fig. 9:2. The rapid drop in the number of iterations for $w \geq 6$ is due to the memory limitation of the current implementation.

9.6. Upper bound for the entropy rate

Here we describe a protocol which will give us an easy-to-understand and compute upper bound to the entropy rates of QWs. If one is not aware of the quantum nature of the walk on which the information source (the black box) is based, she or he might follow a measurement protocol which is suitable for classical walks, thus ignoring the internal quantum coin state. In this case the outputs of the black box are assumed to be described by a classical Markov chain. The absence of the additional information carried by the coin leads to a less efficient encoding and, thus, higher entropy rates. This statement is also supported by the fact that a function of a Markov chain — a hidden Markov chain — has a higher or equal entropy rate than the original chain [141], meaning essentially an upper bound (and lower encoding efficiency).

Let us propose the protocol which ignores the hidden coin (memory) of the QW in the black box. The measurement protocol consists of the following steps:

1. Initialize the black box: this puts the walker to state $|0, c_0\rangle$. Set position indicator $x = 0$.
2. Let the black box work: The walk evolves for w steps. Following, the black box von Neumann measures the position. Finally, the black box outputs a random position outcome $y \in [x \ominus w, x \oplus w]$.
3. Make a note that a $x \rightarrow y$ transition happened.
4. Repeat from 2. with y (the current position state) as the new x .

After applying the protocol above for infinitely many times, the probabilities of $x \rightarrow y$ transitions can be calculated as relative frequencies. In this way, a stochastic transition matrix $P_{x \rightarrow y}$ describing the QW-driven process is obtained. We stress that in this way it is implicitly assumed that the system can be described via a time stationary classical Markov chain — which is not true for the QW based system. Finally, the entropy rate is calculated using Eq. (2:13).

We again use the translation invariance (See. Eq. (9:6)) of the system to get rid of the infinite alphabet (positions): instead of absolute positions we encode the δ shifts. Like in the classical case, we

introduce $p(\delta)$ by Eq. (9:1), which is the probability of a δ length shift. Finally, the upper bound entropy rate H_w^{bound} can be readily determined by Eq. (9:2): It is the Shannon entropy of the distribution of the arising position differences (shifts) in the stationary case.

We numerically calculated the upper bound for one-dimensional QW and the actual entropy rate of one-dimensional CW-driven black boxes using the above upper bound protocol. We used the Monte Carlo method to numerically simulate the behavior of the black boxes, repeating the protocol until $p(\delta)$ appeared to converge. We found that $p(\delta)$ corresponding to the one-dimensional QW in all cases converges to

$$p(\delta) = \sum_{c=\{L,R\}} \text{Tr} \left\{ |\delta, c\rangle \langle \delta, c| U^w \tilde{\rho}_0 (U^w)^\dagger \right\}, \quad (9:36)$$

where

$$\tilde{\rho}_0 = \frac{1}{2} \left(\sum_{c'=\{L,R\}} |0, c'\rangle \langle 0, c'| \right) \quad (9:37)$$

is a state localized at a single position with a completely mixed coin. Note that since $\tilde{\rho}_0$ is completely mixed in coin space, the effect of the initial $|c_0\rangle$ is lost, which is expected for a Markov chain. This result is in perfect agreement with our result given in the previous section: The system always forgets its initial state.

To illustrate the possible effects appearing on finite systems, we also performed simulations with finite M -cycles (one-dimensional cycle graphs with M vertices). Increasing w beyond $M/2$ in such a system causes an interesting effect: The CW starts to evolve towards the uniform distribution. As a consequence, the entropy rate becomes close to its absolute bound H_{limit} defined in Eq. (9:4). In contrast to that, QWs do not mix due to the unitary nature of the system. Consequently, the self-overlap of the wave function might induce fluctuations in the entropy rate. In this self-overlapping regime the entropy production of CWs are usually higher.

Increasing the w waiting time even further, the unitary nature of QWs eventually produces more interesting effects in finite systems: a behavior similar to collapses and revivals [178] can be observed in the upper bound of entropy rate as a function of w and in the entropy rate itself. The appearance of these phenomena demonstrates the fundamental difference between the unitary and stochastic time evolutions. We illustrate these results in Fig. 9:3.

The result in Eq. (9:36) allows us to approximate the scaling of the entropy rate. For the approximation we use the weak limit theory of quantum walks [161–163]. For high number of unitary steps (high w 's) the shape of the symmetric probability distribution of a one-dimensional Hadamard QW can

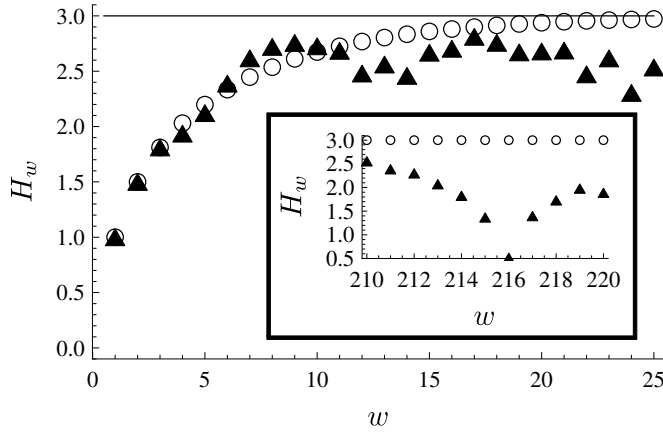


Figure 9.3: Entropy rate H_w of periodically measured walks as the function of waiting time w . We used QW (triangles) with Hadamard coin (see Eq. (9:7)) and the unbiased CW (circles) on the cycle graph with 16 vertices. For the QWs we plotted the protocol giving the upper bound. The straight line corresponds to the theoretical entropy rate limit of Eq. (9:4): $H_{\text{limit}} = \log_2 M - 1 = 3$ bits. In the inset plot, we show traces of the collapse and revive like effects on the same system for high w waiting times: For $w = 216$ the time evolution operator comes very close to a simple permutation matrix, resulting in a very predictable behavior and an entropy rate upper bound $H_{216}^{\text{bound}} \approx 0.514$ bits. Meanwhile, the CW is totally mixing, resulting in an unpredictable outcome, with the maximal possible entropy rate $H_{\text{limit}} = 3$ bits. We calculated all plotted data numerically using the Monte Carlo method until convergence occurred.

be approximated with the formula

$$p(x, w) = \frac{1}{\pi w \sqrt{1 - \frac{2x^2}{w^2}} \left(1 - \frac{x^2}{w^2}\right)}. \quad (9:38)$$

This weak limit is valid for $x \in [-w/\sqrt{2}; w/\sqrt{2}]$. Note that this distribution corresponds to the rescaled asymptotic position distribution of the Hadamard walk started from the initial state localized at the origin, with a totally mixed initial coin state $\tilde{\rho}_0$, as in Eq. (9:37). Consequently,

$$p(\delta) = p(x, w)|_{x=\delta}. \quad (9:39)$$

Employing (9:2) the upper bound of the entropy rate can be readily approximated by the integral

$$H_w^{\text{approx}} = - \int_{-w/\sqrt{2}}^{w/\sqrt{2}} p(x, w) \cdot \log_2 p(x, w) dx, \quad (9:40)$$

which evaluates to

$$H_w^{\text{approx}} \approx -0.163164 + \log_2 w. \quad (9:41)$$

It is apparent that the scaling of the upper bound of entropy rate goes with $\log_2 w$, in contrast with the scaling of the classical system (*cf.* Eq. (9:3)), which goes with $\approx 1/2 \log_2 w = \log_2 \sqrt{w}$. This result

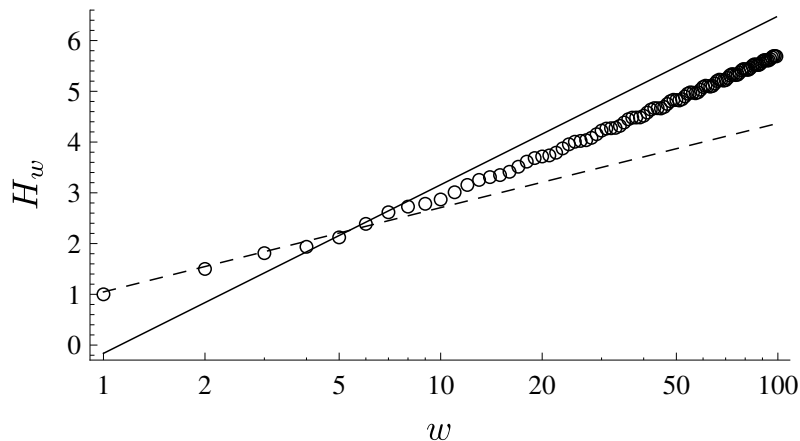


Figure 9:4. Upper bound of the entropy rate H_w^{bound} of a one-dimensional QW with Hadamard coin (see Eq. (9:7)), denoted by circles, for infinite or finite ($w \ll M$) systems. We used high precision numerical simulations on cycles with ($w \ll M$), and plotted the converged results. The dashed line corresponds to the analytically calculated entropy rate of CWs (see Eq. (9:3)), while the continuous line corresponds to the weak-limit-based approximation of Eq. (9:41).

can be interpreted as the consequence of the ballistic spreading of the QW. Our numerical calculations showed that although the weak limit theorem predicts the $\log_2 w$ scaling in the long time limit, the actual scaling of the upper bound rate is for lower waiting times are still close to the classical $\log_2 \sqrt{w}$. Even for the regime around $w \approx 500$, we obtained scaling with $\log_2 w^{0.94}$. We illustrate these results in Fig. 9:4.

We move on to discuss the scaling of the exact entropy rate H_w^{QW} . Using the weak limit approach calculating integrals similar to (9:40) reveal the scaling of other initial states, i. e., the initial states giving the maximum and minimum entropy production H_{max} and H_{min} of (9:30) and (9:31). In both cases the scaling is proportional to $\log_2 w$, consequently, the precisely calculated H_w^{QW} entropy rate is also scales with $\log_2 w$. Thus, the ballistic spreading dominates the entropy rate for high w values.

In summary, the measurement protocol proposed in this section gives a straightforward way to measure, calculate, and approximate the upper bound of entropy rates of QW driven message sources. Since, the exact entropy rate can be quite hard to calculate, the easy-to-calculate and -measure upper bound is a proper tool for distinguishing walks by their entropy production if the waiting times w is long enough. We summarize the results given by all proposed methods in Fig. 9:2.

9.7. Analysis of independent systems — the “most quantum” case

The walkers living in the black box are measured periodically. During the definition of the system, we explicitly stated that all measurements are performed on the same system. Every measurement means a loss of coherence for quantum walks — thus a step towards the classical world. One can consider the “most quantum” case, when at every iteration step the position measurement is carried out on a

new, undisturbed system. That is, in the first iteration step we perform a position measurement on a QW which took w undisturbed steps, and then we discard the system. In the second iteration step, we perform a position measurement on another QW which took $2w$ undisturbed steps, and then we discard the system. All further steps are performed accordingly. In fact, this “most quantum” approach is quite popular in the literature of quantum walks, for example works dealing with the recurrence properties [150–153] and hitting times [35, 147] use this approach.

For the most quantum case the X_k sequence of stochastic variables is given by

$$p(X_k = x) = |S_x U^{w \cdot k} |0, c_0\rangle|^2, \quad (9:42)$$

where S_x is the position measurement projector given in (9:9) and c_0 is the initial coin state of the QW. Since the quantum systems are all independent, there are no correlations between subsequent measurements, *i.e.* all X_k 's are independent random variables. In this case, the entropy rate calculation reverts back to the calculation of the Shannon entropy (*cf.* Eq. (2:14)):

$$H^{\text{mq}} = \lim_{k \rightarrow \infty} H(X_k). \quad (9:43)$$

Let us use our result about the scaling of the Shannon entropy for one-dimensional QWs on the infinite line

$$H(X_k) \approx \log_2 k. \quad (9:44)$$

Employing this, the entropy rate of the system is

$$H^{\text{mq}} = \lim_{k \rightarrow \infty} H(X_k) = \lim_{k \rightarrow \infty} \log_2 k = \infty. \quad (9:45)$$

This divergent result is a straightforward consequence of the spreading of the system on an infinite line. In fact, one would obtain the same result for the entropy rate of independent classical walks.

Still, one can address a question about the entropy rates on finite systems. For the classical case on finite cycles with odd number of edges, the entropy rate is given by Eq. (9:4) due to the mixing behavior of the system. However, since in the quantum case the system is unitary, mixing does not occur but collapses and revivals might appear as discussed in Sec. 9.6. Consequently, the entropy rate of independent unitary QWs does not exist due to the lack of convergence. Similarly, for one-dimensional CWs on cycles with even number of sites, due to the oscillation of the Shannon entropy limit given in Eq. (9:4), the entropy rate does not exist. In summary, we draw the conclusion that for the case of the independent systems — which is the “most quantum” scenario — the entropy rate is not a suitable tool

for describing the per symbol asymptotic information generation.

9.8. The quantum entropy rate of periodically measured QWs

So far, we used the classical information theory description, and in particular the Shannon entropy. However, when quantum mechanical systems are considered for information storage or encoding, the von Neumann entropy

$$S(\rho) = -\text{Tr}(\rho \log \rho) \quad (9:46)$$

takes the place of the Shannon entropy. Operationally meaning, the von Neumann entropy gives the maximum number of bits which can be encoded in the quantum mechanical system ρ without any uncertainty (error). As the Shannon entropy appears in the definition of the entropy rate, one can extend the definition of the von Neumann entropy too, to form the so-called quantum entropy rate [179]

$$Q = \lim_{N \rightarrow \infty} \frac{1}{N} S(\rho_N). \quad (9:47)$$

This section is devoted to investigate our (quantum) black boxes with respect to this quantum entropy rate quantity.

The QWs living in the black box are the perfect candidates for calculating the quantum entropy rate, albeit the original protocol should be modified as follows. At every iterations we let the walker evolve for w steps, after that we perform a *non-selective* position measurement. Thus, the state of the system at iteration step N is

$$\rho_N = \sum_x S_x U^w \rho_{N-1} (U^w)^\dagger S_x, \quad (9:48)$$

where S_x -s are the projectors of the von-Neumann position measurement, which for one-dimensional QWs are given in (9:9). Considering the initial state ρ_0 , the quantum state at iteration step N is

$$\rho_N = \sum_{x_1, \dots, x_{N-1}, x_N} p(x_N, x_{N-1}, \dots, x_1) \times \left\{ \frac{S_{x_N} U^w S_{x_{N-1}} U^w \dots S_{x_1} U^w \rho_0 (U^w)^\dagger S_{x_1} \dots (U^w)^\dagger S_{x_{N-1}} (U^w)^\dagger S_{x_N}}{p(x_N, x_{N-1}, \dots, x_1)} \right\}, \quad (9:49)$$

where we used (9:8). Note that the operators in the curly bracket are proper density operators. The spectra of ρ_N must be calculated in order to determine the von-Neumann entropy (9:46). However, it is

straightforward to see that

$$S(\rho_N) \leq \log(2 + 4Nw) \quad (9:50)$$

for all N -s. At iteration step N the walker took Nw steps, thus the quantum state occupy a $4Nw + 2$ dimensional subspace in the Hilbert space at most (including the coin space). Since the quantum state with the highest von-Neumann entropy is the completely mixed state i. e. $S = \log(2 + 4Nw)$, the entropy rate of the walker at iteration step N cannot exceed this theoretical limit. Thus, the quantum entropy rate of the periodically measured quantum walks are

$$Q = \lim_{N \rightarrow \infty} \frac{1}{N} S(\rho_N) \leq \lim_{N \rightarrow \infty} \frac{1}{N} \{\log(2 + 4Nw)\} = 0. \quad (9:51)$$

Which holds true for all waiting times w . It is straightforward to see that this result holds for all QWs both on finite and infinite systems. We can draw the conclusion that the quantum entropy rate (9:47) is not suitable tool for our purpose.

9.9. Conclusions

In classical information theory, the asymptotic per symbol information content of a classical stochastic process is given by the entropy rate. There are countless dynamical systems in physics, which produce a sequence of symbols as the output, thereby realizing a classical stochastic process. In this chapter we studied an example of physical systems enclosed in a black box: the periodically measured classical and quantum walks. We posted the question whether the value of the entropy rate reflects some properties of the walk enclosed in the box, and in particular, whether the quantumness of the walk is reflected in the entropy rate? The quantum system enclosed in a black box is repeatedly disturbed by the projective measurement. One can approach the previous question following a deeper line of thoughts: How "quantum" a frequently measured system really is?

We have found that the entropy rates of the classical and the quantum mechanical models are indeed different and they reflect some features of the underlying dynamics. Although we used the classical definition of the entropy rate, the rich behavior of the quantum world is still apparent. We have given an elaborate method to determine the exact entropy rate of one-dimensional discrete time quantum walks. We have discovered that the internal coin state — which is not effected by the position measurements — serves as a memory, which allows us to develop a more sophisticated coding, thus achieving a lower entropy rate. In fact, quantum walks are quantum Markov chains, and despite the nonlinear functional connection between the unitary quantum Markov chain and the corresponding periodically measured

classical stochastic process, just from the subsequent position measurement values the total quantum states of the walker can be reconstructed. In this sense, the best encoding given by the entropy rate can be considered as the actual encoding of the quantum states of the periodically measured quantum walk. This is one of our main results.

We have shown that the exact entropy rate of the quantum walks can be calculated as the expected value of the Shannon entropy of the position distributions with respect to the asymptotic coin state distribution. We found that in the case of frequent measurements the exactly calculated entropy rate can be lower than the rate of classical walks, due to the improved predictability provided by the coin state.

We also gave an easy-to-measure and -calculate upper bound protocol that describes the entropy production of one-dimensional QWs when the observer considers the output sequence as a classical Markov chain, thus neglecting the information extractable from the subsequent outputs. In both the approximate and the exact cases the scaling of the entropy rate tends to $\log_2 w$ for high w 's in contrast with the $\log_2 \sqrt{w}$ scaling of the classical walks. This is due to the ballistic spread of quantum walks. Also, in both cases we found that the entropy rate is independent of the initial state of the one-dimensional QW.

To answer our original question regarding the quantumness of the walk hidden in the box with respect to the entropy rate, we would suggest using either the exact or the approximate method depending on the waiting time w (the time between subsequent position measurements). For low w -s the exact entropy rate is easy to determine, and it is straightforward to distinguish between the classical and quantum models. For $w \gg 1$ the $\log_2 w$ scaling produces higher entropy rates, and using the approximate protocol is enough to distinguish the two possible walk models.

For the sake of completeness, we also investigated the "most quantum" scenario, where each position von Neumann measurement is performed on a new, undisturbed system. In this case, the subsequent outputs of the black box are independent random variables. We found that in this case the entropy rate does not converge, neither for classical nor quantum walks, and consequently is not a suitable tool for studying them. We have also studied the quantum entropy rate model where, the von Neumann entropy replaces the Shannon entropy. For this study, we modified the definition of the black boxed quantum walk: the box performs non-selective measurement instead of the default selecting position measurement. However, we found that the quantum entropy rate is always zero.

The fact however that the periodically measured one-dimensional QW has a definite classical entropy rate also provides that it can be simulated using a well-designed classical walk, at least in terms of the black box output sequences. This statement is quite surprising as one can even reconstruct the quantum states of the system just from the outputs. However, on the other hand the observed non-trivial behaviors in the entropy rate: collapses-revivals, non-monotonicity suggest that the underlying system does not follow the rules of a classical random walk. We note here that all our results given in this section

are presented and valid for one-dimensional walks, but the developed methods are quite general, and presumably could be applied for more general systems.

Summary

Introduction

Quantum walks [29–31, 34–37] are quantum mechanical extensions of classical random walks. As random walks are suitable tools used in statistical physics and computational sciences, quantum walks found their applications in quantum physics and quantum information theory [45, 46]. For example, they are suitable models for describing quantum transport [39–41, 44], scattering [32, 170, 171] and topological effects [57–60] in solid state materials. From the quantum information point of view, quantum walks are considered universal computational primitives [54, 55]. Their simplicity and the rapidly growing number of applications soon caught the attention of experimentalists, too. Quantum walks have been successfully realized in a rich variety of physical systems, ranging from trapped atoms [110, 111] and ions [112, 113] to various photonic systems [115–124].

The central focus point of this very thesis is the discrete time quantum walk (QW) (Sec. 1.1), which is a non-trivial extension of the classical random walk. Here, the non-triviality is given by the introduction of the so-called coin space, an internal Hilbert space, thus, the departure from the scalarity of classical random walks. These QWs are unitary by design — they correspond to a closed system dynamics. However, physical processes in nature are subject to noise in general, which might disturb the unitary evolution of closed quantum systems, essentially leading to an open system dynamics. In this thesis we studied quantum walks with some kind of disturbed time evolution.

In the first model we studied, the transport (step) process of the walk was disturbed by some noise corresponding to classical randomness (See Chapter 4). We described this noise as a change in the connectivity of the underlying graph given by dynamical percolation. To study this problem we adapted the asymptotic theory for random unitary operations (See Chapter 3) and also developed it further to suit our needs and to get a better physical insight.

Another way to break the unitarity of the QWs is naturally given through the apparatus of quantum mechanics: measurement inevitably disturbs the unitary evolution. Frequent (*e.g.* periodic) selective measurements result in a stochastic evolution between (quantum) states. We employ the tools of classical information theory to characterize the information (or disorder) generation of such process in terms of the entropy rate (See Chapter 2). As classical walks are the textbook example of the entropy rate, its extension to QW based processes possibly can give us some deeper understanding on the fundamental differences between simple classical and quantum mechanical systems.

General method for determining the asymptotics of percolation quantum walks

The first disordered system we studied is the discrete time quantum walk on dynamical percolation graphs. In this model all edges of the underlying graph have a finite probability that they become broken under unit time step, *i.e.* the walker cannot pass through at that given time step. The time evolution of a discrete time quantum walk on a percolation (imperfect) graph is not trivial since percolation graphs are non-regular. To bypass this non-triviality, we choose to maintain the unitarity by introducing reflections: a walker cannot pass through the broken edge naturally, instead it suffers a reflection in its internal coin degree (See Sec. 5.1). The complete, statistical time evolution is then given by a random unitary operation (RUO map), which is also a trace preserving quantum operation (quantum channel).

We have adapted the general theory for solving the asymptotic dynamics of such RUO maps to the general percolation quantum walk problem (See Sec. 5.3), with the crucial and most important part being the construction of the attractor space: An invariant subspace of the RUO map. We have shown that due to the product form of the discrete time quantum walk dynamics, the coin operator part and the shift part — which also corresponds to the graph topology — can be solved independently. We termed the coin part as “coin condition” and the shift part as “shift conditions”. This separation technique allowed us to parametrize the parts of the problem independently, thus, one might solve a given graph for a family of coins, or a given coins for a family of graphs, or even both. We have illustrated that on translation-invariant regular graphs the shift conditions simplify considerably allowing us to keep the size of the graph as a free parameter (See Sec. 5.4). We note that the attractor space cannot depend on the probabilities used at the construction of the RUO map as long as the set of unitaries used does not change. This results that neither phase-transitions, nor any non-asymptotic effects can be observed in the attractors.

Naturally, the size of these problems increases exponentially in the following sense. The RUO map corresponding to the time evolution results from the summation of many (weighted) unitaries. The number of unitaries goes with the number of possible configurations, which is exponential with respect to the number of edges. We have shown that as discrete time quantum walks correspond to nearest neighbor steps, thus, their unitaries are sparse matrices. Consequently, superoperators can be constructed in polynomial time on regular graphs (See Sec. 5.2). We note that during our studies we performed several numerical tests to confirm our analytical results and to generate figures, and we found this result particularly useful.

In summary, our new results presented in Chapter 5 are the following. We have applied the asymptotic theory of RUOs on percolation quantum walks. We have shown that a coin-step separation can be

performed, allowing us to solve the problem in parts. Thus, more general problems can be addressed. We showed that the shift conditions corresponding to the step part simplify considerably on regular translation-invariant graphs (*e.g.* lattices), allowing for studying whole families of graphs at once. We have also shown that the superoperators corresponding to the dynamics can be constructed polynomially on regular graphs with respect to the number of sites. This is particularly useful in numerical analysis, as the number of configurations grow exponentially with the number of sites, which would make any brute-force approaches fruitless.

Pure state ansatz for random unitary operations

To determine the asymptotics of random unitary operations (RUO maps) one should find the so-called attractor space. This invariant subspace is spanned by the fixed points of dynamics, called attractors. These attractors could be considered as eigenoperators (eigenvectors) of the RUO map (superoperator) corresponding to unit magnitude eigenvalues. However, there are no direct implications on the physical meaning of attractors. In fact, the complete attractor space is a linear space, and the set of possible asymptotic states (proper density operators) is a convex subspace within. In summary, the general theory (See Sec. 3.2) for obtaining asymptotics of RUO maps provides only little help when someone wants to focus on the physical relevance of attractors. Moreover, the attractors are linear operators on the Hilbert space, thus their sizes scale quadratically with respect to the dimension of the Hilbert space, and naturally their analysis is more involving than the analysis based on pure quantum states.

We have addressed the problem of giving a direct physical interpretation to attractors, and as a by-product we managed to make the analysis much more easier to perform: We introduced the pure state ansatz (See Chapter 6). The unitaries used for building up the RUO map can share common eigenstates: pure states which are eigenstates of all building-block unitaries corresponding to the same eigenvalues. We have shown that these states are fixed points of the RUO dynamics, thus they can be used to form attractors of rank one. We termed these attractors as p-attractors. Moreover, the common eigenstates span a decoherence free subspace, a subspace within the attractor space carrying relevant physical meaning and importance. We have to note that naturally not all attractors can be constructed via common eigenstates: the completely mixed state — a trivial attractor due to the unitality of RUO maps — is one notable example of non-p-attractors. However, for some relevant RUOs the attractor space is fully determined by p-attractors and the completely mixed state. In this case the asymptotic time evolution is an incoherent mixture of the unitary evolution on the p-attractor space (decoherence free subspace) and the completely mixed state projected to its orthogonal complement. Here we note that this surprisingly compact asymptotics can be observed in some percolation quantum walks.

To summarize, we have given a refined approach to determine the asymptotic attractor space of RUO maps (Chapter 6). This approach is based on the construction of common eigenstates of the unitaries building up the random unitary dynamics. Naturally, finding eigenstates is less involving than finding eigenoperators of the RUO dynamics. Our pure eigenstate ansatz allows for giving a direct physical meaning for relevant parts of the attractor space, *e.g.* the pure eigenstates form a decoherence free subspace. We have also shown that not all attractors can be constructed from common eigenstates, the completely mixed state being an obvious exception. However, in some physically relevant cases the p-attractors resulting from the pure eigenstate ansatz and the trivial completely mixed solution span the complete attractor space. We have shown that in this case the asymptotic dynamics is given as an incoherent mixture of the unitary dynamics on the decoherence free subspace and the completely mixed state on its orthogonal complement.

One-dimensional percolation walks: explicit solutions and edges states

The problem of discrete time quantum walks on one-dimensional percolation graphs is the first step to understand a family of open systems. At the first glance one might see the problem being quite straightforward: one-dimensional quantum walks are intensively researched and one-dimensional percolation graphs seem to be rather trivial classically. However, the combination of these two basic models is surprisingly new, and more interestingly non-trivial: Most of the studies performed on these systems are either numerical or phenomenological and even numerical results are very limited by their exponential computational costs (Sec. 4.2).

In Chapter 7 we applied our general method for percolation quantum walks (Chapter 5) in tandem with the pure state ansatz (Chapter 6) to explicitly solve the most general $SU(2)$ coin problem of quantum walks on the percolation cycle and line graphs. These are the most basic examples of one-dimensional graphs representing the reflective and periodic boundary conditions. We have acquired the solution explicitly (Sec. 7.1). In most of the cases the attractor space consists of p-attractors and the trivial completely mixed solutions, however, degeneracy in special cases might lead to another non p-attractor. We have shown that the asymptotics are non-trivial and depend on the coin we choose: apart from the trivial completely mixed asymptotic state, stationary states with some quantum coherence, periodic and quasi-periodic asymptotic limit cycles might emerge. We have also shown that the actual asymptotic dynamics (limit cycles) are only observable on the complete coin-position density operator — the asymptotic position density operator is always stationary in time. These results are quite a departure from the complete mixing of classical walks on percolation graphs.

We also commented on the physical form of the common eigenstates we found. They correspond to

edge states (Sec. 7.2) on line graphs in most of the cases (for most coin operators). These edge states are exponentially localized at the boundaries of the system. Apart from these states forming a decoherence free subspace some interesting physical consequences can be drawn. For example, one can start the walk in a pure state corresponding to a completely flat position distribution, to find the asymptotic state being exponentially localized to one of the boundaries of the system. We again note that such effects cannot be observed in classical percolation walks.

To give a summary, in Chapter 7 we have applied our methods to solve the asymptotic dynamics of one-dimensional percolation walks explicitly. We have managed to solve the complete $SU(2)$ problem on the two basic one-dimensional graphs: the cycle and the line graph with N vertices. We note that these results are amongst the first closed form, fully analytical solutions obtained for percolation quantum walks. We have shown that the obtained asymptotics are rather non-trivial: apart from the classically available complete mixture, stationary states having quantum coherence and limit cycles can appear. We also analyzed the physical appearance of the solutions, and discovered that on the linear graph for most of the coin operators edge states can appear, *i.e.* eigenstates exponentially localized at the dedicated boundaries of the system.

Two-dimensional percolation walks: symmetry breaking and trapping

The natural step after completely solving a one-dimensional problem is to look at its higher dimensional counterparts. Even just closed (unitary) quantum walks on two-dimensional lattices (Sec 1.1.2) exhibit more colorful behavior in comparison with the one-dimensional model. A notable example being the Grover trapping. Similarly, two-dimensional percolation graphs offer more challenges and, in addition, more physically relevant problems, *e.g.* non-trivial phase transitions.

Similarly to the one-dimensional case, in Chapter 8 we applied our general method and the pure state ansatz to investigate some special two-dimensional walks analytically. For that analysis we have chosen the two most studied examples of two-dimensional walks: the Hadamard and the Grover walk. For the underlying graph we considered two finite derivatives of the Cartesian square lattice: the carpet corresponding to reflective boundaries and the torus corresponding to periodic boundaries. The solution of the Hadamard walk (Sec. 8.2) yielded a number of differences with respect to its one-dimensional counterpart: While the one-dimensional Hadamard walk always lead to a flat distribution in position (*i.e.* there are no edge states), the two-dimensional one can feature position inhomogeneity in the asymptotics. We also showed that these inhomogeneous solutions (common eigenstates) in fact are sensitive to the orientation of the graph. While in certain cases a unitary (closed) Hadamard walk on the $M \times N$ and $N \times M$ graphs yields a simply rotated position distribution, percolation — which is a symmetric noise

— can break this rotational symmetry.

The solution of the Grover walk (Sec. 8.3) resulted in a whole family of common eigenstates with finite support. These states are responsible for the appearance of trapping (localization) in the unitary (closed system) case, and surprisingly we found them to appear in the percolation case too. That is, the trapping effect survives the strong decoherence induced by the dynamical percolation. As being fixed points of the dynamics, these states form a decoherence free subspace, moreover due to their finite support they are practically insensitive to boundaries or to the size of the graphs: they might be used for information storage. We also commented on the implications of such pure eigenstates on the definition of trapping (localization): Trapping is usually defined in the literature as a situation where the probability to find the particle at its original position is non-vanishing. However, this definition is rather impractical on finite graphs. We suggest that the appearance of robust eigenstates with finite (exponentially decaying) support might be a better indicator for trapping due to the insensitivity to the size of the underlying graph. We note that both the Hadamard and the Grover walks are examples of RUO maps, where the pure eigenstate ansatz are highly beneficial: the attractor space is completely determined by the common eigenstates (p-attractors) and a single trivial non-p attractor, corresponding to the completely mixed state.

To summarize our new results of Chapter 8, we employed our analytical methods to analyze two notable quantum walks on two-dimensional percolation graphs. First, we investigated the two-dimensional Hadamard walk and gave its attractors in a closed analytical form. We have shown that in contrast with its one-dimensional counterpart, it can exhibit position inhomogeneity. Moreover, we have shown that the percolation model is sensitive to certain rotations, *i.e.* with respect to the unitary model some symmetries are broken. We also studied the Grover walk, and obtained its attractor space in a closed analytical form. We have shown that the trademark trapping effect of the Grover walk survives the particularly strong decoherence of percolation. This is due to the family of common eigenstates with finite support, spanning a decoherence free subspace. We also noted on the implication of such states on the definition of trapping.

Calculating the entropy rate of quantum walk driven stochastic processes

Quantum mechanical systems can be disturbed in several ways. Up to now, we have studied a system where the disorder was introduced to the system as an uncontrollable noise coming from the environment. Here, we consider another approach where the system is disturbed by periodical selective measurements. One can ask the natural question that how much quantumness a closed system can maintain when it is frequently disturbed? We approach this problem by studying the information (disorder) a frequently

measured system generates by using the classical quantity of entropy rate (Chapter 2). Approaching from the classical information theory, the entropy rate gives the asymptotic per symbol information content of a stochastic process. As one typical textbook example of the entropy rate is the classical walk, one might find it interesting to address the problem of the entropy rate of quantum walks.

As the classical entropy rate has a sound operational (and physical) meaning, we first studied the problem in terms of classical information theory via embedding both the classical and quantum walks in a black box (Sec. 9.1). We defined a stochastic process corresponding to the periodic von Neumann position measurement of a discrete time quantum walk (Sec. 9.3). Employing the definition of the entropy rate we have successfully given an exact method to calculate the entropy rate of this system. In contrast with the classical random walk, which is a Markov chain, the studied discrete time quantum walk cannot be considered as a classical Markov chain in terms of position measurement outcomes, albeit the quantum walk itself is a quantum Markov chain.

In fact, we have shown that the internal coin states keeping coherences after every position measurement serve as a memory. However, the unitary quantum Markov chain nature of the system can be employed: the actual coin state and, more importantly, the complete quantum state can be deduced from the mere position measurement data. This allowed us to calculate the entropy rate of the model as the entropy rate of a classical Markov chain extended with the coin states (Sec. 9.4). Moreover, we also found that the entropy rate does not depend on the initial state, and the system in the asymptotic limit always forgets its initial state. As the number of coin states can be infinite in the asymptotic limit, we have also given an approximation (Sec. 9.5) to calculate the upper and lower bounds of the entropy rate using finite (truncated) basis (matrices). The given method allowed us to calculate the entropy rate of frequently measured discrete time quantum walks and compare it with the frequently measured classical walk. We found (Sec. 9.5) that due to the implicit memory represented by the coin degree of freedom the entropy rates of the frequently measured one-dimensional Hadamard walks are lower than the corresponding classical walk.

Summarizing Sections 9.1 - 9.5, we have defined a stochastic process corresponding to periodically measured quantum and classical walks. We have given an elaborate method for calculating the entropy rate of quantum walks. We have shown that the quantum walk does not behave as a classical Markov chain on positions, however, it can be viewed as a classical Markov chain on the position-coin basis. We have also given a method to calculate the lower and the upper bound of the entropy rate using finite (truncated) basis. We concluded that for frequent measurements due to the memory effect of the coin the entropy rate of the quantum model (one-dimensional Hadamard walk) is usually lower than its classical counterpart. We note here that the methods we have given are rather general and should be adaptable for higher dimensional quantum walks or other discrete time quantum Markov chains as well.

Determining the scaling of the entropy rate and comparison with other approaches

The entropy rate of the periodically measured quantum and classical walks can indeed be calculated and compared. However, the calculation can become rather involving as the frequency of the periodic measurements becomes lower. In fact, in the worst case the problem becomes exponential (Sec. 9.5) with respect to the dimension of the corresponding Markov chains (matrices).

To overcome this problem we have proposed a protocol (Sec. 9.6) which gives an easy to calculate and measure upper bound to the entropy rate. If one does consider the quantum mechanical system as a classical Markov chain, *i.e.* strictly encodes it with a position transition matrix, she will necessarily face an encoding which is suboptimal, resulting in a higher entropy rate (upper bound). The functional dependence between the correct representation and the position only representation and the corresponding entropy rate inequality is given by the theory of hidden Markov models. We have shown that the scaling of this upper bound rate can be approximated with the help of the weak limit theorem. We have also shown that in tandem with the exact calculation approach a lower bound scaling can be given. We found that in both cases the scaling of the entropy rate for rare measurement is $\log_2 w$, where w is the time between two subsequent measurements. In comparison, this value for the classical walk is $\frac{1}{2} \log_2 w$. The pre-factor difference is due to the ballistic and diffusive spreading of the two models. We drew the conclusion that in the rarely measured limit, the entropy rate is dominated by the spreading behavior of the models, and the quantum version surpasses its classical counterpart. We also considered finite systems (Sec. 9.6), *i.e.* cycle graphs. On these graphs, the classical walk results in complete mixing, while the quantum case shows a non-monotonous behavior due to the unitarity evolution: collapses and revivals might occur.

We have also investigated the "most quantum" case (Sec. 9.7), which corresponds to the scenario when every measurement is performed on a new, undisturbed system. Since there is no correlation between the subsequent outcomes, the entropy rate is simply the entropy of the position distribution of the systems in the infinite limit. On infinite systems this is infinity, and on finite systems due to the collapse-revival behavior of finite unitary quantum systems, there is no convergence in the entropy rate. Thus, the "most quantum" case cannot be studied in terms of the entropy rate.

We calculated the so-called quantum entropy rate (Sec. 9.8) as well. To this end we had to modify the system to have a non-selective measurement. We have shown that the von Neumann entropy in the definition of the quantum entropy rate grows logarithmically with the number of iterations, and thus the entropy rate itself is zero in the asymptotic limit.

To summarize Sections 9.6 - 9.8, we have studied the behavior of the entropy rate of frequently

measured quantum walks using analytical tools. We have given an easy to calculate and measure upper bound approximation for the entropy rate, which is based on the theory of hidden Markov models. We showed that the scaling of the entropy rate with respect to the number of steps between subsequent measurement can be calculated using a weak limit approach. We drew the conclusion that in the limit of rare measurements the spreading of the walk model dominates the entropy rate. Should someone distinguish between the classical and quantum models based on the entropy rates of their periodic position measurements for frequent measurements one should use the exact method giving back the delicate differences, whereas in the rare measurement limit one could safely rely on the upper bound approach. We also investigated the “most quantum” approach, which is a popular approach to characterize some properties of quantum walks. However, here it did not yield any results due to lack of convergence. We finally gave the quantum entropy rate of the system and determined that it is exactly zero in all cases. The fact that the studied quantum models have an exact entropy rate in most of the cases also provides that its outputs can be simulated using well designed classical walks. In this sense the quantum mechanical properties of the system are hidden. On the other hand a number of non-trivial effects we found: memory-like behavior, non-monotonous entropy rate, collapses and revivals reveals the quantum nature of the walk.

Outlook

The methods given for percolation quantum walks gave us a very strong toolset for studying and understanding these systems. The growing interest in this field, and the fruitful experiments further motivate our studies in this direction. The next step could be to study the asymptotics of some other graph structures or multiparticle walks. One could also possibly search for the application of the given methods and results in quantum information theory. Another direction is to study the percolation of other quantum walk models. Our preliminary results on the continuous time quantum walk model suggests that there are non-trivial solutions as well, albeit the model is naturally more restricted due to the absence of the coin state.

The asymptotic theory of random unitary operations clearly benefit from the pure eigenstate ansatz. However, in more general cases the theory can be extended to non-trace-preserving maps, *i.e.* sources and drains can be introduced and steady states could be studied with the theory. It would be rather interesting to find a way to extend the pure state ansatz to this generalized model. Another interesting aspect is the question of the convergence rates. In some models the rate of convergence might carry an important physical meaning, *e.g.* traces of phase transitions. Consequently, developing any method for this purpose might be prosperous.

We intended the study of the entropy rate of discrete time quantum walks as a first step towards a deeper understanding of the concept of entropy rate itself and also the classical and quantum borderline in terms of information theory. A straightforward extension would be to calculate the entropy rate of more general quantum systems and draw the conclusion on how quantum mechanics itself is reflected in this quantity. Another approach would be to find definitions and measurement processes which gives some way to estimate the quantumness of a given system in terms of the classical or quantum entropy rate. A promising candidate would be for example the quantum dynamical entropy. We hope that further studies in this field will lead to some ways to gather a deeper understanding on the mysterious border between the classical and quantum world.

List of new scientific results

1. I have developed a general method for solving the asymptotics of discrete time quantum walks on percolation graphs. This general method is based on the attractor-space formalism of the asymptotic method of random unitary operations, which I separated into two parts by making a difference between the coin toss and position step. I have shown that the separation process allows for solving the problem for whole families of graphs and coins. I have also shown that the superoperator describing the dynamics of the percolation quantum walk can be constructed polynomially on regular graphs with respect to the number of sites [I].
2. I presented a method for determining the asymptotic attractors of random unitary operations. The core of this method is to find the common eigenstates of the dynamics, which can be used to form attractors with a direct physical meaning. I have shown that these common eigenstates span a decoherence-free subspace. I have also shown that in some cases the complete attractor space can be determined via common eigenstates and the trivial attractor (corresponding to the completely mixed state). I determined the formula of the asymptotic time evolution in this case, which is given as an incoherent mixture of the unitary dynamics on the decoherence-free subspace spanned by common eigenstates and the completely mixed state on its orthogonal complement. I have also illustrated the method on discrete time quantum walks on dynamical percolation graphs and pointed out the important differences with respect to the general method [II].
3. I have explicitly solved the asymptotic dynamics of one-dimensional percolation quantum walks by employing the methods I developed. I have given the attractor space in a closed form for the percolation cycle and linear graph for the complete $SU(2)$ problem. I have shown that there are non-trivial asymptotics: stationary states with quantum coherences and limit cycles can appear. I have analyzed the physical form of the solutions and discovered that on the linear graph the solutions are edge states for most of the coin operators [III].
4. I have explicitly solved the asymptotic dynamics of the two-dimensional Hadamard and Grover walks on the percolation torus and carpet. I have shown that in contrast to its one-dimensional counterpart, the Hadamard walk exhibits asymptotic position inhomogeneity. I have also discovered that the percolation model in certain cases is sensitive to rotation, in contrast with the corresponding undisturbed (unitary) quantum walk. I have found that the common eigenstates of the Grover walk have finite support, thus the walk keeps its trapping property in the percolation case [II].

5. I have defined a stochastic process based on the periodically measured quantum and classical walks. I have given a general method for calculating the classical entropy rate of these stochastic processes. I have shown that the frequently measured quantum walk behaves as a classical Markov chain in the position-coin state basis, and the entropy rate of this Markov chain is equal to the entropy rate of the previously defined stochastic process. I have also given a method for calculating the lower and upper bounds of this entropy rate. I have found that in the regime of frequent measurements, the entropy rate of the quantum-walk-based model is usually lower, due to the memory effect of the coin state of the particle [IV].

6. I have developed an approximation protocol to give an upper bound to the exact entropy rate of the periodically measured quantum walks. I have estimated the scaling of the entropy rate of the one-dimensional Hadamard walk with respect to the time (number of discrete steps) between measurements using the so-called weak limit theorem. I have found that for rare measurements the entropy rate is dominated by the ballistic spreading of the quantum walk, thus the entropy rate is higher than in the classical case. I have also studied finite systems and discovered that collapses and revivals can occur in the quantum walk based system. I have also calculated the "most quantum case" and the quantum entropy rate of the model to give a comparison. I found that both of these models are inconclusive for periodically measured walks. On the other hand, the classical-entropy-rate approach I proposed is a suitable tool to capture some of the quantum features of the system [IV].

Összefoglalás

(Summary in Hungarian)

Bevezetés

A kvantumos bolyongások [29–31, 34–37] a klasszikus véletlen bolyongások kvantummechanikai kiterjesztései. Ahogy a véletlen bolyongás a statisztikus fizika és a számítástudomány elfogadott eszköze, hasonlóan a kvantumos bolyongás is felhasználhatónak bizonyult a kvantumfizikában és a kvantuminformáció elméletben [45, 46]. A kvantumos bolyongások megfelelő modellt jelentenek számos fizikai jelenség leírására, többek között a kvantumos transzport [39–41, 44], szórás [32, 170, 171] és a szilárdtestekben tapasztalható topologikus effektusok [57–60] tanulmányozására. A kvantuminformáció-elmélet szempontjából a kvantumos bolyongások univerzális számítási primitívet jelentenek [54, 55]. Egyszerűségük és a potenciális alkalmazások ugrásszerűen gyarapodó száma hamar felkeltette a kísérleti fizikusok figyelmét is. Kvantumos bolyongásokat immáron a fizikai rendszerek széles családjában sikerült demonstrálni, a csapdázott ionokon [112, 113] és atomokon [110, 111] keresztül a fotonikus rendszerekig [115–124].

Jelen disszertáció gerincét a diszkrét idejű kvantumos bolyongás adja (1.1. alfejezet), mely a klasszikus véletlen bolyongás egy nemtriviális kiterjesztése. Itt a nemtrivialitást az úgynevezett érmetér bevezetése okozza, mely egy belső szabadsági fokhoz tartozó Hilbert tér, így e definíció a klasszikus véletlen bolyongások skalárságát bontja fel. A bolyongások időfejlődését unitér dinamika írja le, emiatt alapvetően zárt rendszernek tekinthetőek. Valójában a természetben lezajló folyamatok az esetek túlnyomó többségében valamilyen zaj hatásának vannak kitéve, mely megzavarhatja a zárt kvantumrendszerek unitér időfejlődését, nyíltrendszer dinamikát eredményezve. A jelen disszertációban tárgyalt kvantumos bolyongások mindegyikének dinamikáját valamilyen módon megzavarjuk.

Az általunk vizsgált első modellben a bolyongás „lépés” műveletét zavartuk meg egy klasszikus véletlenszerűség okozta zajjal (Lásd 4. fejezet). Ezt a zajt a bolyongás gráfjának dinamikus perkolációjával írtuk le. E probléma tanulmányozásának érdekében a véletlen unitér műveletek (Lásd 3. fejezet) általános aszimptotikus elméletének eszközeit használtuk fel, miközben azokat a cél és a jobb fizikai rálátás érdekében továbbfejlesztettük.

A kvantumos bolyongások unitaritásának megtörésére a kvantummechanika egy természetes módot is kínál: a mérés szükségszerűen megzavarja az unitér dinamikát. Gyakori (periodikus) szelektív mérések egy kvantumállapotok között zajló sztochasztikus folyamatot eredményeznek. Egy ilyen folyamat információ produkcióját vizsgáljuk meg a klasszikus információelméletben található entrópia-ráta mennyiségének segítségével. Mivel a klasszikus véletlen bolyongások jelentik az entrópia-ráta iskolapéldáját, reményeink

szerint a kvantum bolyongások entrópia-rátájának meghatározása és a két modell összehasonlítása rávilágíthat az egyszerű klasszikus és kvantumrendszerek közötti alapvető különbségekre, ezzel elárulva valamit a rejtélyes klasszikus-kvantum határátmenetről.

Általános módszer a perkolációs kvantum bolyongások aszimptotikájának meghatározására

Az első általunk vizsgált rendezetlen rendszer a perkolációs gráfon történő diszkrét idejű bolyongás volt. Ebben a modellben a bolyongás gráfjának minden éléhez egy véges valószínűséget rendelünk, mely azt írja le hogy az adott él milyen valószínűséggel válik „hibássá” egységnyi időlépés alatt. A „hibás” éleken a bolyongás nem tud átlépni az adott időpillanatban. A perkolációs (zajos) gráfokon való diszkrét idejű bolyongás leírása nem triviális feladat, mivel a perkoláció miatt a gráf regularitása is sérül. E probléma feloldására mi egy irodalomban ismert módszert választottunk: a bolyongás unitaritását egy visszaverődés (reflexió) bevezetésével megtartjuk. Mivel a bolyongás egy hibás élen nem tud átmenni, ezért helyette a belső érmeállapotában történik egy reflexió (Lásd 5.1. alfejezet). Egy ilyen rendszer teljes, sztochasztikus időfejlődését egy véletlen unitér leképezés (RUO) írja le, mely konstrukciója miatt egy trace-megőrző kvantumművelet (kvantumcsatorna).

Az ilyen RUO leképezések aszimptotikájának meghatározását leíró elméletet adaptáltuk a perkolációs kvantum bolyongás problémájára (Lásd 5.3. alfejezet.). Ebben az elméletben a legfontosabb, nélkülözhetetlen lépés az úgynevezett attraktortér megkonstruálása, mely a RUO leképezés egy invariáns altere. Megmutattuk, hogy a diszkrét idejű kvantum bolyongások operátorszorzattal adott dinamikája miatt az érméhez tartozó és a léptető operátorhoz tartozó részek (utóbbi a gráf topológiájának is megfelelő) szeparálhatóak és külön oldhatóak meg. Az érméhez tartozó egyenleteket „érme feltételeknek” a léptetőoperátorhoz tartozó részeket „léptető feltételeknek” neveztük. A szeparációs technika segítségével ezek a részek külön paramétrezhetők, így lehetőséget adva a minél általánosabb problémák megoldására. Megmutattuk, hogy translációinvariáns reguláris gráfok esetére a léptető feltételek számottevően leegyszerűsödnek, lehetővé téve azt, hogy a gráf mérete paraméterként szerepeljen a megoldásban (5.4. alfejezet). Itt fontos megjegyeznünk, hogy az attraktor-tér független a RUO leképezés konstrukciójakor felhasznált valószínűségektől egészen addig, míg a felhasznált unitér operátorok halmaza nem változik. Emiatt az attraktorokban (aszimptotikában) fázisátalakulások vagy a rövid távú dinamika jelei nem figyelhetőek meg.

Alapvetően a perkolációs gráfok problémájának mérete exponenciálisan növekvő a következő értelemben: Az időfejlődést megadó RUO leképezés unitér műveletek súlyozott összeadásának eredménye. Ezen unitérek száma a lehetséges gráf-konfigurációk számával megy, mely exponenciális az élek számával.

Megmutattuk, hogy mivel a kvantumos bolyongások csak legközelebbi szomszéd lépéseket (interakciókat) tartalmaznak, ezért az unitérek ritka mátrixok és ebből kifolyólag a RUO leképezéseket leíró szuperoperátorok polinomiális idő alatt megkonstruálhatóak (lásd 5.2. alfejezet). Itt megjegyezzük, hogy munkánk során rendszeresen használtunk numerikus eszközöket analitikus eredményeink ellenőrzésére és ábrák rajzolására, így a polinomiális konstrukció eredményét gyakorlatban is felhasználtuk és igen hasznosnak találtuk.

Összefoglalva, az 5. fejezetben bemutatott új eredményeink a következők. Sikerrel alkalmaztuk a RUO leképezések aszimptotikus elméletét perkolációs kvantumos bolyongásokra. Megmutattuk, hogy érme-léptetés szeparáció hajtható végre, mely segítségével a probléma részekre osztható és részenként oldható meg. E megközelítés segítségével általánosabb problémák oldhatóak meg. Megmutattuk, hogy a „léptető feltételek” (melyek a léptető operátornak felelnek meg) számottevően leegyszerűsödnek transzlációinvariáns reguláris gráfokon, így hozzájárulva ahhoz hogy gráfok teljes családját tanulmányozzuk egyszerre. Továbbá megmutattuk, hogy a RUO időfejlődést leíró szuperoperátorok a gráf méretével polinomiálisan skálázódó erőforrást felhasználva megkonstruálhatóak reguláris gráfokon. Ez egy különösen hasznos eredmény, hiszen a konfigurációk száma exponenciálisan nő a gráf méretével, így a „nyers erő” (brute force) numerikus módszerek csupán igen kis rendszerek tanulmányozását tennék lehetővé.

Tiszta állapot ansatz a véletlen unitér műveletekben

A véletlen unitér műveletek (RUO) aszimptotikájának meghatározása az úgynevezett attraktor-tér megkonstruálásán keresztül történik. Eme invariáns alteret a dinamika fixpontjai feszítik ki, melyeket attraktoroknak nevezünk. Ezeket az attraktorokat tekinthetjük a RUO leképezés (mint szuperoperátor) egységnyi abszolútértékű sajátértékeihez tartozó sajátoperátorainak (sajátvektorainak). Fontos megjegyeznünk, hogy ezen felül az attraktorok fizikai alakjára, jelentésére nincsenek megkötések. Valójában a teljes attraktortér egy lineáris tér, melyen belül található a tényleges aszimptotikus állapotok (melyek sűrűségoperátorok) konvex tere. Tömören megfogalmazva, a RUO leképezések (3.2. alfejezet) aszimptotikáját megadó általános elmélet kevés támpontot ad, ha valaki az attraktorok közvetlen fizikai jelentésére vagy értelmezésére kíváncsi. Megjegyezzük ezen felül, hogy mivel az attraktorok lineáris operátorok a Hilbert téren ezért az ő méretük négyzetesen növekszik a Hilbert tér méretével, emiatt analízisuk erőforrásigényesebb szemben egy pusztán tiszta állapotokra szorító analízissel.

Ebben a részben az attraktorok fizikai alakjának kérdését tűztük ki célul, miközben az analízist sikerült lényegesen egyszerűbbé tennünk: bevezettük a „tiszta állapot ansatz”-ot (6.1. alfejezet). A RUO leképezés megkonstruálásakor felhasznált unitér operátoroknak közös sajátállapotaik lehetnek: tiszta állapotok, melyek minden RUO-t alkotó unitérnek sajátállapotai ugyanazzal a sajátértékkel. Megmutattuk, hogy

ezek az állapotok a RUO-val leírt időfejlődés fixpontjai, emiatt belőlük egy rangú attraktorok építhetők. Ezeket az attraktorokat p-attraktoroknak neveztük el. Ezen felül a közös sajátállapotok egy dekoherencia-mentes alteret feszítenek ki, mely altér az attraktor-téren belül található, és valódi fizikai jelentéssel bír. Meg kell jegyeznünk, hogy nem minden attraktor konstruálható meg a közös sajátállapotokból: a teljesen kevert állapot (mely a RUO leképezések unitalitása miatt megjelenő triviális attraktor) az egyik ilyen attraktor. Bizonyos releváns esetekben viszont az attraktor-tér teljesen meghatározható p-attraktorok és az előbb említett teljesen kevert állapot segítségével. Ebben az esetben az aszimptotikus időfejlődés egy inkoherens keveréke a p-attraktorok alterén történő unitér időfejlődésnek (mely egy dekoherencia mentes altér) és az eme tér ortogonális alterére vetített teljesen kevert állapotnak. Megjegyezzük, hogy ez a meglepően egyszerűen leírható aszimptotika később még elő fog kerülni némely perkolációs bolyongás során.

Összefoglalva, egy új megközelítést adtunk meg mely segítségével a RUO leképezések aszimptotikus attraktor tere meghatározható (6. fejezet). E megközelítés alapja a RUO leképezést felépítő unitér operátorok közös sajátállapotainak megkonstruálása. Ezen sajátállapotok megkeresése számottevően egyszerűbb, mint a RUO leképezés sajátoperátorainak megkeresése. Az általunk megadott tiszta állapot ansatz lehetővé teszi, hogy az attraktor-tér bizonyos részeihez közvetlen fizikai jelentést rendeljünk. Példának okáért megemlítjük, hogy a közös sajátállapotok dekoherencia-mentes alteret feszítenek ki. Megmutattuk, hogy nem minden attraktor konstruálható meg tiszta sajátállapotok segítségével, a RUO-k unitalitása miatt mindig megjelenő teljesen kevert állapot egy közülük. Továbbá azt is megmutattuk, hogy ha az attraktor-tér tiszta állapotokból és a teljesen kevert állapotból megkonstruálható, akkor az aszimptotikus dinamika igen egyszerűen megadható, az pusztán a közös sajátállapotok terén vett unitér időfejlődésből és az e térre ortogonális alterre vetített teljesen kevert állapot inkoherens keverékéből áll össze.

Egydimenziós perkolációs bolyongások: explicit megoldások és élállapotok

Az egydimenziós perkolációs gráfokon vett kvantum bolyongások problémájának megoldása jelenti az első lépést a nyílt rendszerek egy egész családjához. Első ránézésre a probléma egyszerűnek tűnhet: az egydimenziós kvantum bolyongások az irodalomban igen részletesen leírt és megértett rendszerek, és az egydimenziós gráfok perkolációjának problémája klasszikusan megoldottnak tekinthető. Ezzel szemben e két alapvető modell kombinációja meglepően újszerű és érdekes módon nemtriviális: az ilyen rendszerek tanulmányozása eddig főként numerikus vagy fenomenologikus eszközökkel történt, melyeket erősen bekorlátoz a probléma exponenciális számítási igénye (4.2. alfejezet).

A 7. fejezetben a perkolációs bolyongásokra megadott általános módszerünket (5. fejezet) alkalmaztuk

a tiszta állapot ansatz-zal (6. fejezet) karöltve, hogy segítségükkel explicit módon megoldjuk a legáltalánosabb, $SU(2)$ érmével hajtott kvantum bolyongások problémáját perkolációs gyűrűn és vonalon. Ezek az egyszerű egydimenziós gráfok a fizikában gyakran megjelenő visszaverő és periodikus határfeltételeket testesítik meg. A problémát explicit módon, zárt alakban sikerült megoldanunk (7.1. alfejezet). A legtöbb esetben az attraktor teret p -attraktorok és a teljesen kevert állapothoz tartozó attraktor határozza meg, habár speciális (degenerált) esetekben egy másik nem- p -attraktor is megjelenhet. Megmutattuk, hogy az aszimptotika nagyban függhet az általunk választott érmeoperátortól: a teljesen kevert végállapottól kezdve stacionárius, koherenciát részben megőrző állapotok, illetve periodikus és kvázi-periodikus határciklusok is létrejöhetnek. Azt is megmutattuk, hogy a tényleges aszimptotikus dinamika csupán az érmetéren figyelhető meg, a pozíció sűrűségoperátor mindig stacionárius. Ezek az eredményeink élesen eltérnek a klasszikus bolyongásoknál mindig fennálló teljes keveredéstől.

Megvizsgáltuk továbbá az általunk talált közös sajátállapotok fizikai alakját. Ezek az állapotok a vonal gráfokon a legtöbb esetben (a legtöbb érmeoperátor esetében) élállapotoknak felelnek meg (7.2 alfejezet), azaz exponenciálisan lokalizáltak a rendszer határain. Ez a megfigyelés néhány érdekes fizikai jelenséget is maga után von, példának okáért a bolyongást egy pozícióban teljesen uniform eloszlásnak megfelelő tisztaállapotból indítva a végállapotot exponenciálisan lokalizálnak találhatjuk a rendszer egyik szélén. Újfént megjegyezzük, hogy az ilyen effektusok klasszikus bolyongásokon nem megfigyelhetőek.

Összefoglalva, a 7. fejezetben az eddig kidolgozott módszereinket alkalmaztuk, hogy megoldjuk az egydimenziós perkolációs kvantum bolyongások általános problémáját. Sikeresen megoldottuk a teljes $SU(2)$ problémát két alapvető egydimenziós gráfon, a gyűrűn és a vonalon, miközben a rendszer méretét szabad paraméterként hagytuk. Megjegyezzük, hogy ezek az eredmények a perkolációs kvantum bolyongásokra kiszámolt első analitikus, zárt alakú eredmények közé tartoznak. Megmutattuk, hogy a lehetséges aszimptotikus viselkedések eléggé sokszínűek lehetnek: a klasszikusan is elérhető teljes keveredéstől kezdve stacionárius, kvantum koherenciát megőrző állapotok és határciklusok is kialakulhatnak. Továbbá megvizsgáltuk ezen aszimptotikus megoldások fizikai alakját és azt találtuk, hogy a vonal gráfon a legtöbb érmeoperátorra élállapotok (a rendszer szélein megjelenő exponenciális lokalizált tiszta állapotok) jelennek meg.

Kétdimenziós perkoláció bolyongások: szimmetriasérülés és csapdázás

Az egydimenziós probléma teljes megoldását követően természetes továbblépés egy magasabb dimenzió probléma megvizsgálása. Már a zárt (unitér) kétdimenziós kvantum bolyongások (1.1.2. fejezet) is sokkal érdekesebb jelenségeket mutathatnak az egydimenziós modellhez képest. Ilyen jelenségekre egy kiváló példa a Grover csapdázás (lokalizáció). Hasonképpen a kétdimenziós perkolációs gráfok elmélete

sokkal több kihívást és releváns problémát rejt.

Az egydimenziós esettel analóg módon a 8. fejezetben az általunk megadott általános módszert és tiszta állapot ansatz-ot használtuk hogy a kétdimenziós bolyongások néhány érdekes esetét analitikusan megoldjuk. A két legnépszerűbb kétdimenziós bolyongást választottuk: a Hadamard és a Grover bolyongást. Az analízisben a bolyongás gráfjaként kétféle véges négyzettrácsot vettünk: a szőnyeg gráfot, mely a visszaverő határfeltételeknek felel meg és a tóruszt mely a periodikus határfeltételeknek felel meg. Mindegyik esetben a gráf méreteit szabad paraméterként meghagytuk. A Hadamard bolyongásra kapott megoldás (Sec. 8.2) az egydimenziós megfelelőjéhez képest számos eltérést mutatott: Mialatt az egydimenziós Hadamard bolyongás mindig sík pozícióeloszlást eredményez aszimptotikusan (tehát nincsenek élállapotok), addig a kétdimenziós modell mutathat pozíció inhomogenitást. Azt is megmutattuk, hogy ezek az inhomogén megoldások (tiszta sajátállapotok) érzékenyek a gráf orientációjára. Míg egyes esetekben az unitér Hadamard bolyongás az $M \times N$ és $N \times M$ gráfokon pusztán egy elforgatott pozícióeloszlást eredményez, a perkolációs változatban ez a fajta szimmetria sérül: az eloszlás teljesen megváltozik.

A Grover bolyongásra kapott megoldásban (Sec. 8.3) véges tartójú közös sajátállapotok egész seregét találtuk. Ezek az állapotok felelnek a csapdázás (lokalizáció) megjelenésért az unitér (zártrendszer dinamikát követő) esetben, de meglepő módon megjelennek a perkolációs esetben is. Ebből kifolyólag a csapdázás jelensége túléli a dinamikus perkoláció jelentette erős dekoherenciát. Ezek az állapotok dekoherencia-mentes alteret feszítenek ki, és véges tartójuk miatt a gráf méretére vagy határfeltételeire sem érzékenyek: a gyakorlatban információtárolásra is alkalmasak lehetnek. Egy ilyen nagy dekoherencia-mentes alter megjelenése számunkra nem várt eredmény volt. A véges tartójú sajátállapotok a csapdázás definíciójára vonatkozó következményeit is átgondoltuk: az irodalomban a csapdázást (lokalizációt) általában úgy definiálják, hogy a részecske megtalálási valószínűsége a kezdeti helyén a teljes időfejlődés alatt nagyobb mint zérus. Ez a definíció viszont nem alkalmazható megfelelően véges gráfokon. Javaslatunk szerint a robusztus, véges (exponenciálisan lecsengő tartójú) sajátállapotok megjelenése a csapdázás egy jobb indikátora lehetne, mivel az a gráf méretére és határaitra érzéketlen. Megjegyezzük, hogy mind a Hadamard mind a Grover bolyongások olyan RUO leképezések ahol a tiszta állapot ansatz igen jó eredménnyel alkalmazható: a teljes attraktor-tér meghatározható a közös sajátállapotok segítségével definiált attraktorokkal (p-attraktorok) és az egyetlen triviális nem-p-attraktorról mely a teljesen kevert állapotnak felel meg.

A 8. fejezet eredményeit összefoglalva: Alkalmaztuk az általunk javasolt analitikus módszereket, hogy két népszerű kétdimenziós kvantum bolyongást vizsgáljunk perkolációs gráfokon. Először a kétdimenziós Hadamard bolyongást analizáltuk és adtuk meg zárt alakban attraktorait. Megmutattuk, hogy szemben az egydimenziós Hadamard bolyongással itt inhomogenitás is felléphet. Továbbá megmutattuk, hogy a perkolációs modell érzékeny bizonyos elforgatásokra, az unitér modell bizonyos szimmetriái sérülnek. Megvizsgáltuk a Grover bolyongást is, melynek szintén meghatároztuk az attraktorait zárt alakban.

Megmutattuk, hogy a Grover bolyongásra jellemző csapdázási jelenség megtalálható a perkolációs modellben is. E jelenség túlélése a véges tartójú közös sajátállapotok megjelenésének köszönhető, melyek egy dekoherenciamentes alteret is kifizítenek. Ezen állapotok megjelenése miatt a csapdázás definíciójának kiterjesztését javasoltuk.

Az entrópia-ráta kiszámítása kvantumos bolyongás alapú stochasztikus folyamatokban

A kvantummechanikai rendszereket többféle módon is megzavarhatjuk. Eddig egy olyan rendszert tárgyaltunk, ahol a rendezetlenséget a környezetből érkező zaj okozta. Itt egy másik megközelítést fogunk megvizsgálni, melyben a rendszert periodikus szelektív mérésekkel zavarjuk meg. A következő kérdést tehetjük fel: mennyi kvantumosságot mutat egy olyan alapvetően zárt rendszer melyet rendszeres méréssel zavarunk meg? Ezt a problémát a rendszerből kinyerhető információ (rendezetlenség) tükrében vizsgáljuk meg a klasszikus információelméletből ismert entrópia-ráta eszközével (2. fejezet). A klasszikus információelmélet szemszögéből nézve az entrópia-ráta egy stochasztikus folyamat aszimptotikus szimbólumonkénti információtartalmát írja le. Mivel az entrópia-ráta egyik iskolapéldája a klasszikus véletlen bolyongás, kézenfekvőnek tűnik hogy a kvantumos bolyongások entrópia-rátájának problémáját megvizsgáljuk.

Mivel a klasszikus entrópia-ráta rendelkezik egy megfelelő operacionális és fizikai jelentéssel, a problémát a klasszikus információelmélet határain belül vizsgáltuk meg. Ehhez a klasszikus vagy kvantumos bolyongásokat egy fekete dobozba rejtettük (9.1. alfejezet), és ehhez rendeltünk egy stochasztikus folyamatot. Ezt a diszkrét idejű kvantumos bolyongások esetén a periodikus pozíció von Neumann méréssel definiáltuk (9.3. alfejezet). Az entrópia-ráta alapdefinícióját felhasználva sikeresen megadtunk egy módszert a rendszer entrópia-rátájának kiszámítására. Szemben a klasszikus bolyongásokkal, melyek Markov láncok, a vizsgált diszkrét idejű bolyongás nem tekinthető klasszikus Markov folyamatnak a pozíció mérési eredményeken, habár maga a bolyongás egy kvantumos Markov lánc.

Megmutattuk, hogy a belső érmeállapot a pozíciómérések után is megőriz némi koherenciát, így egyfajta memóriaként működik. Továbbá azt is megmutattuk, hogy a rendszer kvantumos Markov lánc tulajdonsága kihasználható: az aktuális érmeállapot, sőt, a rendszer teljes kvantumállapota rekonstruálható a pozíciómérések kimeneteleiből. Ez lehetővé tette számunkra, hogy a modell entrópia-rátáját egy érmeállapotokra is kiterjesztett klasszikus Markov lánc entrópia-rátájaként számítsuk ki (9.4. alfejezet). Továbbá azt is megfigyeltük, hogy a rendszer entrópia-rátája nem függ a kezdeti állapottól, tehát a rendszer aszimptotikusan mindig elfelejti kezdeti állapotait. Mivel az érmeállapotok száma végtelen is lehet, ezért egy az érmeállapotok vágásán alapuló közelítő módszert is megadtunk (9.5. alfejezet), mely

segítségével a rendszer entrópia-rátájának egy alsó és felső határa is kiszámítható. A megadott módszerek lehetővé tették, hogy meghatározzuk a sűrűn mért kvantumos bolyongások entrópia-rátáját és összevessük azt a sűrűn mért klasszikus bolyongásokéval. Azt találtuk (9.5. fejezet), hogy az érmeállapot mint implicit memória megjelenése miatt a sűrűn (gyakran) mért egydimenziós Hadamard bolyongások entrópia-rátája tipikusan kisebb mint a megfelelő klasszikus bolyongásoké.

Összefoglalva a 9.1 - 9.5. alfejezeteket, először egy stochasztikus folyamatot rendeltünk a periodikusan mért kvantumos (és klasszikus) bolyongásokhoz. Egy részletes módszert adtunk meg a klasszikus bolyongások entrópia-rátájának kiszámítására. Megmutattuk, hogy a kvantumos bolyongások nem tekinthetők a pozíció mérési eredmények közötti klasszikus Markov láncnak, viszont pozíció-érme bázison már annak tekinthetők. Módszert adtunk meg az entrópia-ráta alsó és felső határainak kiszámítására a bázisállapotok vágásával. Azt találtuk, hogy a sűrű mérések esetében az érme memóriaszerű viselkedése a kvantumos modellben (egydimenziós Hadamard bolyongás) tipikusan alacsonyabb entrópia-rátát eredményez mint a megfelelő klasszikus bolyongásé. Fontosnak tartjuk kiemelni, hogy az általunk megadott módszerek általánosak és könnyen kiterjeszthetők magasabb dimenziós bolyongásokra vagy más diszkrét idejű kvantumos Markov láncokra is.

Az entrópia-ráta skálázódásának meghatározása és összehasonlítás más megközelítésekkel

A periodikusan mért kvantumos és klasszikus bolyongások entrópia-rátája kiszámítható és összehasonlítható. Azonban ezek a számítások rendkívüli módon komplikálhattá válhatnak, ahogy a mérések közötti időt növeljük. Valójában a legrosszabb esetben a probléma exponenciálissá válik (9.5. alfejezet) a megfelelő Markov láncok dimenzióját (mátrixok méretet) tekintve.

Ezt a problémát elkerülendő egy protokollt adtunk meg (9.6. alfejezet) mely egy könnyen kiszámítható és mérhető felső határt ad meg az entrópia-rátára: Ha valaki a kvantumos bolyongást szigorúan klasszikus Markov láncként kezeli, azaz a pozíciók közötti stochasztikus (átmeneti) mátrixként írja le a mérési kimeneteket, szükségszerűen egy szuboptimális kódolást fog találni, mely magasabb entrópia-rátával társul. A korrekt reprezentáció és a pozícióra szorítókozó reprezentáció közötti függvénykapcsolatot és a kapcsolódó entrópia-ráta egyenlőtlenséget a rejtett Markov modellek elmélete szolgáltatja. Megmutattuk, hogy ezen felső határt jelentő entrópia-ráta közelíthető az úgynevezett weak limit elméletek segítségével. Azt is megmutattuk, hogy az egzakt kiszámítási mód segítségével akár egy alsó határhoz tartózkodó skálázódás is kiszámítható. Minden kvantumos esetben az entrópia-ráta $\log_2 w$ -vel skálázódik, ahol w két egymást követő mérés között eltelt idő (a periodikus mérések periódusideje). Összehasonlításképpen, ez a mennyiség klasszikus bolyongások esetén $\frac{1}{2} \log_2 w$. A szorzófaktorban megjelenő különbség a ballisztikus és diffúzív

terjedések következménye. Azt a konklúziót vontuk le, hogy a ritkán mért határesetben az entrópia-rátát a rendszerek terjedése uralja, azaz itt a kvantumozott változat túlszárnyalja a klasszikus megfelelőjét. Véges rendszereket (gyűrű gráfokat) is megvizsgáltunk (9.6. alfejezet) a módszer segítségével. Azt találtuk, hogy ezeken a gráfokon a klasszikus bolyongások teljes keveredést mutatnak, ezzel szemben a kvantumozott rendszer nem-monoton viselkedést mutat az unitaritás miatt: kollapszusok és feléledések (collapses and revivals) történhetnek.

Megvizsgáltuk a „teljesen kvantumozott” esetet is (9.7. alfejezet), melyben minden egyes mérést egy új, addig zavartalanul fejlődő rendszeren végzünk el. Miután ebben az esetben nincs korreláció az egymást követő mérések között, az entrópia-rátát egyszerűen a végtelen határesetig elfejlesztett rendszer pozíció eloszlásának entrópiája adja meg. Ez azonban végtelen kvantumozott rendszereken végtelen, véges kvantumozott rendszereken viszont nem konvergens az előbb említett kollapszus-feléledés viselkedés miatt. Azt a konklúziót vontuk le, hogy a „teljesen kvantumozott” eset nem vizsgálható az entrópia-ráta segítségével.

Az úgynevezett kvantumozott entrópia-rátát (9.8. fejezet) is kiszámítottuk. Ehhez szükség volt a mérés definíciójának szelektívtről nem szelektívtré történő változtatására. Megmutattuk, hogy a kvantumozott entrópia-ráta definíciójában található Neumann entrópia logaritmikusan nő az iterációkkal, ezért maga a kvantumozott entrópia-ráta (mely lineáris növekedést feltételez) zérus lesz.

A 9.6 - 9.8. alfejezeteket összefoglalandó, analitikus eszközök segítségével vizsgáltuk meg a periodikusan mért kvantumozott bolyongásokat. A rejtett Markov modellek elméletének segítségével egy egyszerűen kiszámítható és mérhető protokollt adtunk meg, mely segítségével az entrópia-rátára egy felső határ adható meg. Megmutattuk, hogy az entrópia-ráta skálázódása a mérések között eltelt idő függvényében megadható a "weak limit" elméletek segítségével. Arra a következtetésre jutottunk, hogy a ritka mérések határesetében az entrópia-rátát a bolyongások terjedése uralja. Az entrópia-ráta tükrében ezek alapján a kvantumozott és klasszikus rendszerek megkülönböztethetőek: a sűrű mérések esetében az egzakt módszer segítségével megtalálható a két rendszer közötti finom különbség, míg a ritka mérések határában a sokkal könnyebben kiszámítható felső határt adó protokoll biztonsággal vezet eredményre. Szintén megvizsgáltuk a „teljesen kvantumozott” esetet is, mely a kvantumozott bolyongások vizsgálatánál igen gyakran előforduló megközelítés. Ebben az esetben az entrópia-rátát nem találtuk konvergensnek. Végezetül a kvantumozott entrópia-rátát is megvizsgáltuk és azt találtuk, hogy az minden esetben zérus. Az, hogy az esetek túlnyomó részében a megvizsgált kvantumozott modelleknek létezik klasszikus entrópia-rátája, azt is magával vonja, hogy egy megfelelően tervezett klasszikus bolyongással e rendszerek kimenetei szimulálhatóak. Ilyen értelemben a kvantummechanikai tulajdonságok végig rejtve maradnak a klasszikus információelmélet szemszögéből. Másrészt a feltárt nem-triviális jelenségek, mint az érme memóriaszerű viselkedése, a nem-monoton entrópia-ráta és a kollapszusok-feléledések felfedik a bolyongás kvantumozott természetét.

Kitekintés

A perkolációs kvantums bolyongásokhoz általunk megadott módszerek jól megalapozott eszköztárat biztosítanak e rendszerek tanulmányozásához és megértéséhez. A területet övező növekvő figyelem és a gyümölcsöző kísérletek tovább motiválják ezirányú kutatásainkat. A következő kézenfekvő lépés más gráfok vagy többrészesek bolyongások vizsgálata lehet. Lehetségesnek tartjuk, hogy a megadott módszerek és eredmények a kvantuminformáció területén is közvetlenül felhasználhatóak. Egy másik irányt jelenthet a perkoláció jelenségének vizsgálata másféle kvantumos bolyongás definíciókat használva. Az előzetes eredményeink folytonos idejű bolyongások esetére azt mutatják, hogy itt is fellépnek nem-triviális effektusok, annak ellenére hogy a modell alapvetően kevésbé gazdag az érmetér hiánya miatt.

A véletlen unitér műveletek aszimptotikus elméletében közvetlenül felhasználható a tiszta állapot ansatz. Az általános módszer kiterjeszhető trace nem-megőrző rendszerekre is, azaz források és nyelők is bevezethetőek. Ígéretesnek tűnhet a tiszta állapot ansatz kiterjesztése ilyen általános rendszerekre. Egy másik érdekes kérdéskör a konvergencia, hiszen ez bizonyos modellekben igen fontos fizikai relevanciával bír, pl.: fázisátalakulások válhatnának tetten érhetővé.

A diszkrét idejű kvantumos bolyongások entrópia-rátájának meghatározásának kérdéskörét egy kezdeti lépésnek szántuk, mely segítségével az entrópia-ráta és a klasszikus-kvantumos határátmenet mélyebb megértését reméljük. Kézenfekvő továbblépési lehetőség az entrópia-ráta kiszámítása általános kvantumos rendszerekre és ezen keresztül a kvantummechanika sajátosságainak felismerése. Egy hasonló megközelítést jelenthet olyan definíciók és mérési eljárások megadása ami segítségével egy rendszer kvantumossága jellemezhető valamilyen entrópia-ráta-szerű mennyiség tükrében. Ehhez ígéretes jelöltnek tűnik az úgynevezett kvantumos dinamikus entrópia (quantum dynamical entropy). Azt reméljük, hogy a témában történő további kutatásaink segítségével egy kis betekintést nyerhetünk a klasszikus és kvantumos világ között húzódó rejtélyes határmezsgyébe.

Új tudományos eredmények

(List of new scientific results in Hungarian)

1. Általános módszert adtam meg a perkolációs diszkrét idejű kvantum bolyongások aszimptotikájának megoldására. E módszer a véletlen unitér műveletek attraktor-tér formalizmusán alapszik, melyet a diszkrét idejű bolyongások időfejlődésének definíciójában található érme-lépés operátorok szerint szeparáltam. Megmutattam, hogy a szeparáció segítségével érmék és gráfok egész családjaira oldható meg az aszimptotika. Azt is megmutattam, hogy a véletlen unitér dinamikát leíró szuperoperátor reguláris gráfokon a csúcsok számának függvényében polinomiálisan megkonstruálható [I].
2. Megadtam egy módszert véletlen unitér műveletek aszimptotikus attraktorainak meghatározására. A módszer gerincét a dinamika közös sajátállapotainak megtalálása jelenti, mely segítségével olyan attraktorokat lehet konstruálni, melyek direkt fizikai jelentést hordoznak. Megmutattam, hogy ezek a sajátállapotok egy dekoherencia-mentes alteret feszítenek ki. Azt is megmutattam, hogy némely esetben a teljes attraktor-tér megadható a közös sajátállapotok és a triviális attraktor (teljesen kevert állapot) segítségével. Erre az esetre is meghatároztam az aszimptotikus időfejlődést, mely a dekoherencia-mentes altéren történő unitér dinamika és az erre merőleges altérre vetített teljesen kevert állapot inkoherens keverékéből áll. Illusztráltam továbbá a megadott módszert a perkolációs gráfokon történő diszkrét idejű bolyongáson és rámutattam a közös sajátállapotokon alapuló módszer és az általános módszer közötti fontos különbségekre [II].
3. Explicit módon megoldottam az egydimenziós perkolációs kvantum bolyongások aszimptotikáját az általam kifejlesztett módszerek segítségével. Zárt alakban megadtam az attraktor-tér formuláját a teljes $SU(2)$ problémára perkolációs gyűrű és lánc gráfokon. Megmutattam, hogy az aszimptotika nemtriviális, kvantumkoherenciát mutató stacionárius állapotok és határciklusok is létrejöhetnek. Az aszimptotikus megoldások fizikai alakját is vizsgáltam, és felfedeztem, hogy lánc gráfokon a legtöbb érme esetében élállapotok lépnek fel [III].
4. Perkolációs tórusz és szőnyeg gráfokon explicit módon megoldottam a kétdimenziós Hadamard és Grover bolyongások aszimptotikus dinamikáját. Megmutattam, hogy a kétdimenziós Hadamard bolyongás az egydimenziós változatával szemben pozíció-inhomogenitást mutat. Azt is megmutattam, hogy a kétdimenziós Hadamard bolyongás a perkolációs esetben elveszti bizonyos elforgatási szimmetriáit. A Grover bolyongás esetén azt találtam, hogy a közös sajátállapotok véges tartóval rendelkeznek, tehát a bolyongás a perkolációs esetben is megtartja a zárt rendszerre (unitér eset) jellemző csapdázás jelenségét [II].

5. Módszert adtam meg a periodikusan mért kvantumoz bolyongások entrópia-rátájának kiszámításához. Megmutattam, hogy a periodikusan mért kvantumoz bolyongások klasszikus Markov-láncként viselkednek a pozíció-érmeállapot bázison és ennek a Markov-láncknak az entrópia-rátája megegyezik az előzőleg definiált sztochasztikus folyamatéval. Ezen entrópia-ráta felső és alsó határának kiszámítására is megadtam egy módszert. Sűrű mérések esetére azt találtam, hogy a kvantumoz bolyongások entrópia-rátája általában alacsonyabb mint a megfelelő klasszikus bolyongásé, mely az érmeállapot memóriaszerű viselkedésének következménye [IV].
6. Kidolgoztam egy közelítő protokollt, melynek segítségével a periodikusan mért kvantumoz bolyongások entrópia-rátája felülről közelíthető, illetve a ritka mérések esetére skálázódása kiszámítható. Egydimenziós Hadamard bolyongás esetére kiszámítottam az entrópia-ráta skálázódását a mérések közt eltelt idő (diszkrét lépések száma) függvényében. Azt találtam, hogy ritka mérések esetében az entrópia-rátát a kvantumoz bolyongás ballisztikus terjedése határozza meg, tehát az entrópia-ráta magasabb mint a klasszikus rendszer esetében. A véges rendszerek esetét is megvizsgáltam, és azt találtam, hogy az entrópia-rátában kollapszusok és feléledések is megjelenhetnek. Összehasonlítás céljából az úgynevezett kvantumoz entrópiát és a "legkvantumozabb" mérési eljárás esetét is megvizsgáltam. Azt találtam, hogy ezek a megközelítések triviális eredménnyel szolgálnak, nem árulnak el semmit a rendszer kvantumosságáról. Ezzel szemben az általam megadott klasszikus entrópia-rátán alapuló módszer önmagában alkalmas eszköz lehet a vizsgált rendszer kvantumosságának felderítésére [IV].

List of publications

Related publications

- [I] B. Kollár, T. Kiss, J. Novotný, I. Jex, *Asymptotic Dynamics of Coined Quantum Walks on Percolation Graphs*, Phys. Rev. Lett. **108**, 230505 (2012)
- [II] B. Kollár, J. Novotný, T. Kiss, I. Jex, *Percolation induced effects in two-dimensional coined quantum walks: analytic asymptotic solutions*, New J. Phys. **16**, 023002 (2014)
- [III] B. Kollár, J. Novotný, T. Kiss, I. Jex, *Discrete time quantum walks on percolation graphs*, Eur. Phys. J. Plus **129**, 103 (2014)
- [IV] B. Kollár, M. Koniorczyk, *Entropy rate of message sources driven by quantum walks*, Phys. Rev. A **89**, 022338 (2014)

Other publications

- [V] B. Kollár, M. Štefaňák, T. Kiss, I. Jex, *Recurrences in three-state quantum walks on a plane*, Phys. Rev. A **82**, 012303 (2010)
- [VI] M. Štefaňák, B. Kollár, T. Kiss, I. Jex, *Full revivals in 2D quantum walks*, Phys. Scr. **T140**, 014035 (2010)
- [VII] M. Štefaňák, S. M. Barnett, B. Kollár, T. Kiss, I. Jex, *Directional correlations in quantum walks with two particles*, New J. Phys. **13**, 033029 (2011)

Acknowledgement

I would like to thank my supervisor, Tamás Kiss for his guidance throughout my years as a PhD student at the University of Pécs and the Wigner Research Centre for Physics. I would also like to thank my unofficial co-supervisor Igor Jex, for his support and encouragement over my frequent visits to the Czech Technical University in Prague. Without their professional and personal support, and strong scientific collaboration this work could not have been completed.

I would like to express my gratitude towards all the employees of the Institute of Physics, and Institute of Mathematics and Informatics at the University of Pécs for their support, especially Mátyás Koniorczyk for the many insightful and stimulating discussions we had.

I thank all the members of the Department of Physics at the Czech Technical University in Prague, for creating the friendly atmosphere and for making Prague my second home, especially colleagues Jaroslav Novotný, Aurél Gábris, and Martin Štefaňák, who also dedicated his valuable time to read the manuscript and add his indispensable suggestions to it.

I would also like to thank all the members of the Department of Quantum Optics and Quantum Information, János Asbóth, Péter Ádám, Zoltán Darázs, András Dombi, Péter Domokos, András Gilyén, József Janszky, Orsolya Kálmán, Zsolt Kis, László Kecskés, Gábor Kónya, Zoltán Kurucz, Dávid Nagy, Nóra Sándor, Péter Sinkovicz, Viktor Szalay, Gergely Szirmai, Géza Tóth, and András Vukics, whom I had the opportunity to work with, for creating and maintaining an inspiring and familiar atmosphere.

Last, but not least, I would like to thank my parents, and my dear wife for believing in me, encouraging me, and providing their loving understanding and support without which I could not have been able to get this far.

Appendix

A. Entropy rate of one-dimensional Hadamard walk for waiting time $w = 2$

We show our calculation scheme for the entropy rate of QW driven stochastic process X_k [Eq. (9:5)], using the simplest nontrivial example of the one-dimensional Hadamard walk, driven by the coin (9:7). Let us stick to the simplest case, when we initialized the walk in the coin state $|L\rangle_C$ at the origin, thus $c_0 = L$ and $w = 2$. We apply U^2 on $|\psi_0\rangle = |0, L\rangle$, resulting in the following quantum state:

$$U^2|0, L\rangle = \frac{1}{2}| -2, L\rangle + \frac{1}{2}(-|0, L\rangle + |0, R\rangle) + \frac{1}{2}|2, R\rangle. \quad (\text{A:1})$$

This yields some elements of $P_{\alpha \rightarrow \beta}$ (see Eq. (9:22)):

$$\begin{aligned} P_{L \rightarrow L} &= 1/4 \\ P_{L \rightarrow -L+R} &= 1/2 \\ P_{L \rightarrow R} &= 1/4. \end{aligned} \quad (\text{A:2})$$

We repeat this process again for the newly obtained coin states $|R\rangle_C$ and $\frac{1}{\sqrt{2}}(-|L\rangle_C + |R\rangle_C)$, thus we apply U^2 again, and we calculate new elements of the transition matrix $P_{\alpha \rightarrow \beta}$ as follows:

$$\begin{aligned} P_{-L+R \rightarrow L} &= 1 \\ P_{R \rightarrow L} &= 1/4 \\ P_{R \rightarrow L+R} &= 1/2 \\ P_{R \rightarrow R} &= 1/4. \end{aligned} \quad (\text{A:3})$$

Note that in this second step, only a single new coin state $\frac{1}{\sqrt{2}}(|L\rangle + |R\rangle)$ appeared. Thus, we apply again U^2 on this new state to obtain the following:

$$P_{L+R \rightarrow R} = 1. \quad (\text{A:4})$$

We arrived to a complete coin state circle as no new coin states appeared, thus the $P_{\alpha \rightarrow \beta}$ transition matrix is complete. In the abstract coin state basis of $L, -L + R, R, L + R$ it takes the form

$$P_{\alpha \rightarrow \beta} = \frac{1}{4} \begin{pmatrix} 1 & 2 & 1 & 0 \\ 4 & 0 & 0 & 0 \\ 1 & 0 & 1 & 2 \\ 0 & 0 & 4 & 0 \end{pmatrix}. \quad (\text{A:5})$$

$\mu(\alpha)$ is found readily as the left eigenvector of $P_{\alpha \rightarrow \beta}$ corresponding to eigenvalue 1. Expanded in the same basis as the transition matrix, it takes the form of

$$\mu(\alpha) = \frac{1}{6} (2, 1, 2, 1). \quad (\text{A:6})$$

The single step missing is the calculation of the Shannon entropies $H(p_\alpha(\delta))$, which can be done in a straightforward manner, resulting in the following:

$$\begin{aligned} H(p_L(\delta)) &= \frac{3}{2} \text{ bits} \\ H(p_{-L+R}(\delta)) &= 1 \text{ bit} \\ H(p_R(\delta)) &= \frac{3}{2} \text{ bits} \\ H(p_{L+R}(\delta)) &= 1 \text{ bit}. \end{aligned} \quad (\text{A:7})$$

Finally, employing Eq. (9:21), the entropy rate is

$$H_2^{\text{QW}} = \frac{4}{3} \text{ bits}. \quad (\text{A:8})$$

In this particular example we restricted ourselves to initial state $|L\rangle_C$. One can repeat the process for a general initial coin state $|c_0\rangle_C = l|L\rangle_C + r|R\rangle_C$ with $|l|^2 + |r|^2 = 1$. After a more involving but still straightforward calculation it turns out that the size of $P_{\alpha \rightarrow \beta}$ is still finite in this case, and the entropy rate is $4/3$ bits independently from the initial coin state. Moreover, this result holds true even for any mixed initial coin states.

We repeat the calculation of entropy rate for $w = 2$ from initial coin state $c_0 = L = (LR)$ to demonstrate the refined method using property (9:24). We write the transitions corresponding to the abstract LR coin state

$$\begin{aligned} P_{LR \rightarrow LR} &= 1/2 \\ P_{LR \rightarrow -L+R} &= 1/2. \end{aligned} \quad (\text{A:9})$$

Investigating $\frac{1}{\sqrt{2}}(-|L\rangle_C + |R\rangle_C)$ leads to

$$P_{-L+R \rightarrow LR} = 1, \quad (\text{A:10})$$

and, hence, we obtain the transition matrix

$$P_{\alpha \rightarrow \beta} = \frac{1}{2} \begin{pmatrix} 1 & 1 \\ 2 & 0 \end{pmatrix}, \quad (\text{A:11})$$

in the basis of LR and $-L+R$. The asymptotic coin distribution $\mu(\alpha)$ turns out to be $\frac{1}{3}(2, 1)$. According to Eq. (9:24), the Shannon entropy of LR reads

$$H(p_{LR}(\delta)) = H(p_L(\delta)) = H(p_R(\delta)). \quad (\text{A:12})$$

Thus, by employing Eq. (9:21), we obtain

$$H_2^{\text{QW}} = \frac{4}{3} \text{ bits} \quad (\text{A:13})$$

again.

B. Approximating entropy rates of one-dimensional QWs

In the following we demonstrate the approximative method for determining $\mu(\alpha)$ for the case of $w = 2$ and $c_0 = L (= LR)$. Here we note that for $w = 2$ the approximation is not necessary, but it is comparable with our previous results and it is easier to follow than the $w > 2$ cases. We restrict ourselves to the calculation of the exact mapping only for the initial state, thus

$$\begin{aligned} P_{LR \rightarrow LR} &= 1/2 \\ P_{LR \rightarrow -L+R} &= 1/2. \end{aligned} \quad (\text{B:14})$$

Since we do not wish to calculate further, using Eq. (9:27) we get the following maps

$$\begin{aligned} P_{-L+R \rightarrow LR} &= 1/2 \\ P_{-L+R \rightarrow ?} &= 1/2, \end{aligned} \quad (\text{B:15})$$

where we used “?” to mark the set of unknown coin states $|?\rangle_C$ which we do not wish to determine (see Eq. (9:29)). To build a proper stochastic matrix we need an additional set of rules for the state “?”,

which, again using Eq. (9:27), are

$$\begin{aligned} P_{? \rightarrow LR} &= 1/2 \\ P_{? \rightarrow ?} &= 1/2. \end{aligned} \tag{B:16}$$

Thus, the transition matrix on the basis of LR and $-L + R, ?$ is

$$P_{\alpha \rightarrow \beta} = \frac{1}{2} \begin{pmatrix} 1 & 1 & 0 \\ 1 & 0 & 1 \\ 1 & 0 & 1 \end{pmatrix}. \tag{B:17}$$

The corresponding asymptotic coin distribution is $\frac{1}{4}(2, 1, 1)$. Using Eq. (9:32) we finish our calculation, in this particular case $H_{\max} = 3/2$ bits and $H_{\min} = 1$ bit. Thus, the exact entropy rate is in the interval

$$H_2^{\text{QW}} = 1.3125 \pm 0.0625 \text{ bits}, \tag{B:18}$$

which is surprisingly close to the exact $4/3$ bits.

We move to the case of $w = 3$. For convenience, we use $c_0 = L (= LR)$ as the initial state. We apply U^3 on $|\psi_0\rangle = |0, L\rangle$ resulting in the following:

$$\begin{aligned} U^3|\psi_0\rangle &= \frac{1}{\sqrt{8}} (| -3, L\rangle + | -1\rangle_P \otimes (-2|L\rangle_C + |R\rangle_C) \\ &\quad - |1, L\rangle + |3, R\rangle). \end{aligned} \tag{B:19}$$

Thus, we have transitions

$$\begin{aligned} P_{LR \rightarrow LR} &= 3/8 \\ P_{LR \rightarrow -2L+R} &= 5/8. \end{aligned} \tag{B:20}$$

Continuing with the new, yet undiscovered coin state, we obtain

$$\begin{aligned} P_{-2L+R \rightarrow LR} &= 1/4 \\ P_{-2L+R \rightarrow 4L-3R} &= 5/8 \\ P_{-2L+R \rightarrow L-2R} &= 1/8. \end{aligned} \tag{B:21}$$

We end our calculation here and introduce the unknown coin state “?” once again. Using Eq. (9:27) we

complete the transition matrix, arriving at

$$P_{\alpha \rightarrow \beta} = \begin{pmatrix} 3/8 & 5/8 & 0 & 0 & 0 \\ 1/4 & 0 & 5/8 & 1/8 & 0 \\ 1/4 & 0 & 0 & 0 & 3/4 \\ 1/4 & 0 & 0 & 0 & 3/4 \\ 1/4 & 0 & 0 & 0 & 3/4 \end{pmatrix}, \quad (\text{B:22})$$

which is written with respect to the basis $(LR, -2L + R, 4L - 3R, L - 2R, ?)$. From here, $\mu(\alpha)$, $p_\alpha(\delta)$ can be determined readily. With the use of Eq. (9:32), the entropy rate for the one-dimensional Hadamard QW is in the interval

$$H_3^{\text{QW}} = 1.54 \pm 0.08 \text{ bits}. \quad (\text{B:23})$$

If we iterate the above procedure further, the interval (uncertainty) shrinks, i. e., the precision of the entropy rate increases. For 11 iterations the entropy rate of the one-dimensional Hadamard QWs with $w = 3$ is

$$H_3^{\text{QW}} = 1.499 \pm 0.004 \approx 3/2 \text{ bits}. \quad (\text{B:24})$$

Bibliography

- [1] K. Pearson, *Nature* **72**, 294 (1905).
- [2] L. Rayleigh, *Nature* **72**, 318 (1905).
- [3] M. Kac, *Am. Math. Month.* , 369 (1947).
- [4] F. Spitzer, F. Spitzer, F. Spitzer, and A. Mathematician, *Principles of random walk* (Springer, 1964).
- [5] L. Lovász, *Combinatorics, Paul Erdős is eighty* **2**, 1 (1993).
- [6] B. D. Hughes, *Random walks and random environments* (Clarendon Press Oxford, 1996).
- [7] P. Révész, *Random walk in random and non-random environments* (World Scientific, 2005).
- [8] A. Einstein, *Ann. der Phys.* **322**, 549 (1905).
- [9] A. Einstein, *Ann. der Phys.* **324**, 371 (1906).
- [10] M. Von Smoluchowski, *Z. Phys.* **17**, 557 (1916).
- [11] A. Einstein, *Investigations on the Theory of the Brownian Movement* (Courier Dover Publications, 1956).
- [12] P. Gaspard, G. Györgyi, I. Kondor, L. Sasvari, and T. Tél, *From Phase Transitions to Chaos: Topics in Modern Statistical Physics* , 322 (1992).
- [13] E. F. Fama, *Financial Analysts Journal* , 55 (1965).
- [14] J. Masoliver, M. Montero, and G. H. Weiss, *Phys. Rev. E* **67**, 021112 (2003).
- [15] E. Scalas, *Physica A: Statistical Mechanics and its Applications* **362**, 225 (2006).
- [16] A. Király and I. M. Jánosi, *Phys. Rev. E* **65**, 051102 (2002).
- [17] D. Kelker, *J. Am. Stat. As.* **68**, 821 (1973).
- [18] H. Daniels, *Adv. Appl. Prob.* , 607 (1974).
- [19] E. A. Codling, M. J. Plank, and S. Benhamou, *J Roy. Soc. Int.* **5**, 813 (2008).
- [20] W. Breymann, T. Tél, and J. Vollmer, *Chaos: An Interdisciplinary Journal of Nonlinear Science* **8**, 396 (1998).
- [21] Z. Rácz, *Phys. Rev. Lett.* **55**, 1707 (1985).
- [22] B. Bergersen and Z. Rácz, *Phys. Rev. Lett.* **67**, 3047 (1991).
- [23] F. Iglói and H. Rieger, *Phys. Rev. B* **57**, 11404 (1998).
- [24] F. Iglói and H. Rieger, *Phys. Rev. E* **58**, 4238 (1998).
- [25] T. Antal and I. Scheuring, *Bull. math. biol.* **68**, 1923 (2006).
- [26] B. A. Huberman, P. L. Pirolli, J. E. Pitkow, and R. M. Lukose, *Science* **280**, 95 (1998).
- [27] A. Blum, T.-H. H. Chan, and M. R. Rwebangira, *ANALCO* **6**, 238 (2006).
- [28] M. Mohseni, P. Rebentrost, S. Lloyd, and A. Aspuru-Guzik, *J. Chem. Phys.* **129**, 174106 (2008).
- [29] Y. Aharonov, L. Davidovich, and N. Zagury, *Phys. Rev. A* **48**, 1687 (1993).
- [30] D. A. Meyer, *J. Stat. Phys.* **85**, 551 (1996).
- [31] E. Farhi and S. Gutmann, *Phys. Rev. A* **58**, 915 (1998).
- [32] M. Hillery, J. Bergou, and E. Feldman, *Phys. Rev. A* **68**, 032314 (2003).
- [33] M. Szegedy, in *Foundations of Computer Science, 2004. Proceedings. 45th Annual IEEE Symposium on* (IEEE, 2004) pp. 32–41.

- [34] A. M. Childs, E. Farhi, and S. Gutmann, *Quant. Inf. Proc.* **1**, 35 (2002).
- [35] J. Kempe, *Cont. Phys.* **44**, 307 (2003).
- [36] N. Konno, in *Quantum Potential Theory*, edited by U. Franz and M. Schürmann (Springer, 2008) pp. 309–452.
- [37] S. E. Venegas-Andraca, *Quant. Inf. Proc.* **11**, 1015 (2012).
- [38] F. Grunbaum and L. Velázquez, Preprint [arXiv:1111.6630](https://arxiv.org/abs/1111.6630) (2011).
- [39] O. Mülken, V. Pernice, and A. Blumen, *Phys. Rev. E* **76**, 051125 (2007).
- [40] O. Mülken and A. Blumen, *Phys. E: Low-dimensional Systems and Nanostructures* **42**, 576 (2010).
- [41] O. Mülken and A. Blumen, *Phys. Rep.* **502**, 37 (2011).
- [42] Z. Zimboras, M. Faccin, Z. Kadar, J. D. Whitfield, B. P. Lanyon, and J. Biamonte, *Nat. Sci. Rep.* **3** (2013).
- [43] D. Lu, J. D. Biamonte, J. Li, H. Li, T. H. Johnson, V. Bergholm, M. Faccin, Z. Zimborás, R. Laflamme, J. Baugh, *et al.*, Preprint [arXiv:1405.6209](https://arxiv.org/abs/1405.6209) (2014).
- [44] A. Anishchenko, A. Blumen, and O. Mülken, *Quant. Inf. Proc.* **11**, 1273 (2012).
- [45] L. Diósi, *A short course in quantum information theory: an approach from theoretical physics*, Vol. 827 (Springer, 2011).
- [46] D. Petz, *Quantum information theory and quantum statistics* (Springer, 2007).
- [47] N. Shenvi, J. Kempe, and K. B. Whaley, *Phys. Rev. A* **67**, 052307 (2003).
- [48] A. Ambainis, *Int. J. Quant. Inf.* **1**, 507 (2003).
- [49] A. Ambainis, J. Kempe, and A. Rivosh, in *Proc. 16th ACM-SIAM symposium on Discrete algorithms* (Society for Industrial and Applied Mathematics, 2005) pp. 1099–1108.
- [50] N. B. Lovett, M. Everitt, M. Trevers, D. Mosby, D. Stockton, and V. Kendon, *Nat. Comp.* **11**, 23 (2012).
- [51] M. Santha, in *Theory and Applications of Models of Computation*, Lecture Notes in Computer Science, Vol. 4978, edited by M. Agrawal, D. Du, Z. Duan, and A. Li (Springer Berlin Heidelberg, 2008) pp. 31–46.
- [52] A. Gábris, T. Kiss, and I. Jex, *Phys. Rev. A* **76**, 062315 (2007).
- [53] V. Potoček, A. Gábris, T. Kiss, and I. Jex, *Phys. Rev. A* **79**, 012325 (2009).
- [54] A. M. Childs, *Phys. Rev. Lett.* **102**, 180501 (2009).
- [55] N. B. Lovett, S. Cooper, M. Everitt, M. Trevers, and V. Kendon, *Phys. Rev. A* **81**, 042330 (2010).
- [56] A. M. Childs, D. Gosset, and Z. Webb, *Science* **339**, 791 (2013).
- [57] T. Kitagawa, M. S. Rudner, E. Berg, and E. Demler, *Phys. Rev. A* **82**, 033429 (2010).
- [58] J. Asbóth, *Phys. Rev. B* **86**, 195414 (2012).
- [59] J. Asbóth and H. Obuse, *Phys. Rev. B* **88**, 121406 (2013).
- [60] M. S. Rudner, N. H. Lindner, E. Berg, and M. Levin, *Phys. Rev. X* **3**, 031005 (2013).
- [61] S. Moulieras, M. Lewenstein, and G. Puentes, *J. Phys. B: Atomic, Molecular and Optical* **46**, 104005 (2013).
- [62] I. Carneiro, M. Loo, X. Xu, M. Girerd, V. Kendon, and P. L. Knight, *New J. Phys.* **7**, 156 (2005).
- [63] O. Maloyer and V. Kendon, *New J. Phys.* **9**, 87 (2007).
- [64] R. Vieira, E. P. Amorim, and G. Rigolin, *Phys. Rev. Lett.* **111**, 180503 (2013).
- [65] R. Vieira, E. P. Amorim, and G. Rigolin, *Phys. Rev. A* **89**, 042307 (2014).
- [66] Ł. Paweła, P. Gawron, J. Miszczak, and P. Sadowski, Preprint [arXiv:1407.1184](https://arxiv.org/abs/1407.1184) (2014).
- [67] A. Romanelli, *Phys. Rev. A* **85**, 012319 (2012).

-
- [68] A. Romanelli and G. Segundo, *Phys. A: Stat. Mech. Appl.* **393**, 646 (2014).
- [69] M. Christandl, N. Datta, A. Ekert, and A. J. Landahl, *Phys. Rev. Lett.* **92**, 187902 (2004).
- [70] V. Kendon, *Math. Struct. Comp. Sci.* **17**, 1169 (2007).
- [71] P. Ribeiro, P. Milman, and R. Mosseri, *Phys. Rev. Lett.* **93**, 190503 (2004).
- [72] G. Abal, R. Siri, A. Romanelli, and R. Donangelo, *Phys. Rev. A* **73**, 042302 (2006).
- [73] C. Cedzich, T. Rybár, A. Werner, A. Alberti, M. Genske, and R. Werner, *Phys. Rev. Lett.* **111**, 160601 (2013).
- [74] H. Lavička, V. Potoček, T. Kiss, E. Lutz, and I. Jex, *Eur. Phys. J. D* **64**, 119 (2011).
- [75] E. Camilleri, P. P. Rohde, and J. Twamley, Preprint [arXiv:1401.1869](https://arxiv.org/abs/1401.1869) (2014).
- [76] N. Inui, N. Konno, and E. Segawa, *Phys. Rev. E* **72**, 056112 (2005).
- [77] C. S. Hamilton, A. Gábris, I. Jex, and S. M. Barnett, *New J. Phys.* **13**, 013015 (2011).
- [78] M. Stefanak, I. Bezdekova, I. Jex, and S. Barnett, Preprint [arXiv:1309.7835](https://arxiv.org/abs/1309.7835) (2013).
- [79] M. Stefanak, I. Bezdekova, and I. Jex, Preprint [arXiv:1405.7146](https://arxiv.org/abs/1405.7146) (2014).
- [80] T. D. Mackay, S. D. Bartlett, L. T. Stephenson, and B. C. Sanders, *J. Phys. A* **35**, 2745 (2002).
- [81] N. Inui, Y. Konishi, and N. Konno, *Phys. Rev. A* **69**, 052323 (2004).
- [82] C. Chandrashekar, R. Srikanth, and S. Banerjee, *Phys. Rev. A* **76**, 022316 (2007).
- [83] Y. Shikano and H. Katsura, *Phys. Rev. E* **82**, 031122 (2010).
- [84] D. R. Hofstadter, *Phys. Rev. B* **14**, 2239 (1976).
- [85] G. D. Paparo and M. A. Martin-Delgado, *Nat. Sci. Rep.* **2** (2012), doi:10.1038/srep00444.
- [86] Y. Omar, N. Paunković, L. Sheridan, and S. Bose, *Phys. Rev. A* **74**, 042304 (2006).
- [87] M. Štefanák, T. Kiss, I. Jex, and B. Mohring, *J. Phys. A: Math. Gen.* **39**, 14965 (2006).
- [88] J. K. Gamble, M. Friesen, D. Zhou, R. Joynt, and S. Coppersmith, *Phys. Rev. A* **81**, 052313 (2010).
- [89] S. D. Berry and J. B. Wang, *Phys. Rev. A* **83**, 042317 (2011).
- [90] K. Mayer, M. C. Tichy, F. Mintert, T. Konrad, and A. Buchleitner, *Phys. Rev. A* **83**, 062307 (2011).
- [91] B. C. Sanders, S. D. Bartlett, B. Tregenna, and P. L. Knight, *Phys. Rev. A* **67**, 042305 (2003).
- [92] T. Di, M. Hillery, and M. S. Zubairy, *Phys. Rev. A* **70**, 032304 (2004).
- [93] C. Chandrashekar, *Phys. Rev. A* **74**, 032307 (2006).
- [94] H. Jeong, M. Paternostro, and M. S. Kim, *Phys. Rev. A* **69**, 012310 (2004).
- [95] P. Pathak and G. Agarwal, *Phys. Rev. A* **75**, 032351 (2007).
- [96] A. Wójcik, T. Łuczak, P. Kurzyński, A. Grudka, T. Gdala, and M. Bednarska-Bzdęga, *Phys. Rev. A* **85**, 012329 (2012).
- [97] S. K. Goyal, F. S. Roux, A. Forbes, and T. Konrad, *Phys. Rev. Lett.* **110**, 263602 (2013).
- [98] C. S. Hamilton, R. Kruse, L. Sansoni, C. Silberhorn, and I. Jex, *Phys. Rev. Lett.* **113**, 083602 (2014).
- [99] W. Dür, R. Raussendorf, V. M. Kendon, and H.-J. Briegel, *Phys. Rev. A* **66**, 052319 (2002).
- [100] K. Eckert, J. Mompart, G. Birkel, and M. Lewenstein, *Phys. Rev. A* **72**, 012327 (2005).
- [101] R. Côté, A. Russell, E. E. Eyler, and P. L. Gould, *New J. Phys.* **8**, 156 (2006).
- [102] B. C. Travaglione and G. J. Milburn, *Phys. Rev. A* **65**, 032310 (2002).
- [103] P. L. Knight, E. Roldán, and J. E. Sipe, *Opt. Comm.* **227**, 147 (2003).
- [104] J. Ghosh, *Phys. Rev. A* **89**, 022309 (2014).

- [105] O. Kálmán, T. Kiss, and P. Földi, *Phys. Rev. B* **80**, 035327 (2009).
- [106] P. Földi, O. Kálmán, and F. Peeters, *Phys. Rev. B* **80**, 125324 (2009).
- [107] K. Manouchehri and J. Wang, *J. Phys. A: Math. Theor.* **41**, 065304 (2008).
- [108] J. Boehm, M. Bellec, F. Mortessagne, U. Kuhl, S. Barkhofen, S. Gehler, H.-J. Stoeckmann, I. Foulger, S. Gnutzman, and G. Tanner, Preprint [arXiv:1409.2382](https://arxiv.org/abs/1409.2382) (2014).
- [109] J. Wang and K. Manouchehri, *Physical Implementation of Quantum Walks* (Springer, 2013).
- [110] M. Karski, L. Förster, J.-M. Choi, A. Steffen, W. Alt, D. Meschede, and A. Widera, *Science* **325**, 174 (2009).
- [111] M. Genske, W. Alt, A. Steffen, A. H. Werner, R. F. Werner, D. Meschede, and A. Alberti, *Phys. Rev. Lett.* **110**, 190601 (2013).
- [112] H. Schmitz, R. Matjeschk, C. Schneider, J. Glueckert, M. Enderlein, T. Huber, and T. Schaetz, *Phys. Rev. Lett.* **103**, 090504 (2009).
- [113] F. Zähringer, G. Kirchmair, R. Gerritsma, E. Solano, R. Blatt, and C. F. Roos, *Phys. Rev. Lett.* **104**, 100503 (2010).
- [114] C. Ryan, M. Laforest, J. Boileau, and R. Laflamme, *Phys. Rev. A* **72**, 062317 (2005).
- [115] A. Peruzzo, M. Lobino, J. C. F. Matthews, N. Matsuda, A. Politi, K. Poulios, X.-Q. Zhou, Y. Lahini, N. Ismail, K. Wörhoff, Y. Bromberg, Y. Silberberg, M. G. Thompson, and J. L. O'Brien, *Science* **329**, 1500 (2010).
- [116] L. Sansoni, F. Sciarrino, G. Vallone, P. Mataloni, A. Crespi, R. Ramponi, and R. Osellame, *Phys. Rev. Lett.* **108**, 010502 (2012).
- [117] A. Crespi, R. Osellame, R. Ramponi, V. Giovannetti, R. Fazio, L. Sansoni, F. De Nicola, F. Sciarrino, and P. Mataloni, *Nat. Phot.* **7**, 322 (2013).
- [118] J. D. A. Meinecke, K. Poulios, A. Politi, J. C. F. Matthews, A. Peruzzo, N. Ismail, K. Wörhoff, J. L. O'Brien, and M. G. Thompson, *Phys. Rev. A* **88**, 012308 (2013).
- [119] D. Bouwmeester, I. Marzoli, G. Karman, W. Schleich, and J. Woerdman, *Phys. Rev. A* **61**, 013410 (1999).
- [120] M. A. Broome, A. Fedrizzi, B. P. Lanyon, I. Kassal, A. Aspuru-Guzik, and A. G. White, *Phys. Rev. Lett.* **104**, 153602 (2010).
- [121] P. Xue, H. Qin, B. Tang, and B. C. Sanders, *New J. Phys.* **16**, 053009 (2014).
- [122] A. Schreiber, K. N. Cassemiro, V. Potoček, A. Gábris, P. J. Mosley, E. Andersson, I. Jex, and C. Silberhorn, *Phys. Rev. Lett.* **104**, 050502 (2010).
- [123] A. Schreiber, K. N. Cassemiro, V. Potoček, A. Gábris, I. Jex, and C. Silberhorn, *Phys. Rev. Lett.* **106**, 180403 (2011).
- [124] A. Schreiber, A. Gábris, P. P. Rohde, K. Laiho, M. Štefaňák, V. Potoček, C. Hamilton, I. Jex, and C. Silberhorn, *Science* **336**, 55 (2012).
- [125] Y.-C. Jeong, C. Di Franco, H.-T. Lim, M.-S. Kim, and Y.-H. Kim, *Nat. Comm.* **4** (2013).
- [126] G. Palla and G. Vattay, *New J. Phys.* **8**, 307 (2006).
- [127] A. Fekete, G. Vattay, and M. Pósfai, *Phys. Rev. E* **79**, 065101 (2009).
- [128] H. Kesten, *Percolation theory for mathematicians* (Birkhäuser Boston, 1982).
- [129] G. Grimmett, *Percolation*, Die Grundlehren der mathematischen Wissenschaften in Einzeldarstellungen

- (Springer, 1999).
- [130] J. E. Steif, in *Fractal geometry and stochastics IV*, edited by C. Bandt, M. Zähle, and P. Mörters (Springer, 2009) pp. 145–174.
- [131] A. Romanelli, R. Siri, G. Abal, A. Auyuanet, and R. Donangelo, *Phys. A: Stat. Mech. Appl.* **347**, 137 (2005).
- [132] A. C. Oliveira, R. Portugal, and R. Donangelo, *Phys. Rev. A* **74**, 012312 (2006).
- [133] G. Abal, R. Donangelo, F. Severo, and R. Siri, *Phys. A: Stat. Mech. Appl.* **387**, 335 (2008).
- [134] G. Leung, P. Knott, J. Bailey, and V. Kendon, *New J. Phys.* **12**, 123018 (2010).
- [135] N. B. Lovett, M. Everitt, R. M. Heath, and V. Kendon, Preprint [arXiv:1110.4366](https://arxiv.org/abs/1110.4366).
- [136] F. L. Marquezino, R. Portugal, G. Abal, and R. Donangelo, *Phys. Rev. A* **77**, 042312 (2008).
- [137] Z. Darázs and T. Kiss, *J. Phys. A: Math. Theor.* **46**, 375305 (2013).
- [138] J. Novotný, G. Alber, and I. Jex, *J. Phys. A: Math. Theor.* **42**, 282003 (2009).
- [139] J. Novotný, G. Alber, and I. Jex, *Centr. Eur. J. Phys.* **8**, 1001 (2010).
- [140] J. Novotný, G. Alber, and I. Jex, *J. Phys. A: Math. Theor.* **45**, 485301 (2012).
- [141] T. M. Cover and J. A. Thomas, *Elements of information theory* (John Wiley & Sons, 2012).
- [142] D. Petz, in *John von Neumann and the foundations of quantum physics* (Springer, 2001) pp. 83–96.
- [143] R. Alicki, A. Łoziński, P. Pakoński, and K. Życzkowski, *J. Phys. A: Math. Gen.* **37**, 5157 (2004).
- [144] I. Csiszár, G. O. Katona, and G. Tardos, *Entropy, Search, Complexity*, Bolyai Society Mathematical Studies, Vol. 16 (Springer, 2007).
- [145] S. K. Goyal, T. Konrad, and L. Diósi, Preprint [arXiv:1401.0196](https://arxiv.org/abs/1401.0196) (2013).
- [146] R. Portugal, S. Boettcher, and S. Falkner, Preprint [arXiv:1408.5166](https://arxiv.org/abs/1408.5166) (2014).
- [147] J. Kempe, *Prob. theor. rel. fields* **133**, 215 (2005).
- [148] J. Keating, N. Linden, J. Matthews, and A. Winter, *Phys. Rev. A* **76**, 012315 (2007).
- [149] G. Pólya, *Math. Ann.* **84**, 149 (1921).
- [150] M. Štefaňák, I. Jex, and T. Kiss, *Phys. Rev. Lett.* **100**, 020501 (2008).
- [151] M. Štefaňák, T. Kiss, and I. Jex, *Phys. Rev. A* **78**, 032306 (2008).
- [152] M. Štefaňák, T. Kiss, and I. Jex, *New J. Phys.* **11**, 043027 (2009).
- [153] T. Kiss, L. Kecskés, M. Štefaňák, and I. Jex, *Phys. Script.* **T135**, 014055 (2009).
- [154] Z. Darázs and T. Kiss, *Phys. Rev. A* **81**, 062319 (2010).
- [155] F. A. Grünbaum, L. Velázquez, A. H. Werner, and R. F. Werner, *Comm. Math. Phys.* **320**, 543 (2013).
- [156] A. C. Oliveira, R. Portugal, and R. Donangelo, Preprint [arxiv:0706.3181](https://arxiv.org/abs/0706.3181).
- [157] G. Abal, R. Donangelo, F. L. Marquezino, and R. Portugal, *Math. Struct. Comp. Sci.* **20**, 999 (2010).
- [158] C. Chandrashekar, Preprint [arXiv:1103.2704](https://arxiv.org/abs/1103.2704) (2011).
- [159] L. K. Grover, *Phys. Rev. Lett.* **79**, 325 (1997).
- [160] L. K. Grover, *Phys. Rev. Lett.* **80**, 4329 (1998).
- [161] G. Grimmett, S. Janson, and P. F. Scudo, *Phys. Rev. E* **69**, 026119 (2004).
- [162] K. Watabe, N. Kobayashi, M. Katori, and N. Konno, *Phys. Rev. A* **77**, 062331 (2008).
- [163] N. Konno and H. Yoo, *J. Stat. Phys.* **150**, 299 (2013).
- [164] F. W. Strauch, *Phys. Rev. A* **74**, 030301 (2006).

- [165] A. P. Hines and P. Stamp, *Phys. Rev. A* **75**, 062321 (2007).
- [166] A. M. Childs, *Comm. Math. Phys.* **294**, 581 (2010).
- [167] A. M. Childs, R. Cleve, E. Deotto, E. Farhi, S. Gutmann, and D. A. Spielman, in *Proc. 35th Annual ACM Symposium on Theory of Computing*, STOC '03 (ACM, New York, NY, USA, 2003) pp. 59–68.
- [168] A. M. Childs and J. Goldstone, *Phys. Rev. A* **70**, 022314 (2004).
- [169] O. Mülken, A. Blumen, T. Amthor, C. Giese, M. Reetz-Lamour, and M. Weidemüller, *Phys. Rev. Lett.* **99**, 090601 (2007).
- [170] E. Feldman and M. Hillery, *Phys. Lett. A* **324**, 277 (2004).
- [171] E. Feldman and M. Hillery, *J. Phys. A: Math. Theor.* **40**, 11343 (2007).
- [172] E. Feldman, M. Hillery, H.-W. Lee, D. Reitzner, H. Zheng, and V. Bužek, *Phys. Rev. A* **82**, 040301 (2010).
- [173] H. Spohn, *J. Math. Phys.* **19**, 1227 (1978).
- [174] M. Koniorczyk, P. Rapčan, and V. Bužek, *Phys. Rev. A* **72**, 022321 (2005).
- [175] J. Novotný, G. Alber, and I. Jex, *Phys. Rev. Lett.* **107**, 090501 (2011).
- [176] X. Feng, Y. Deng, and H. W. Blöte, *Phys. Rev. E* **78**, 031136 (2008).
- [177] J. L. Jacobsen, *J. Phys. A: Math. Theor.* **47**, 135001 (2014).
- [178] C. Chandrashekar, *Centr. Eur. J. Phys.* **8**, 979 (2010).
- [179] R. Alicki and M. Fannes, *Quantum Dynamical Systems* (Oxford University Press, 2001).